THE UNIVERSITY
of EDINBURGH

The two-reggeon exchange to all loop orders

Joscha Reichel

A thesis presented for the degree of

Doctor of Philosophy

School of Physics and Astronomy

University of Edinburgh

United Kingdom

2019

Abstract

In the limit of very large centre-of-mass energy s the two-parton scattering amplitude is well approximated by the exchange of reggeons in the t channel. In particular, the leading contributions to the signature-even two-reggeon exchange are described by the famous Balitsky–Fadeev–Kuraev–Lipatov (BFKL) evolution equation. In this thesis we demonstrate that it is possible to solve this equation iteratively, and in this way calculate the associated amplitude to any loop order in perturbative QCD.

The key idea is to analyse the evolution of the two-reggeon wavefunction in two complementary regions. The so-called soft region is characterised by the small momentum of one of the reggeons. There, the wavefunction obeys a simplified evolution equation and evaluates to a polynomial in the soft momentum. This region is the exclusive source of the singularities of the signature-even amplitude. Consequently, the complementary region is described by purely finite integrals which can be evaluated without dimensional regularisation, directly in terms of a class of iterated polylogarithms. The contributions from both regions are combined and shown to recover the result of the full BFKL evolution. All the above methods are algorithmic and work to any loop order.

We resum the singularities of the amplitude to all loop orders and match the result to the predictions made by the soft factorisation theorem to shed light on the universal infrared behaviour of two-parton scattering. This lets us extract the all-order soft anomalous dimension in the high-energy limit whose properties we analyse in detail. In particular, it turns out to be an entire function of the coupling which can be approximated by a simple oscillating function well beyond the perturbative regime.

The finite terms of the signature-even amplitude show intricate combinations of transcendental numbers. At low loop orders they are the well-known values of the Riemann

zeta function evaluated at integer arguments. However, examining the amplitude at eleven loops and beyond reveals that a broader class of numbers — so-called single-valued multiple zeta values — is needed to describe the two-reggeon exchange. Moreover, finite terms that originate in the soft region are readily resummed and allow us to derive a modified evolution equation for the complementary hard region. In fact, there are more hints of all-order resummation which we discuss towards the end of this thesis hoping they will inspire future research in this area.

Lay summary

Scattering amplitudes are the current paradigm to describe particle interactions at a fundamental level. While not directly observable they determine the probability of the outcome of a scattering experiment and are therefore at the interface of theoretical and experimental physics. Being able to calculate scattering amplitudes accurately leads to better predictions which can be contrasted with experimental data to test and improve our understanding of the world of elementary particles.

Amplitudes are typically difficult to calculate. So difficult that, for realistic processes, the mathematics needed to compute them exactly is unknown. Instead, one usually approximates them as a series of contributions that decrease in size and importance but increase in complexity. Put simply, the more terms of the series we are able to compute the more accurate the predictions for the amplitude are. This idea is known as perturbation theory. Due to the increased complexity usually only a few terms of the series can be calculated, limiting the the accuracy at which we can predict the outcome of a scattering experiment.

It is sometimes useful to consider special limits of particle interactions, like collisions of two particles with minimal deflection also known as *forward scattering*. For experimentalists this limit is of interest because a fair share of events that occur at high-energy colliders (like the LHC) fall into this category. On the other hand, it enables theoreticians to make very precise predictions as the associated amplitudes simplify in special limits. More recently, special-limit calculations have been used as boundary data that — together with other theoretical constraints — determine the physics also away from the limit.

In this thesis we demonstrate that it is possible to calculate arbitrarily many terms of the series that describes the forward scattering of two particles. At very large energies the interaction between the two particles is mediated by the exchange of two unobservable "virtual" particles called reggeons. The key idea behind our calculation is to split the space of kinematic configurations, i.e. the distribution of the available energy onto the two reggeons, into two momentum regions. Mathematically, the two regions have very different properties which we exploit individually to compute the amplitude in a disjoint fashion.

Like many scattering amplitudes, the one we study in this work exhibits so-called long-distance singularities. These divergent terms cancel upon computing probabilities and reflect the arbitrariness of defining individual partons as final states in the mathematical framework, quantum field theory (QFT), and underlying model, quantum chromodynamics (QCD). As such they offer unique insights into the inner workings and characteristics of both QFT and QCD and allow for very general conclusions. For example, it is known that the long-distance behaviour of two-particle scattering amplitudes is universal and governed by a single quantity, called the soft anomalous dimension. Since our approach enables us to compute *all* long-distance singularities we will be able to extract the exact form of the soft anomalous dimension at very high energies. As explained above, this type of exact result is very rare in realistic theories like QCD.

The regular (i.e. non-divergent) terms on the other hand we find to have an intricate structure made of transcendental numbers beyond the well-known values of the Riemann zeta function at integer arguments. The calculations outlined in this work enable us to study this structure for the first time since only the first two regular terms had previously been known. The aforementioned momentum regions naturally split the regular terms into two sets, one of which can again be written as an exact solution while the other one remains, for the most part, a perturbative series. We hope that this analysis carried out at the end of the thesis will inspire future research in this area.

Declaration

I declare that the thesis has been composed by myself and that the work has not be submitted for any other degree or professional qualification. I confirm that the work submitted is my own, except where work which has formed part of jointly-authored publications has been included. My contribution and those of the other authors to this work have been explicitly indicated below. I confirm that appropriate credit has been given within this thesis where reference has been made to the work of others.

The calculations and results presented in chapter 3 and section 5.1 are largely based on the work published in ref. [1] as "Infrared singularities of QCD scattering amplitudes in the Regge limit to all orders" by myself, my supervisor Einan Gardi and my collaborators Simon Caron-Huot and Leonardo Vernazza. This study was conceived by all of the authors. I carried out the majority of the calculations and contributed significantly to all parts of the above reference.

The remaining parts, in particular chapter 4, are based on unpublished work with the same collaborators.

Acknowledgements

I would like to express my deep gratitude to my supervisor and collaborator Einan Gardi. It is beautiful and inspiring how he seems to strike a perfect balance between being a teacher and a researcher and I thank him for countless helpful discussions. Very inspiring has also been the collaboration with Leonardo Vernazza and Simon Caron-Huot. Together with Einan they are the people whose questions and ideas have shaped me most as a physicist over the last four-odd years.

Moreover, I want to extend my thanks to the whole "particle physics theory" group here at the Higgs Centre in Edinburgh, first and foremost to Jenni Smillie and Arjun Berera for being such pleasant and interested interviewers, Rafael Hernández Jiménez for casual discussions covering everything from cosmology to Oaxaca, and Susi Ehret for a hundred or more witty lunch breaks.

I owe special thanks to Cyril Pietsch who held the line in Munich after I left and never let the resulting distance harm our friendship. The same goes for Ela Nagaj who welcomed me so warmly when I moved to Scotland and Leon Goertz whose door is always open when I visit my home town.

Thank you Luisa Brown for letting me see this charming city through the eyes of a local musician. Merci Anne Amoureux for your views, your words, and the smiles we share whilst sharing so much more.

Last but not least I would like to thank my parents, Kerstin and Michael, for being such loving, intelligent, curious and open-minded people. Because of you I can wander the world with my eyes wide open, not afraid of the new and the unknown.

Contents

Chapter 1

Introduction

The high-energy limit of QCD scattering has always been a subject of much theoretical interest, see e.g. [2–9]. In particular, the Balitsky-Fadin-Kuraev-Lipatov (BFKL) equation [2–4] provides a theoretical framework to resum high-energy (or rapidity) logarithms to all orders in perturbation theory. It was used extensively to investigate a range of physical phenomena including the small-x behaviour of deep-inelastic structure functions and parton densities, and jet production with large rapidity gaps. The non-linear generalisations of BFKL, known as the Balitsky-JIMWLK equation [10–15], extends the range of phenomena further, e.g. to describe gluon saturation in heavy-ion collisions.

On the theoretical front a separate line of investigation concerns the structure of partonic scattering amplitudes in the high-energy limit [16–29]. Scattering amplitudes of quarks and gluons are dominated at high energies by the t-channel exchange of effective excitations dubbed reggeised gluons or reggeons. In this context the BFKL equation and its generalisations provide again a highly-valuable tool: by solving these equations iteratively one can compute high-energy logarithms order-by-order in perturbation theory [25, 26].

The real part of a $2 \to 2$ partonic amplitude (i.e. its signature-odd part, see eq. (1.3)) is governed by an odd number of reggeised gluons. The leading high-energy logarithms simply exponentiate, dressing the t-channel gluon propagator by a power of s/t. In Regge theory (see e.g. ref. [30] and the original ref. [31]) this behaviour corresponds

to a Regge pole in the complex angular momentum plane. QCD amplitudes can thus be factorised in the high-energy limit into a t-channel reggeised gluon exchange which captures the dependence on the energy, and energy-independent impact factors that depend on the colliding partons. However, this simple picture in which a single reggeised gluon is exchanged does not extend beyond leading logarithms (LL). Multiple exchanges, which now form Regge cuts, contribute to the real part of the amplitude starting at next-to-next-to-leading logarithmic accuracy (NNLL) and to the imaginary part at NLL. This was recently demonstrated explicitly in ref. [26], where these effects were computed through three loops, by constructing an iterative solution of the relevant BFKL or Balitsky-JIMWLK equation, describing the evolution of three reggeised gluons and their mixing with a single reggeised gluon.

In this work we extend this study, focusing on the imaginary part of $2 \to 2$ partonic amplitudes, which are governed by the exchange of an even number of reggeised gluons, which also form Regge cuts. The leading logarithmic corrections to the even amplitude are determined to all orders by a wavefunction of a pair of reggeised gluons, which solves the celebrated BFKL evolution equation. This iterative solution, which will be central to the present work, can be famously described by ladder graphs, where an additional rung is generated at each order in the loop expansion.

The signature-even $2 \to 2$ scattering amplitude exhibits singularities associated with small momentum transfers, so-called infrared or soft divergencies. While not physical objects themselves infrared singularities are of great interest to theoreticians. They are a ubiquitous feature of quantum field theory (QFT) with massless excitations and, as such, a natural candidate to study universal properties of amplitudes. For example, infrared factorisation theorems guarantee that soft singularities factorise and exponentiate as governed by a renormalisation group equation. They are thus uniquely determined by the value of an anomalous dimension — the soft anomalous dimension. This statement holds for all kinematic configurations but is particularly appealing in the high-energy limit: Indeed, the gluon Regge trajectory $\alpha_g(t)$ is infrared-singular and its exponentiation along with the energy logarithms, which is a manifestation of reggeisation, is readily consistent with infrared factorisation. The correspondence between the structure of amplitudes in the high-energy limit, which is governed by rapidity evolution equations, on the one hand, and the structure of infrared singularities on the other, becomes more

complicated at subleading orders. While both separately provide means to explore the structure of amplitudes to all orders in perturbation theory, the interplay between the two provides additional insight in either direction, as demonstrated multiple times over the past few years [21–26].

Infrared singularities of massless scattering amplitudes are now fully known, for general colour, kinematics and any number of partons, through three loops, owing to an explicit computation of the soft anomalous dimension at this order [32, 33]. While through two loops infrared singularities are governed exclusively by a sum over colour dipoles formed by pairs of the hard-scattered partons [34–37], at three loops one encounters for the first time infrared singularities that are simultaneously sensitive to the colour and kinematics of three and four hard partons. Subsequently, ref. [26] specialised these results to the high-energy limit, and provided a detailed comparison between the singularity structure deduced from the soft anomalous dimension and what has been established there through three loops via computations in the high-energy limit. While full consistency was found, remarkably, it was shown that at three loops (see eq. (4.11) there) the real part of the amplitude is only sensitive to non-dipole corrections starting at $\mathrm{N^3LL}$ accuracy, while in the imaginary part of the amplitude they appear already at NNLL accuracy.

As an application of the interplay between these limits, it was recently demonstrated [38] that the functional form of the three-loop soft anomalous dimension in general kinematics can in fact be fully recovered via a bootstrap procedure using the high-energy limit of $2 \to 2$ scattering, alongside other information, as input. The bootstrap programme of the soft anomalous dimension can be extended beyond three loops, provided that information from special kinematic limits is available. The imaginary part of $2 \to 2$ amplitudes is a natural place to start; indeed, already in ref. [25], a non-dipole contribution at four loops and NLL accuracy could be predicted using BFKL theory.

The same reference [25] demonstrated, by direct computation and using an appropriate normalisation, that the finite terms of the amplitude up to four loops are given by zeta numbers of weight equal to the loop order. This *homogeneous-weight* property is believed to be a general feature and true to all loop orders. Testing this conjecture is difficult however due the complexity of the multi-loop integrals that enter the amplitude

beyond four loops. Consequently, it is also unknown which types on transcendental numbers make up higher loop orders; due to the trivial momentum dependence of the amplitude this number-theoretical approach may be the only way to uncover its all-order properties.

In the present work we continue to investigate the high-energy limit of $2 \to 2$ scattering in QCD, focusing on the imaginary (signature-even) part of the amplitude, which is governed, as mentioned above, by the exchange of a pair of reggeised gluons that satisfy the BFKL evolution equation. The leading-order equation is sufficient to determine an infinite tower of high-energy logarithms in the soft anomalous dimension[1].

Although the BFKL Hamiltonian has been diagonalised in many instances [5], to study partonic amplitudes requires us to use the dimensionally-regulated Hamiltonian which is comparatively less understood. Instead of a direct computation like shown in ref. [25] we propose a different approach to its iterative loop expansion. The key idea is to consider what we call the *soft limit* of the BFKL evolution. This limit selects configurations where one of the reggeised gluons has a small momentum w.r.t. the other. The approach is inspired by three observations: First, the two-reggeised-gluon wavefunction is finite at any loop order. Second, the singularities of the amplitude are controlled by the above soft limit. Third, the BFKL evolution is closed in the soft limit. As we will demonstrate, the full BFKL evolution can then be recovered by carefully summing contributions from the soft limit and its kinematic complement.

Focusing on the singularities first, we evolve the wavefunction in the limit of one soft reggeised gluon and find that the BFKL Hamiltonian simplifies dramatically. In fact, it will not only enable us to calculate the wavefunction to any loop order in this limit but also find an exact solution for the all-order singular amplitude (see eq. (5.18)). Later, we demonstrate how one can extract from it the soft anomalous dimension at NLL (see eq. (5.23) with (5.24)) which turns out to be an entire function of the coupling.

The finite amplitude on the other hand receives contributions from all kinematic configurations and thus cannot be calculated from the above limit. However, away from the soft limit the evolution of the wavefunction as well as computation of the amplitude can

[1]We refer to these as next-to-leading logarithms, owing to their suppression by one logarithm compared to the reggised-gluon corrections to the real part of the amplitudes.

be performed in strictly two dimensions since they involve only finite integrals, as explained above. In two dimensions, the BFKL evolution is related to a set of differential equations which are conveniently solved in terms of single-valued harmonic polylogarithms (SVHPLs). This, again, is an entirely algorithmic procedure and works to any loop order. Integrating the wavefunction over the remaining two-dimensional momentum yields finite terms that recover the full signature-even amplitude when combined with the results of the soft limit.

The structure of the thesis is as follows. In section 1.1 we recall the basic notions regarding the high-energy limit of $2 \to 2$ amplitudes and introduce vocabulary used throughout this work. Chapter 2 then explains how the BFKL evolution equation can be solved iteratively to determine the two-reggeised-gluon wavefunction and the imaginary part of the amplitude. In section 2.2 we reformulate the equation so as to explicitly display the fact that the evolution retains infrared finiteness and recover the four-loop results of ref. [25]. In chapter 3 we consider the soft approximation, show that the evolution closes in this limit, and exploit this simplification to derive all-order solutions for the wavefunction and amplitude.

Chapter 4 in turn covers BFKL evolution in strictly two dimensions. There, we again focus on the wavefunction first and describe the two-dimensional iteration in detail, see section 4.3. The transition to the amplitude is more elaborate than in the soft case and is discussed in section 4.4. Throughout the chapter we distinguish clearly between soft and hard (i.e. non-soft) finite terms so as to avoid confusion when we recover the full finite amplitude in section 4.5.

With the results of both soft and hard configurations at hand we examine their resummation properties in chapter 5. The concept of soft factorisation is introduced in section 5.1 and we demonstrate how one can extract the soft anomalous dimension in the high-energy limit from the single poles of the $2 \to 2$ scattering amplitude. We study the implications of our results, obtain a closed-form expression for the soft anomalous dimension at NLL and verify the consistency of our BFKL-based result with infrared exponentiation.

The finite amplitude shows signs of exponentiation, too. In particular, the soft wavefunction can be resummed and used to define a modified evolution for the remaining

hard terms. Furthermore, the part of the BFKL Hamiltonian that vanishes for colour-octet exchanges turns out to be associated to a fully resummable amplitude. These results are presented in section 5.2 and should provide clues to future research in this area.

Lastly, we summarise our results and offer a final conclusion and outlook in chapter 6.

1.1 Prelude: The signature-even amplitude

This is a good moment to introduce some basic concepts and notation which will be useful in the context of the BFKL equation introduced in the next chapter. To this end let us consider a $2 \to 2$ scattering amplitude $\mathcal{M}_{ij\to ij}$, where i, j can be a quark or a gluon. The momenta are assigned as indicated in figure 1.1.

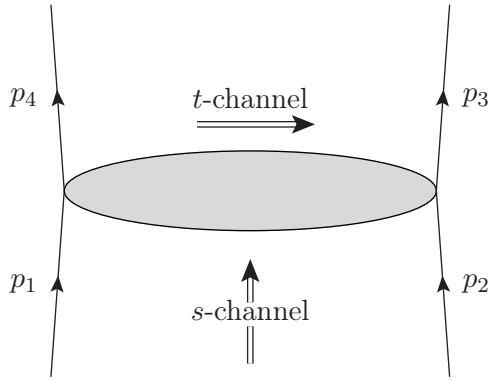

Figure 1.1: The t-channel exchange dominating the high-energy limit, $s \gg -t > 0$. The figure also defines our conventions for momenta assignment and Mandelstam invariants. We shall assume that particles 1 and 4 (2 and 3) are of the same type and have the same helicity.

The high-energy limit corresponds to a configuration of forward scattering, such that the Mandelstam variables satisfy $s \gg -t > 0$. In this limit scattering amplitudes show a factorised behaviour: schematically,

$$\mathcal{M}_{ij\to ij}(s,t) = D_i(t) \times \mathcal{M}(s,t) \times D_j(t) \tag{1.1}$$

with $D_{i,j}$ the so-called impact factors and $\mathcal{M}$ the energy-dependent t-channel interaction. Impact factors depend on the species of the particles i and j as well as the momentum exchanged between them, t. They can be calculated perturbatively and are

known for quarks, gluons and photons to the next-to-leading order [39–41]. Importantly, they contain a trivial $\mathcal{O}(\alpha_s^0)$ contribution such that, in general,

$$D_i(t) = 1 + \alpha_s D_i^{(1)}(t) + \mathcal{O}\left(\alpha_s^2\right). \tag{1.2}$$

The t-channel interaction on the other hand has a universal character and produces (upon loop expansion) the infamous "large logarithms", $\log|s/t|$, which impede the convergence of the perturbative series. For example, the exchange of a single gluon in the t channel receives contributions that feature such large logarithms starting at one loop. The leading terms, i.e. the ones maximally enhances by powers of $\log|s/t|$, follow the pattern $\alpha_s^{\ell+1}\log^\ell|s/t|$ at ℓ loops. These *leading logarithms* (LL) can be resummed and accounted for to all loop orders by the exchange of a single effective excitation dubbed reggeised gluon or reggeon. The exchange of two reggeons, which is at the heart of the present work, exhibits large logarithms from the two-loop order and the leading terms take the form $\alpha_s^{\ell+2}\log^\ell|s/t|$ at ℓ loops. Confusingly enough they are referred to as *next-to-leading logarithms* (NLL) in the literature, purely to distinguish them from the ones produced by the single-reggeon exchange.

In analysing the high-energy limit it is convenient to decompose the amplitude into its odd and even components with respect to $s \leftrightarrow u$ exchange, the so-called *signature*:

$$\mathcal{M}^{(\pm)}(s,t) = \frac{1}{2}\left[\mathcal{M}(s,t) \pm \mathcal{M}(-s-t,t)\right] \tag{1.3}$$

where $\mathcal{M}^{(+)}$, $\mathcal{M}^{(-)}$ are referred to, respectively, as the *even* and *odd* amplitudes. As shown in ref. [26], these have respectively *real* and *imaginary* coefficients, when expressed in terms of the natural signature-even combination of logarithms,

$$\frac{1}{2}\left(\log\frac{-s-i0}{-t} + \log\frac{-u-i0}{-t}\right) \simeq \log\left|\frac{s}{t}\right| - \frac{i\pi}{2} \equiv L \tag{1.4}$$

and have independent factorisation properties in the high-energy limit. Both L and $\log|s/t|$ are usually referred to as *large* or *high-energy* logarithms.

In particular, the amplitudes associated with the aforementioned single- and two-reggeon exchange have odd and even signature, respectively. This, together with eqs. (1.1) and (1.2), makes the study of their leading terms remarkably simple,

$$\mathcal{M}_{ij\to ij}(s,t)\big|^{\text{leading}}_{n\text{-reggeon}} = \mathcal{M}\big|^{\text{leading}}_{n\text{-reggeon}}(s,t) \qquad (n=1,2), \tag{1.5}$$

while subleading contributions are sensitive to the (one-loop) impact factors $D^{(1)}(t)$.[2]

$$\begin{aligned}\mathcal{M}_{ij\to ij}(s,t)\big|^{\text{next-to-leading}}_{n\text{-reggeon}} &= \alpha_s D_i^{(1)}(t)\times\mathcal{M}\big|^{\text{leading}}_{n\text{-reggeon}}(s,t)\\ &+\mathcal{M}\big|^{\text{leading}}_{n\text{-reggeon}}(s,t)\times\alpha_s D_j^{(1)}(t)+\mathcal{M}\big|^{\text{next-to-leading}}_{n\text{-reggeon}}(s,t)\qquad(n=1,2)\end{aligned}\tag{1.6}$$

The analysis carried out in this work concerns the leading contributions to the two-reggeon exchange amplitude, cf. eq. (1.5) with $n = 2$. As argued above these terms are independent of any non-trivial contribution to the impact factors which enables us to identify $\mathcal{M}_{ij\to ij}(s,t)\big|^{\text{leading}}_{2\text{-reggeon}}$ with the signature-even t-channel interaction of two reggeons at next-to-leading logarithmic accuracy, $\mathcal{M}^{(+)}_{ij\to ij,\,\text{NLL}}$.

For completeness and to supplement comments in the main text we briefly introduce the concept of Regge poles and Regge cuts. Starting point is the partial wave expansion of scattering amplitudes. In the case of $2\to 2$ scattering it is well known that the associated amplitude may be written as a series in Legendre polynomials $P_l(\cos\theta)$ whose coefficients are the so-called partial wave amplitudes:

$$\mathcal{M}_{ij\to ij}(s,t)=16\pi\sum_{l=0}^{\infty}(2l+1)a_l(s)P_l(\cos\theta)\tag{1.7}$$

where θ is the scattering angle in the centre-of-mass frame: $\cos\theta = 1+2t/s$. The partial wave amplitudes $a_l(s)$ are functions of the real centre-of-mass energy s and the quantised angular momentum l. One of Regge's key contributions [31] was to promote them to general functions of the complex variables s and l. Applied to high-energy t-channel scattering it was understood that the exchange of a single reggeon is described by partial wave amplitudes with a single pole at $\alpha(t)$ in the complex l plane,[3]

$$a_l(t)\simeq\frac{1}{l-\alpha(t)}.\tag{1.8}$$

This leads to a power behaviour of the associated high-energy amplitude,

$$\mathcal{M}_{ij\to ij}(s,t)\sim f(t)s^{\alpha(t)}\tag{1.9}$$

with some function $f(t)$, and is referred to as a *Regge pole*.

Regge poles are, however, only the simplest example of the corrections brought about by the asymptotic kinematics of the high-energy limit. In general one expects the partial

[2] Recall that impact factors are independent of s and thus signature-even by definition.

[3] One uses crossing symmetry to relate the s-channel partial wave amplitudes $a_l(s)$ to $a_l(t)$.

wave amplitudes to exhibit cuts, i.e.

$$a_l(t) \simeq \frac{1}{(l-\alpha(t))^{\beta(t)}} \tag{1.10}$$

with some function $\beta(t)$, and consequently a more complicated energy dependence of the scattering amplitude. In particular, this is true for the two-reggeon exchange, as mentioned in the introduction. While the concepts of Regge poles and cuts will take a back seat in the perturbative approach taken in the following they are integral to many other works on Regge theory and the high-energy limit.

Chapter 2

The BFKL equation

The well-known BFKL evolution equation predicts the rapidity dependence of two-parton amplitudes in the high-energy limit [3, 4]. It captures the leading contributions enhanced by (large) logarithms of colour-singlet exchanges in the t channel to all loop orders in a similar way that gluon reggeisation does for the colour-octet exchange. In QCD these singlet and octet colour flows are associated with the exchange of one and two reggeised gluons (or reggeons), respectively. The colour-singlet exchange is famously known as the pomeron, named after Isaak Pomeranchuk. By now, the BFKL evolution is textbook material and excellent reviews are available, e.g. ref. [42].

More than two decades after the discovery of the BFKL equation it was realised that it and gluon reggeisation are, in fact, part of a larger framework, which would become known as the Balitsky-JIMWLK equation [10–15]. The Balitsky-JIMWLK equation is built on the language of parallel light-like Wilson lines at different transverse positions to describe the two colliding partons, often called projectiles.

In his 2013 paper [25] Caron-Huot uncovered the connection of the Balitsky-JIMWLK equation and the exchange of reggeons in the t channel by interpreting the logarithm of the projectile Wilson lines as the source of the t-channel reggeons. He thereby showed that the Balitsky-JIMWLK framework is capable of describing the exchange of *any* number of reggeons and at the same time demonstrated how to isolate the evolution of a fixed number of t-channel reggeons. As expected, solving the single-reggeon exchange simply describes the phenomenon of gluon reggeisation and yields the signature-odd

amplitude at LL. Likewise, the two-reggeon exchange is governed by the (even-signature) BFKL equation and captures the NLL contributions.

To extend this discussion we will show how to derive the formulae of ref. [25] directly from the original BFKL equation in the next section. We will see that the signature-even amplitude can be viewed as the result of a two-step procedure. The first step we call the evolution of the wavefunction and it governs the leading logarithm-enhanced loop corrections of the two-reggeon state. It corresponds to the recursive definition of the off-shell amplitude in the language of the original refs. [2–4], can be solved iteratively and is generated by a linear operator whose explicit form we introduce in section 2.1. For fixed-order calculations the operator is applied a finite number of times on the

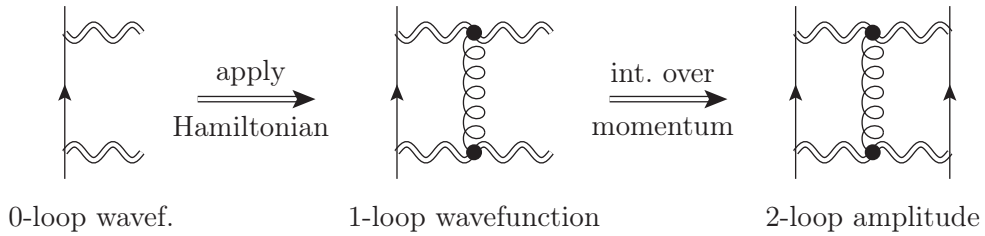

Figure 2.1: Sketch of the relation between ladder graphs and the BFKL evolution using the vocabulary of the main text. The zero-loop wavefunction (left) describes the initial two-reggeon state after emission from a parton/Wilson line. Applying the Hamiltonian once yields the one-loop wavefunction (middle) which contains all NLL one-loop corrections and is represented by a ladder with one rung. Integration of the one-loop wavefunction over the unconstrained momentum generates the two-loop amplitude at NLL and "closes the ladder" by connecting it to the second parton/Wilson line (right).

two-reggeon state yielding the leading perturbative corrections to the wavefunction at the corresponding loop order. The second step then consists of integrating the resulting ℓ-loop wavefunction over the unconstrained momentum producing the $(\ell+1)$-loop corrections to the signature-even amplitude at NLL. Both steps can be illustrated by means of so-called ladder graphs where the action of the Hamiltonian adds a rung and the integration of the wavefunction "closes the ladder", cf. figure 2.1. Note that we will provide a more detailed depiction in the next section, cf. figure 2.2, once the required quantities have been defined.

In the next section we give mathematical meaning to the objects introduced above. This will require us to take an inverse approach, i.e. start with a precise definition of the amplitude and work our way towards the two-reggeon wavefunction. We stress however that the aforementioned two-step approach, sketched in figure 2.1, is a common thread in nearly everything that follows.

2.1 Dimensionally regularised BFKL equation

In this section we introduce the concepts needed to generate the loop expansion of the signature-even $2 \to 2$ scattering amplitude at NLL which we denote $\mathcal{M}^{(+)}_{\text{NLL}}$. An important first observation is that its leading-order contribution, i.e. the exchange of a pair of gluons between the scattering partons,

$$\mathcal{M}^{(+,\text{LO})}_{ij\to ij,\,\text{NLL}} = i\pi\alpha_s^2 \frac{8s}{t} \int \frac{\mathrm{d}^2k}{(2\pi)^2} \frac{p^2}{k^2(p-k)^2} \times (\delta_{ce}\delta_{df} + \delta_{cf}\delta_{de})(T_i^c T_i^d)_{a_1a_4}(T_j^e T_j^f)_{a_2a_3}\delta_{\lambda_1\lambda_4}\delta_{\lambda_2\lambda_3} \quad (2.1)$$

may be written in terms of the tree-level single-gluon exchange

$$\mathcal{M}^{(\text{tree})}_{ij\to ij} = 4\pi\alpha_s \frac{2s}{t}(T_i^c)_{a_1a_4}(T_j^c)_{a_2a_3}\delta_{\lambda_1\lambda_4}\delta_{\lambda_2\lambda_3} \quad (2.2)$$

where λ_i for $i = 1$ through 4 are helicity indices and T the generators of the $SU(3)$ colour group. To expose this relation we first need to regularise the divergent integral in eq. (2.1) which we choose to do by introducing a dimensional regulator $-1 \ll \epsilon < 0$. A convenient normalisation of the integral measure in $2 - 2\epsilon$ dimensions is

$$[\mathrm{D}k] \equiv \frac{\pi}{B_0(\epsilon)} \left(\frac{\mu^2}{4\pi e^{-\gamma_\text{E}}}\right)^\epsilon \frac{\mathrm{d}^{2-2\epsilon}k}{(2\pi)^{2-2\epsilon}} \quad (2.3)$$

where we set the renormalisation scale μ^2 equal to $p^2 = -t$, the only physical scale of the high-energy scattering amplitude. In the above equation $B_0(\epsilon)$ is a ubiquitous loop factor and the first of a class of bubble integrals, cf. eq. (3.8), to become important in section 3.1. For now, it suffices to know that

$$B_0(\epsilon) = e^{\epsilon\gamma_\text{E}} \frac{\Gamma^2(1-\epsilon)\Gamma(1+\epsilon)}{\Gamma(1-2\epsilon)} = 1 - \frac{\zeta_2}{2}\epsilon^2 - \frac{7\zeta_3}{3}\epsilon^3 + \ldots \quad (2.4)$$

where ζ_n are "ordinary" zeta numbers, i.e. the values of the Riemann zeta function at integer argument n, and γ_E is the Euler-Mascheroni constant. With eq. (2.3) the

momentum integral in eq. (2.1) can be evaluated and simply gives

$$\int [\mathrm{D}k] \frac{p^2}{k^2(p-k)^2} = -\frac{1}{2\epsilon}. \tag{2.5}$$

Secondly, we note that the colour factors in eq. (2.1) can be simplified

$$(\delta_{ce}\delta_{df} + \delta_{cf}\delta_{de})(T_i^c T_i^d)_{a_1 a_4}(T_j^e T_j^f)_{a_2 a_3} = \mathbf{T}^2_{s-u}(T_i^c)_{a_1 a_4}(T_j^c)_{a_2 a_3}. \tag{2.6}$$

where the colour operator on the r.h.s. is defined in terms of the usual basis of quadratic Casimirs corresponding to the colour flow through the three channels [24, 43]:

$$\mathbf{T}^2_{s-u} \equiv \frac{\mathbf{T}_s^2 - \mathbf{T}_u^2}{2} \qquad \text{with} \qquad \begin{cases} \mathbf{T}_s = \mathbf{T}_1 + \mathbf{T}_2 = -\mathbf{T}_3 - \mathbf{T}_4 \\ \mathbf{T}_u = \mathbf{T}_1 + \mathbf{T}_3 = -\mathbf{T}_2 - \mathbf{T}_4 \\ \mathbf{T}_t = \mathbf{T}_1 + \mathbf{T}_4 = -\mathbf{T}_2 - \mathbf{T}_3 \end{cases} \tag{2.7}$$

$\mathbf{T}_i$ is the colour charge operator [44] associated with parton i. When acting on an amplitude it produces the quadratic Casimir of the representation corresponding to the parton. Consequently, $\mathbf{T}_s^2$, $\mathbf{T}_u^2$ and $\mathbf{T}_t^2$ have eigenvalues equal to the quadratic Casimirs of the colour flow in the s, u and t channel, respectively.

The leading-order contribution to the signature-even amplitude (2.1) then takes the compact form

$$\mathcal{M}^{(+,\mathrm{LO})}_{ij\to ij,\,\mathrm{NLL}} = i\pi \frac{\alpha_s}{\pi} \frac{B_0(\epsilon)}{2\epsilon} \mathbf{T}^2_{s-u} \mathcal{M}^{(\mathrm{tree})}_{ij\to ij}. \tag{2.8}$$

In the following we will suppress the species indices i, j unless explicitly needed and write $B_0 \equiv B_0(\epsilon)$ for brevity.

Higher-order corrections to the amplitude are governed by the famous BFKL equation [2–4]. For massless-particle scattering it reads

$$\begin{aligned} &\left[\omega - C_A \alpha_g(k^2) + C_A \alpha_g((p-k)^2)\right] F_\omega(p,k) \\ &\qquad = \frac{\omega}{C_T p^2} - \alpha_s C_A C_T \int \frac{\mathrm{d}^2 k'}{(2\pi)^2} f(p,k,k') F_\omega(p,k'), \end{aligned} \tag{2.9}$$

cf. for example eq. (17) of ref. [3]. C_A is the quadratic Casimir in the adjoint representation, C_T a colour factor to be discussed below and $F_\omega(p,k)$ the (Mellin transform of) the off-shell amplitude. $F_\omega(p,k)$ is related to what we call the two-reggeon *wavefunction* $\Omega_x(p,k)$ via

$$\Omega_x(p,k) = \int_{0-i\infty}^{0+i\infty} \mathrm{d}\omega e^{x\omega} F_\omega(p,k) \tag{2.10}$$

where in the original references $x = \ln|s/t|$. The first terms on the r.h.s. of eq. (2.9) vanishes for signature-even exchanges and the integration kernel $f(p,k,k')$ is given by

$$f(p,k,k') \equiv \frac{k^2}{(k')^2(k-k')^2} + \frac{(p-k)^2}{(p-k')^2(k-k')^2} - \frac{p^2}{(k')^2(p-k')^2}. \tag{2.11}$$

Furthermore, $\alpha_g(t)$ is the so-called *gluon Regge trajectory*. It can be expanded in the perturbative series

$$\alpha_g(q^2) = \sum_{n=1}^{\infty} \left(\frac{\alpha_s}{\pi}\right)^n \alpha_g^{(n)}(q^2). \tag{2.12}$$

Given that we work to NLL accuracy, we will only need to consider the gluon Regge trajectory to first order in α_s where, in $4-2\epsilon$ dimensions and with $\mu^2 = p^2$,

$$\alpha_g^{(1)}(q^2) = \frac{B_0}{2\epsilon}\left(\frac{p^2}{q^2}\right)^{\epsilon}. \tag{2.13}$$

The appendix of ref. [2] provides the colour factor C_T for $SU(N_C)$ gauge groups. For $SU(3)$ we find it can be written $C_T = \mathbf{T}_t^2/C_A - 2$, assuming it acts on the leading-order amplitude (2.8). This is in agreement with the expressions derived from the linearised Balitsky-JIMWLK equation [25].

For strictly signature-even t-channel exchanges the BFKL equation (2.9) can then be rearranged to read

$$\begin{aligned}\omega F_\omega(p,k) = \frac{\alpha_s B_0}{\pi}(2C_A - \mathbf{T}_t^2)\int [\mathrm{D}k'] f(p,k,k') F_\omega(p,k') \\ + \frac{\alpha_s B_0}{\pi}\left[\frac{C_A}{2\epsilon}\left(\frac{p^2}{k^2}\right)^{\epsilon} + \frac{C_A}{2\epsilon}\left(\frac{p^2}{(p-k)^2}\right)^{\epsilon}\right] F_\omega(p,k).\end{aligned} \tag{2.14}$$

It suggests to define $x \equiv \alpha_s B_0 L/\pi$ as the Mellin conjugate of ω which effectively removes the two factors of $\alpha_s B_0/\pi$ on the r.h.s. Next we apply the inverse Mellin transform in eq. (2.10) to arrive at

$$\begin{aligned}\frac{\mathrm{d}}{\mathrm{d}x}\Omega_x(p,k) = (2C_A - \mathbf{T}_t^2)\int [\mathrm{D}k] f(p,k,k')\Omega_x(p,k') \\ + \frac{1}{2\epsilon}\left[C_A\left(\frac{p^2}{k^2}\right)^{\epsilon} + C_A\left(\frac{p^2}{(p-k)^2}\right)^{\epsilon}\right]\Omega_x(p,k).\end{aligned} \tag{2.15}$$

where it is useful to define an operator H according to the action of the r.h.s., namely

$$\frac{\mathrm{d}}{\mathrm{d}x}\Omega_x(p,k) = H\Omega_x(p,k). \tag{2.16}$$

Due to the similarity with the Schrödinger equation we shall call H the BFKL *Hamiltonian*. It furthermore motivates the use of the word *wavefunction* for Ω_x (2.10).

In order to obtain the on-shell scattering amplitude one sets $k^2 = (p-k)^2 = 0$ and reapplies H (bar the factor $2C_A - \mathbf{T}_t^2$ as the colour of the on-shell particles is fixed by the physical process) on the wavefunction, making sure that the colour operators inside Ω_x act on the leading-order amplitude

$$\mathcal{M}^{(+)}_{\text{NLL}} = -i\pi \int [\mathrm{D}k'] \frac{p^2}{(k')^2(p-k')^2} \Omega_x(p,k') \mathbf{T}^2_{s-u} \mathcal{M}^{(\text{tree})}. \tag{2.17}$$

Note, that in the high-energy limit the t-channel evolution depends solely on the transverse momenta of the exchanges particles. This gives rise to the two-dimensional integrals with Euclidean signature the BFKL evolution is known for.

Since the effects we discuss in the following originate from the exchange of two reggeons it proves useful[1] to define a *reduced amplitude* by removing the contribution of the one-reggeon exchange:

$$\hat{\mathcal{M}}_{ij\to ij} \equiv e^{-\alpha_g(t) L \mathbf{T}_t^2} \mathcal{M}_{ij\to ij} \tag{2.18}$$

which at NLL and for signature-even scattering becomes

$$\hat{\mathcal{M}}^{(+)}_{\text{NLL}} \equiv e^{-\frac{\alpha_s}{\pi}\alpha_g^{(1)}(t) L \mathbf{T}_t^2} \mathcal{M}^{(+)}_{\text{NLL}}. \tag{2.19}$$

The effect of the exponential can be accounted for by subtracting $\mathbf{T}_t^2/(2\epsilon)$ from H: $\hat{H} \equiv H - \frac{\mathbf{T}_t^2}{2\epsilon}$ such that

$$\hat{H}\Omega_x(p,k) = (2C_A - \mathbf{T}_t^2) \int [\mathrm{D}k'] f(p,k,k') \Omega^{(\ell-2)}(p,k') + \tilde{J}(p,k) \Omega^{(\ell-2)}(p,k) \tag{2.20}$$

where $f(p,k,k')$ was defined in eq. (2.11) and the function $\tilde{J}(p,k)$ is given by

$$\tilde{J}(p,k) = \frac{1}{2\epsilon}\left[C_A \left(\frac{p^2}{k^2}\right)^{\epsilon} + C_A \left(\frac{p^2}{(p-k)^2}\right)^{\epsilon} - \mathbf{T}_t^2 \right]. \tag{2.21}$$

$\tilde{J}(p,k)$ accounts for the Regge trajectories of the individual reggeised gluons, minus the overall Regge trajectory with colour charge $\mathbf{T}_t^2$ which was subtracted in the exponent of the reduced amplitude (2.18).

As we would like to use the BFKL evolution to generate the perturbative series of the (reduced) amplitude at NLL the all-order expression for $\hat{\mathcal{M}}^{(+)}_{\text{NLL}}$ and Ω_x are somewhat

[1] The full advantage of considering the reduced amplitude will become clear in what follows. First, BFKL evolution of the reduced amplitude involves an extra term proportional to $\mathbf{T}_t^2$ in (2.21). This term renders the wavefunction finite. Second, upon performing infrared factorisation of the reduced amplitude one is able to identify the NLL terms that originate in the soft anomalous dimension — see eq. (5.11).

inconvenient to work with. Instead, consider the loop expansion of the wavefunction in the variable $x = \alpha_s B_0 L/\pi$

$$\Omega_x(p,k) = \frac{\alpha_s B_0}{\pi} \sum_{\ell=0}^{\infty} \frac{x^\ell}{\ell!} \Omega^{(\ell)}(p,k). \tag{2.22}$$

With eq. (2.16) it is easy to verify that $\hat{H}$ can be used to generate the ℓ-loop coefficients $\Omega^{(\ell)}(p,k)$ iteratively,

$$\Omega^{(\ell)}(p,k) = \hat{H}\Omega^{(\ell-1)}(p,k). \tag{2.23}$$

Furthermore, writing

$$\hat{\mathcal{M}}^{(+)}_{\text{NLL}}\left(\frac{s}{-t}\right) = \sum_{\ell=1}^{\infty} \left(\frac{\alpha_s}{\pi}\right)^\ell L^{\ell-1} \hat{\mathcal{M}}^{(+,\ell)}_{\text{NLL}} \tag{2.24}$$

lets us isolate the ℓ-loop contributions to the reduced amplitude which can be calculated from the $(\ell-1)$-loop wavefunction by integration, as was sketched in section 1.1. According to eq. (2.17), and with $\mathcal{M}^{(+)}_{\text{NLL}} \to \hat{\mathcal{M}}^{(+)}_{\text{NLL}}$, one has

$$\hat{\mathcal{M}}^{(+,\ell)}_{\text{NLL}} = -i\pi \frac{B_0^\ell}{(\ell-1)!} \int [\mathrm{D}k] \frac{p^2}{k^2(p-k)^2} \Omega^{(\ell-1)}(p,k) \mathbf{T}^2_{s-u} \mathcal{M}^{(\text{tree})}, \tag{2.25}$$

We emphasise that while these corrections are the leading-logarithmic contributions to the even amplitude, we denote them by NLL to recall that the power of the logarithm L is one less than the loop order. This can be contrasted with the single-reggeon contribution to the odd amplitude $\mathcal{M}^{(-)}_{\text{LL}} \sim e^{\mathbf{T}_t^2 \alpha_g(t) L} \mathcal{M}^{(\text{tree})}$. Note that our initial discussion of the leading order contribution, cf. eq. (2.8), fixes the zero-loop wavefunction,

$$\Omega^{(0)}(p,k) = 1, \tag{2.26}$$

because $\mathcal{M}^{(+,1)}_{\text{NLL}} = \hat{\mathcal{M}}^{(+,1)}_{\text{NLL}}$.

As discussed in refs. [25,26], the BFKL equation and its higher-order generalisations can be understood by considering the expectation value of Wilson lines associated to the colour flow of the external partons [10], which are described as "target" and "projectile" in the (high-energy) forward scattering configuration of figure 1.1. The wavefunction then represents the transverse momenta in each of two Wilson lines and the BFKL equation is obtained as an appropriate limit of the more general Balitsky-JIMWLK evolution equation [10]. For the detailed derivations we refer the interested reader to the cited references.

A graphical representation of eq. (2.25) is provided in figure 2.2. As a result of BFKL evolution, the amplitude at NLL accuracy can be represented as a ladder. At order ℓ it is obtained by closing the ladder and integrating the wavefunction of order $(\ell-1)$ over the resulting loop momentum, according to eq. (2.25). The wavefunction $\Omega^{(\ell-1)}(p,k)$ in turn is obtained by applying once the leading-order BFKL evolution kernel to the wavefunction of order $(\ell-2)$. Graphically, this operation corresponds to adding one rung to the ladder.

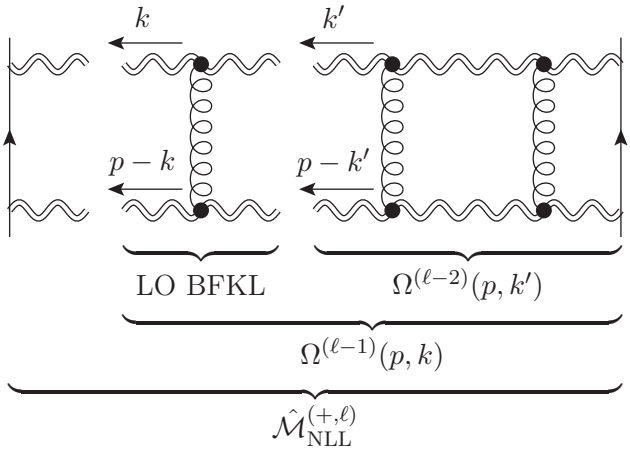

Figure 2.2: Graphical representation of the amplitude at NLL accuracy, as obtained through BFKL evolution. The addition of one rung corresponds to applying once the leading-order BFKL evolution on the wavefunction of order $(\ell-2)$. This gives the wavefunction at order $(\ell-1)$, according to eq. (2.27). Closing the ladder and integrating over the resulting loop momentum gives the reduced amplitude, according to eq. (2.25).

2.2 Evolution of the wavefunction

Eq. (2.25) shows that the ℓ-th order amplitude is obtained in terms of iterated integrals that arise upon evaluating the wavefunction $\Omega^{(\ell-1)}(p,k)$ to order $(\ell-1)$. It is straightforward to compute the first few orders which gives us an opportunity to revisit the findings of ref. [25]. We will be able to explain why a new colour structure emerges for the first time at four loops and explore the general structure of the relevant iterated integrals.

A useful fact is that the evolution admits one well-known solution in the case where the exchanged state is colour-adjoint and $\Omega_x(p,k)$ is constant (i.e. independent of k) [3, 4].

The adjoint exchange gives a signature-even state with the same leading-order trajectory as the reggeised gluon. This enables one to rewrite the Hamiltonian (2.20) as a part which vanishes when $\Omega_x(p,k)$ is constant, plus a part proportional to $(C_A - \mathbf{T}_t^2)$:

$$\Omega^{(\ell-1)}(p,k) = \hat{H}\Omega^{(\ell-2)}(p,k) \qquad \hat{H} = (2C_A - \mathbf{T}_t^2)\hat{H}_{\rm i} + (C_A - \mathbf{T}_t^2)\hat{H}_{\rm m} \tag{2.27}$$

where, explicitly,

$$\hat{H}_{\rm i}\Psi(p,k) = \int [{\rm D}k'] f(p,k,k') \left[\Psi(p,k') - \Psi(p,k)\right] \tag{2.28}$$

$$\hat{H}_{\rm m}\Psi(p,k) = J(p,k)\Psi(p,k) \tag{2.29}$$

and the function $J(p,k)$ is defined by

$$J(p,k) = \frac{1}{2\epsilon} + \int [{\rm D}k'] f(p,k,k') \tag{2.30}$$

$$= \frac{1}{2\epsilon}\left[2 - \left(\frac{p^2}{k^2}\right)^{\epsilon} - \left(\frac{p^2}{(p-k)^2}\right)^{\epsilon}\right] \tag{2.31}$$

The first interesting feature to note is that the $\hat{H}_{\rm i}$ operator in eq. (2.27) vanishes when acting on $\Omega^{(0)}(p,k) = 1$. Therefore the one-loop wavefunction involves a single colour structure:

$$\Omega^{(1)}(p,k) = (C_A - \mathbf{T}_t^2)J(p,k) \tag{2.32}$$

The second colour structure appears for the first time at the second order:

$$\Omega^{(2)}(p,k) = (C_A - \mathbf{T}_t^2)^2 J^2(p,k) + (2C_A - \mathbf{T}_t^2)(C_A - \mathbf{T}_t^2)\int [{\rm D}k'] f(p,k,k') \left[J(p,k') - J(p,k)\right] \tag{2.33}$$

Inserting the explicit form of $J(p,k)$ (2.31) into eq. (2.33) one finds that it involves bubble integrals of the form

$$\int [{\rm D}k][k^2]^{-a}[(q-k)^2]^{-b} = \frac{e^{\epsilon\gamma_{\rm E}}}{4B_0} B_{a,b}(\epsilon)\left(\frac{p^2}{q^2}\right)^{\epsilon}(q^2)^{1-a-b} \tag{2.34}$$

with

$$B_{a,b}(\epsilon) = \frac{\Gamma(1-\epsilon-a)\Gamma(1-\epsilon-b)\Gamma(-1+\epsilon+a+b)}{\Gamma(a)\Gamma(b)\Gamma(2-2\epsilon-a-b)} \tag{2.35}$$

as well as three-mass triangle integrals with massless propagators, such as

$$\int [{\rm D}k'] \frac{(p-k)^2}{(p-k')^2(k-k')^2}\left(\frac{p^2}{(k')^2}\right)^{\epsilon} \tag{2.36}$$

which is represented in figure 2.3.

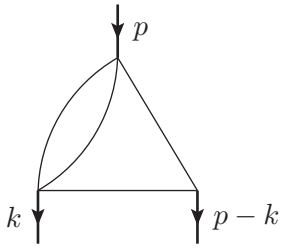

Figure 2.3: Three-mass triangle integral with massless propagators as it appears in the calculation of the wavefunction at two loops. This type of integral contributes to the amplitude only starting at four loops, due to symmetry constraints, as discussed in the main text. The bubble integral (2.34) on one of the edges of the triangle clarifies the origin of the propagator which is raised to power ϵ in eq. (2.36).

The wavefunction at higher orders can be expressed formally by introducing a class of functions

$$\Omega_{\mathrm{i},a_1,\ldots,a_n}(p,k) \equiv \int [\mathrm{D}k'] f(p,k,k') \left[\Omega_{a_1,\ldots,a_n}(p,k') - \Omega_{a_1,\ldots,a_n}(p,k)\right] \tag{2.37}$$

$$\Omega_{\mathrm{m},a_1,\ldots,a_n}(p,k) \equiv J(p,k)\Omega_{a_1,\ldots,a_n}(p,k) \tag{2.38}$$

where $\Omega_{\varnothing}(p,k) \equiv 1$. Each of the indices a_j can take the value "i" or "m", which stand for integration and multiplication, respectively, according to the action of the two Hamiltonian operators in eq. (2.28). In this notation, the one- and two-loop wavefunctions read, respectively,

$$\Omega^{(1)}(p,k) = (C_A - \mathbf{T}_t^2)\Omega_{\mathrm{m}} \tag{2.39}$$

$$\Omega^{(2)}(p,k) = (C_A - \mathbf{T}_t^2)^2\Omega_{\mathrm{m,m}} + (2C_A - \mathbf{T}_t^2)(C_A - \mathbf{T}_t^2)\Omega_{\mathrm{i,m}} \tag{2.40}$$

and this is easily extended to higher loops, for example,

$$\begin{aligned}\Omega^{(3)}(p,k) = (C_A - \mathbf{T}_t^2)^3\Omega_{\mathrm{m,m,m}} + (2C_A - \mathbf{T}_t^2)(C_A - \mathbf{T}_t^2)^2 \left(\Omega_{\mathrm{i,m,m}} + \Omega_{\mathrm{m,i,m}}\right) \\ + (2C_A - \mathbf{T}_t^2)^2(C_A - \mathbf{T}_t^2)\Omega_{\mathrm{i,i,m}}\end{aligned} \tag{2.41}$$

and

$$\begin{aligned}\Omega^{(4)}(p,k) = (C_A - \mathbf{T}_t^2)^4\Omega_{\mathrm{m,m,m,m}} \\ + (2C_A - \mathbf{T}_t^2)(C_A - \mathbf{T}_t^2)^3 \left(\Omega_{\mathrm{m,m,i,m}} + \Omega_{\mathrm{m,i,m,m}} + \Omega_{\mathrm{i,m,m,m}}\right) \\ + (2C_A - \mathbf{T}_t^2)^2(C_A - \mathbf{T}_t^2)^2 \left(\Omega_{\mathrm{m,i,i,m}} + \Omega_{\mathrm{i,m,i,m}} + \Omega_{\mathrm{i,i,m,m}}\right) \\ + (2C_A - \mathbf{T}_t^2)^3(C_A - \mathbf{T}_t^2)\Omega_{\mathrm{i,i,i,m}}.\end{aligned} \tag{2.42}$$

2.3 The amplitude

The wavefunctions written thus far are sufficient to evaluate the reduced amplitude up to five loops. At one and two loops inserting $\Omega^{(0)}(p,k)=1$ and eq. (2.32), respectively, into eq. (2.25) and performing the resulting bubble integrals (2.34) one readily arrives at

$$\hat{\mathcal{M}}^{(+,1)}_{\rm NLL} = -i\pi\frac{B_0}{2\epsilon}\mathbf{T}^2_{s-u}\mathcal{M}^{(\rm tree)} \tag{2.43}$$

$$\hat{\mathcal{M}}^{(+,2)}_{\rm NLL} = i\pi\frac{(B_0)^2}{2}\left[\frac{1}{(2\epsilon)^2}+\frac{9\zeta_3}{2}\epsilon+\frac{27\zeta_4}{4}\epsilon^2+\frac{63\zeta_5}{2}\epsilon^3+\mathcal{O}(\epsilon^4)\right] \times (C_A-\mathbf{T}^2_t)\mathbf{T}^2_{s-u}\mathcal{M}^{(\rm tree)}. \tag{2.44}$$

We notice that the amplitude depends solely on the colour structure $C_A-\mathbf{T}^2_t$, a mere consequence of the fact that the wavefunctions $\Omega^{(0)}$ (2.26) and $\Omega^{(1)}$ (2.39) have only this one colour component.

Based on this one would expect the second colour structure, $2C_A-\mathbf{T}^2_t$, to contribute to the amplitude starting at three loops given that it appears in $\Omega^{(2)}$ (2.40). However, this contribution to the three-loop amplitude $\hat{\mathcal{M}}^{(+,3)}_{\rm NLL}$ cancels by symmetry:

$$\begin{aligned}\int[\mathrm{D}k]\frac{p^2}{k^2(p-k)^2}\Omega_{\rm i,m}(p,k) &= \int[\mathrm{D}k][\mathrm{D}k']\frac{p^2}{k^2(p-k)^2}f(p,k,k')\left[J(p,k')-J(p,k)\right]\\ &= \int[\mathrm{D}k][\mathrm{D}k']\left\{\frac{p^2}{(k')^2(p-k')^2}f(p,k',k)J(p,k')-(k\leftrightarrow k')\right\}=0\end{aligned} \tag{2.45}$$

where we swapped the order of integration over k and k' and used the property

$$\frac{p^2}{k^2(p-k)^2}f(p,k,k')=\frac{p^2}{(k')^2(p-k')^2}f(p,k',k). \tag{2.46}$$

Hence, eq. (2.45) vanishes by antisymmetry with respect to $k\leftrightarrow k'$. Because of this the amplitude at three loops has again a single colour component, proportional to $(C_A-\mathbf{T}^2_t)^2$:

$$\hat{\mathcal{M}}^{(+,3)}_{\rm NLL} = i\pi\frac{B_0^3}{3!}\left[\frac{1}{(2\epsilon)^3}-\frac{11\zeta_3}{4}-\frac{33\zeta_4}{8}\epsilon-\frac{357\zeta_5}{4}\epsilon^2+\mathcal{O}(\epsilon^3)\right] \times (C_A-\mathbf{T}^2_t)^2\mathbf{T}^2_{s-u}\mathcal{M}^{(\rm tree)} \tag{2.47}$$

While this symmetry ensures that there is only one colour structure at three loops, this is no longer the case at four loops. There, one obtains [25]

$$\hat{\mathcal{M}}^{(+,4)}_{\text{NLL}} = -i\pi\frac{B_0^4}{3!}\int[\mathrm{D}k]\frac{p^2}{k^2(p-k)^2}\Big\{(C_A-\mathbf{T}_t^2)^3\Omega_{\text{m,m,m}}(p,k) + (2C_A-\mathbf{T}_t^2)(C_A-\mathbf{T}_t^2)^2\Omega_{\text{m,i,m}}(p,k)\Big\}\mathbf{T}^2_{s-u}\mathcal{M}^{(\text{tree})} \quad (2.48)$$

$$= i\pi\frac{B_0^4}{4!}\Big\{(C_A-\mathbf{T}_t^2)^3\left(\frac{1}{(2\epsilon)^4}+\frac{175\zeta_5}{2}\epsilon+\mathcal{O}(\epsilon^2)\right) + C_A(C_A-\mathbf{T}_t^2)^2\left(-\frac{\zeta_3}{8\epsilon}-\frac{3}{16}\zeta_4-\frac{167\zeta_5}{8}\epsilon+\mathcal{O}(\epsilon^2)\right)\Big\}\mathbf{T}^2_{s-u}\mathcal{M}^{(\text{tree})} \quad (2.49)$$

We see that the integrated result for the amplitude at four loops involves two colour structures, and in the final expression (2.49) we rearranged them so as to single out a factor of C_A. In section 5.1 below we will see that in this form it is easy to compare the amplitude with the structure of infrared divergences. Specifically, we will see that corrections involving the colour structure $(C_A-\mathbf{T}_t^2)^{\ell-1}$ at ℓ loop order emerge directly from the simplest "dipole" formula of the soft anomalous dimension, while other colour structures, namely $C_A^j(C_A-\mathbf{T}_t^2)^{\ell-j-1}$ with $j\geq 1$, identify deviations from the dipole formula, as was first observed in ref. [25] for $\ell=4$.

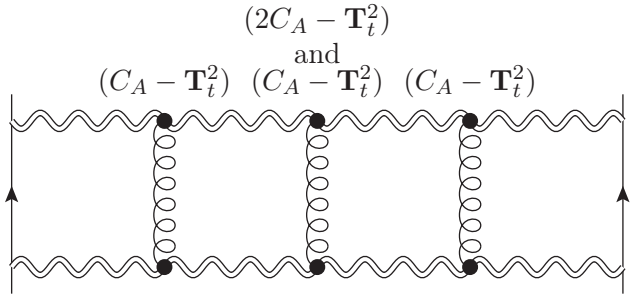

Figure 2.4: Graphical representation of the BFKL ladder at four loops. The fact that $\Omega^{(1)}(p,k)\sim C_A-\mathbf{T}_t^2$ (2.39) in conjunction with the target-projectile symmetry, cf. section 2.4, imply that the first rungs on either side can only give rise to contributions proportional to $C_A-\mathbf{T}_t^2$. As a consequence, distinct colour structures can appear for the first time at four loops.

Inspecting the diagrammatic representation of BFKL evolution in figure 2.2, one can interpret the delayed appearance of a new colour structure as a consequence of the target-projectile symmetry. Recall that for the first rung of the ladder, only the term generated by $\hat{H}_{\text{m}}$ (2.29) contributes, so the wavefunction has a single colour structure

$C_A - \mathbf{T}_t^2$. Considering more rungs, using target-projectile symmetry one can deduce that the same is true for the first rung on the opposite side of the ladder. As a consequence, the two rungs of the three-loop amplitude can each only contribute a factor of $C_A - \mathbf{T}_t^2$ despite that fact that $\Omega^{(2)}(p,k)$ (2.40) contains a term promotional to $2C_A - \mathbf{T}_t^2$. As shown in figure 2.4, distinct colour structures can only appear in the amplitude starting at four loops, where the middle rung — and only that rung — gives rise to both colour factors.

A simple and fast way to extend the study in ref. [25] to higher loops is provided by numerical integration methods. In particular, we find sector decomposition[2] as implemented in `pySecDec`/`SecDec` [46, 47] to be suited to calculate the nested integrals that enter the five-loop amplitude. Provided a high numerical accuracy it is straightforward to extract from the results the rational coefficients of the involved zeta numbers at this loop order. This procedure relies on the observed *homogeneous weight* property of the ℓ-loop amplitude: Assigning $o(\epsilon) = -1$, $o(\pi) = 1$ and $o(\zeta_n) = n$ one sees that the terms of the ℓ-loop amplitude are uniformly of weight $o = \ell$. Given the Laurent series in ϵ of an amplitude we can hence deduce the zeta numbers (or powers of π) that multiply a certain power of ϵ.

Another observation facilitates this procedure at five loops; after dividing the ℓ-loop amplitude by B_0^ℓ (2.4) there are no occurrences of $\zeta_2 = \pi^2/6$ up to four loops, see e.g. the $\mathcal{O}(\epsilon)$ terms of eq. (2.49). If we assume this absence of ζ_2 to be an actual property of the amplitude the finite terms of the five-loop amplitude can only be proportional to one transcendental number, ζ_5, whereas $\zeta_3\zeta_2$ is excluded. At this point this approach may seem rather conjectural. However, over the course of the next two chapters we develop methods that prove this assumption true and we shall briefly return to it at the end of sections 3.3 and 4.5.

To obtain the five-loop amplitude $\hat{\mathcal{M}}_{\text{NLL}}^{(+,5)}$ we integrate the four-loop wavefunction $\Omega^{(4)}(p,k)$ (2.42) according to eq. (2.25). In doing so one is faced with a plethora of multi-loop integrals. Many of them correspond to bubble graphs and can be solved analytically, cf. eq. (2.34). Others vanish by symmetry and a mechanism similar to the one in eq. (2.45). We will return to this symmetry in more detail in section 2.4. The

[2] For a review of sector decomposition methods in the context of multi-loop Feynman integrals, see e.g. ref. [45].

remaining integrals can be computed numerically using `SecDec`, as mentioned above. One of the more difficult examples is shown in figure 2.5. In the depicted case one can integrate out the two internal bubbles and is left with a three-loop integral with two of the propagators raised to non-integer powers:

$$\text{figure 2.5} \sim \int \frac{[\mathrm{D}k][\mathrm{D}k'][\mathrm{D}k'']}{(k^2)^\epsilon((k'')^2)^\epsilon(k-k')^2(k'-k'')^2(p-k)^2(p-k')^2(p-k'')^2} \tag{2.50}$$

After combining all contributions and reconstructing the zeta numbers in case of the

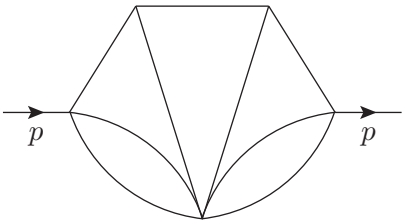

Figure 2.5: Example of a five-loop integral that enters the calculation of the five-loop amplitude $\hat{\mathcal{M}}^{(+,5)}_{\mathrm{NLL}}$. The two bubbles may be integrated out turning it into a three-loop integral with two propagators raised to non-integer powers, cf. eq. (2.50).

numerical results we find

$$\begin{aligned}\hat{\mathcal{M}}^{(+,5)}_{\mathrm{NLL}} = i\pi\frac{B_0^5}{5!}\Bigg\{&(C_A-\mathbf{T}_t^2)^4\left(\frac{1}{32\epsilon^5}-\frac{53\zeta_5}{2}\right)\\ &+C_A(C_A-\mathbf{T}_t^2)^3\left(-\frac{\zeta_3}{16\epsilon^2}-\frac{3\zeta_4}{32\epsilon}+\frac{253\zeta_5}{16}\right)\\ &-\frac{5}{2}C_A^2(C_A-\mathbf{T}_t^2)^2\zeta_5\Bigg\}\mathbf{T}^2_{s-u}\mathcal{M}^{(\mathrm{tree})}.\end{aligned} \tag{2.51}$$

2.4 A note on symmetries

We close this chapter by commenting on the symmetries of the wavefunction and amplitude. Knowledge of these will come in handy in the following chapters.

The wavefunction is symmetric under swapping the two t-channel reggeons, which can be understood from the graphical representation of the BFKL evolution in figure 2.2. Mathematically this implies

$$\Omega^{(\ell)}(p,k) = \Omega^{(\ell)}(p,p-k) \tag{2.52}$$

and can be easily verified by confirming that the functions $f(p,k,k')$ (2.11), $J(p,k)$ (2.31) and $\Omega^{(0)}(p,k)$ (2.26) obey the same symmetry.

While the two reggeons can be *defined* to originate from either the projectile *or* target Wilson line — which gives the corresponding ladder graphs a sense of direction — this is no longer true at the level of the amplitude. There the two cases become indistinguishable and we refer to this as the target-projectile symmetry. It has far-reaching consequences for the amplitude which present themselves in a particularly nice form in the notation introduced in eqs. (2.37) and (2.38).

We illustrated the first example of how this symmetry simplifies the amplitude above eq. (2.45) where we showed that the integral of $\Omega_{\mathrm{i,m}}(p,k)$ is zero. Later, in figure 2.4 we argued that the outer rungs of the four-loop ladder cannot give contributions proportional to $2C_A - \mathbf{T}_t^2$ purely based on the fact that $\hat{H}_{\mathrm{i}}\Omega_{\varnothing} = 0$. However, the idea that constraints have to apply to the first and last rung in the same way works at any loop order. It implies that, in general,

$$\int [\mathrm{D}k] \frac{p^2}{k^2(p-k)^2} \hat{H}_{\mathrm{i}} \Omega_{a_2,\ldots}(p,k) = \int [\mathrm{D}k] \frac{p^2}{k^2(p-k)^2} \Omega_{\mathrm{i},a_2,\ldots}(p,k) = 0. \tag{2.53}$$

For a rigorous proof one proceeds as in eq. (2.45) with $J(p,q)$ replaced by $\Omega_{a_2,\ldots}(p,q)$ (with $q = k$ or k') on the r.h.s.

The target-projectile symmetry does not only constrain the outermost rungs. In the notation of eqs. (2.37) and (2.38) reversal of the rungs directly translates to the reversal of the indices of the wavefunction. The symmetry thus guarantees the equality

$$\int [\mathrm{D}k] \frac{p^2}{k^2(p-k)^2} \Omega_{a_1,\ldots,a_n}(p,k) = \int [\mathrm{D}k] \frac{p^2}{k^2(p-k)^2} \Omega_{a_n,\ldots,a_1}(p,k). \tag{2.54}$$

We hope to have convinced the reader that the symmetries discussed above can reduce the number of functions to be computed significantly. Nonetheless, beyond four loops, computing the needed iterated integrals is all but easy with current methods.

Chapter 3

Singularities

While it might be possible to calculate the wavefunction and amplitude to higher loop orders by, numerically or analytically, computing the iterated integrals generated by the BFKL evolution (2.27) discussed in the last chapter we will take a different route. Instead of considering the amplitude as a whole we will examine its singular and finite terms independently. While the latter are discussed in chapter 4 it turns out that the former can be extracted from a kinematic limit of the BFKL evolution which we refer to as the *soft limit*. We strive to add these singularities to the finite terms calculated in chapter 4 as well as compare them with the predictions made by the infrared factorisation theorem in section 5.1.

With these goals in mind we highlight at this point another important property of $\Omega_x(p,k)$ which can be verified when inspecting eq. (2.27) more carefully (see below): the wavefunction $\Omega^{(\ell-1)}(p,k)$ is finite for $\epsilon \to 0$ to all orders in perturbation theory! This is a non-trivial statement, which becomes evident only after the evolution equation is brought from the form in eq. (2.20) to eq. (2.27). A practical implication is that all divergences in the amplitude must originate in the "last integration", namely going from the wavefunction to the amplitude as in eq. (2.17). Inspecting the latter equation we see that divergences arise only in the $k \to 0$ and $k \to p$ limits, the so-called *soft* limits, where one of the reggeons has a much smaller momentem than the other. (Note that ultraviolet power counting in eq. (2.28) using (2.11) excludes divergences from $k' \gg p, k$.) Due to the symmetry of the integrand, cf. section 2.4, all divergences of

the amplitude can therefore be obtained by evaluating it in one of these two limits, and multiplying the result by two.

3.1 The soft limit

Let us now examine more carefully the evolution of the wavefunction according to eqs. (2.27) and (2.28), verify that the wavefunction is indeed finite, and derive a simplified version of the evolution, valid in the small-k or *soft* approximation: $k \ll p$. The loop integral in eq. (2.28) can in principle receive contributions from two regions; $k \ll k' \sim p$ and $k \sim k' \ll p$. Inspecting the form of $f(p,k,k')$ in the two regions, it is easy to check that only the second region contributes:

$$f(p,k,k')|_{k\ll k'\sim p} \longrightarrow 0 + \frac{p^2}{(p-k')^2(k')^2} - \frac{p^2}{(k')^2(p-k')^2} = 0 \tag{3.1}$$

$$f(p,k,k')|_{k\sim k'\ll p} \longrightarrow \frac{k^2}{(k')^2(k-k')^2} + \frac{1}{(k-k')^2} - \frac{1}{(k')^2} = \frac{2k\cdot k'}{(k')^2(k-k')^2} \tag{3.2}$$

This means that the soft approximation closes under evolution! In the following, we will identify the region $k \sim k' \ll p$ as *soft* and add a subscript "s" to quantities calculated in this limit.

From $J(p,k)$ in eq. (2.31) one gets

$$J_{\rm s}(p,k) = \frac{1}{2\epsilon}\left[1 - \left(\frac{p^2}{k^2}\right)^{\epsilon}\right] \tag{3.3}$$

and the evolution in eq. (2.27) becomes

$$\Omega_{\rm s}^{(\ell-1)}(p,k) = \hat{H}_{\rm s}\Omega_{\rm s}^{(\ell-2)}(p,k) \tag{3.4}$$

$$\begin{aligned}\hat{H}_{\rm s}\Psi(p,k) = (2C_A - \mathbf{T}_t^2)\int [{\rm D}k']\frac{2k\cdot k'}{(k')^2(k-k')^2}\left[\Psi(p,k') - \Psi(p,k)\right] \\ + (C_A - \mathbf{T}_t^2)J_{\rm s}(p,k)\Psi(p,k)\end{aligned} \tag{3.5}$$

where $[{\rm D}k']$ is the previously defined integration measure (2.3). Eq. (3.5) confirms that it is consistent to truncate the Regge evolution to the soft approximation: using the power counting $\Psi(p,k) \sim 1$, we see that the k' integral is saturated by the soft region $k' \sim k$, with no sensitivity to larger scales.

Inserting the wavefunction $\Omega_{\rm s}^{(\ell-1)}(p,k)$ into eq. (2.25) we get the amplitude in the soft limit at the ℓ-th order. In this approximation the last integral becomes divergent and

needs an ultraviolet cutoff, which we fix by requiring $k^2 < p^2$, based on dimensional analysis and consistency with the soft limit (any finite cutoff would be consistent and would not affect the infrared singularities). The integration measure for the last integral therefore reads

$$\int [\mathrm{D}k]_s = \frac{(p^2)^\epsilon e^{\epsilon\gamma_\mathrm{E}}}{2\Gamma(1-\epsilon)B_0} \int_0^{p^2} \mathrm{d}k^2 (k^2)^{-\epsilon} \tag{3.6}$$

where we multiplied by a factor of two, in order to take into account the fact that there is an identical contribution from the region where the reggeised gluon with momentum $(p-k)$ is soft. Inserting this result into eq. (2.25), we get

$$\hat{\mathcal{M}}^{(+,\ell)}_{\mathrm{NLL}} = -\frac{i\pi B_0^{\ell-1}}{(\ell-1)!} \frac{e^{\epsilon\gamma_\mathrm{E}}}{\Gamma(1-\epsilon)} \int_0^{p^2} \frac{\mathrm{d}k^2}{2k^2} \left(\frac{p^2}{k^2}\right)^\epsilon \Omega_\mathrm{s}^{(\ell-1)}(p,k) \mathbf{T}^2_{s-u} \mathcal{M}^{(\mathrm{tree})} + \mathcal{O}(\epsilon^0). \tag{3.7}$$

We stress that this approximation gives correct results only as long as one of the two reggeons has a small momentum. The soft limit and the result in eq. (3.7) gives the complete and correct set of poles in ϵ since the integrand is finite and divergences arise only from the $k \to 0$ limit of integration. It also captures correctly finite terms that originate in the soft limit. However, in the full amplitude (2.25) there will be additional finite contributions from outside the soft region as indicated by the $\mathcal{O}(\epsilon^0)$ terms in the above equation.

The most significant advantage of the soft approximation is that the evolution equation greatly simplifies and that it allows us to obtain closed-form expressions for the wavefunction $\Omega_\mathrm{s}^{(\ell-1)}(p,k)$ and the amplitude $\hat{\mathcal{M}}^{(+,\ell)}_{\mathrm{NLL}}\big|_\mathrm{s}$, as we are going to detail in the following.

3.2 Evolution of the soft wavefunction

In analogy to the exercise done in section 2.2, we start by calculating explicitly the wavefunction at the first few orders in perturbation theory, this time in the soft approximation. The initial condition is still given by eq. (2.26), and the evolution obeys eq. (3.5). Note how the evolution has a much simpler structure compared to the original one (2.28) because the soft approximation turns a two-scale problem into a one-scale problem. It is easy to check that the wavefunction reduces to a polynomial in $\xi = \left(p^2/k^2\right)^\epsilon$ which implies that the integrals involved in eq. (3.5) are simple bubble

integrals of the type

$$\int [\mathrm{D}k'] \frac{2(k\cdot k')}{(k')^2(k-k')^2}\left(\frac{p^2}{(k')^2}\right)^{n\epsilon} = -\frac{1}{2\epsilon}\frac{B_n(\epsilon)}{B_0(\epsilon)}\left(\frac{p^2}{k^2}\right)^{(n+1)\epsilon} \tag{3.8}$$

where the integration measure is given in eq. (2.3). This defines a class of one-loop functions mentioned above eq. (2.4), namely

$$B_n(\epsilon) = e^{\epsilon\gamma_{\mathrm{E}}}\frac{\Gamma(1-\epsilon)}{\Gamma(1+n\epsilon)}\frac{\Gamma(1+\epsilon+n\epsilon)\Gamma(1-\epsilon-n\epsilon)}{\Gamma(1-2\epsilon-n\epsilon)}. \tag{3.9}$$

Using this we can write the action of the soft Hamiltonian (3.5) on any monomial ($m \geq 0$):

$$\hat{H}_{\mathrm{s}}\xi^m = \frac{\xi^m}{2\epsilon}\Big((1-\xi)(C_A-\mathbf{T}_t^2) + \xi\hat{B}_m(\epsilon)(2C_A-\mathbf{T}_t^2)\Big) \tag{3.10}$$

$$= \frac{(C_A-\mathbf{T}_t^2)}{2\epsilon}\left(\xi^m - \xi^{m+1}\left[1-\hat{B}_m(\epsilon)\frac{(2C_A-\mathbf{T}_t^2)}{(C_A-\mathbf{T}_t^2)}\right]\right) \tag{3.11}$$

where we have introduced the loop functions

$$\hat{B}_n(\epsilon) = 1 - \frac{B_n(\epsilon)}{B_0(\epsilon)} = 2n(2+n)\zeta_3\epsilon^3 + 3n(2+n)\zeta_4\epsilon^4 + \ldots \tag{3.12}$$

Note that the odd-looking colour factor in the denominator in eq. (3.11) is cancelled by the overall factor $C_A - \mathbf{T}_t^2$. Given that $\hat{B}_m(\epsilon) = \mathcal{O}(\epsilon^3)$, eq. (3.10) makes manifest the fact that $\hat{H}_s\xi^m$ is finite for $\epsilon \to 0$, in line with our earlier assertion about the finiteness of the wavefunction. Writing the action as in eq. (3.11) will be useful in what follows for determining the all-order structure of the wavefunction.

Applying eq. (3.8) repeatedly up to three loops (which is sufficient to determine the amplitude at four loops) we find

$$\Omega_{\mathrm{s}}^{(0)}(\xi) = 1 \tag{3.13a}$$

$$\Omega_{\mathrm{s}}^{(1)}(\xi) = \frac{(C_A-\mathbf{T}_t^2)}{2\epsilon}(1-\xi) \tag{3.13b}$$

$$\Omega_{\mathrm{s}}^{(2)}(\xi) = \frac{(C_A-\mathbf{T}_t^2)^2}{(2\epsilon)^2}\left\{1-2\xi+\xi^2\left[1-\hat{B}_1(\epsilon)\frac{(2C_A-\mathbf{T}_t^2)}{(C_A-\mathbf{T}_t^2)}\right]\right\} \tag{3.13c}$$

$$\begin{aligned}\Omega_{\mathrm{s}}^{(3)}(\xi) = \frac{(C_A-\mathbf{T}_t^2)^3}{(2\epsilon)^3}\Bigg\{&1-3\xi+3\xi^2\left[1-\hat{B}_1(\epsilon)\frac{(2C_A-\mathbf{T}_t^2)}{(C_A-\mathbf{T}_t^2)}\right]\\ &-\xi^3\left[1-\hat{B}_1(\epsilon)\frac{(2C_A-\mathbf{T}_t^2)}{(C_A-\mathbf{T}_t^2)}\right]\left[1-\hat{B}_2(\epsilon)\frac{(2C_A-\mathbf{T}_t^2)}{(C_A-\mathbf{T}_t^2)}\right]\Bigg\}.\end{aligned} \tag{3.13d}$$

The evaluation of a few additional orders allows us to obtain an ansatz for the $(\ell-1)$-th order wavefunction:

$$\Omega_{\rm s}^{(\ell-1)}(p,k) = \frac{(C_A-\mathbf{T}_t^2)^{\ell-1}}{(2\epsilon)^{\ell-1}}\sum_{n=0}^{\ell-1}(-1)^n\binom{\ell-1}{n}\left(\frac{p^2}{k^2}\right)^{n\epsilon} \times\prod_{m=0}^{n-1}\left\{1-\hat{B}_m(\epsilon)\frac{(2C_A-\mathbf{T}_t^2)}{(C_A-\mathbf{T}_t^2)}\right\} \quad (3.14)$$

The validity of this all-order formula can be proved directly using the action of the Hamiltonian in the second line of eq. (3.10) by noticing first that, independently of the loop order, the term ξ^n can only be generated by acting n times with the second term of eq. (3.10), each of which raises the power of ξ by one. Hence ξ^n will always be accompanied by the product $(-1)^n\prod_{m=0}^{n-1}\left\{1-\hat{B}_m(\epsilon)\frac{(2C_A-\mathbf{T}_t^2)}{(C_A-\mathbf{T}_t^2)}\right\}$. Furthermore, the combinatorial factor $\binom{\ell-1}{n}$ associated with ξ^n simply counts the number of different ways of acting $(\ell-1)$ times with the Hamiltonian, out of which n times with the second term and $\ell-1-n$ times with the first. We emphasise again that the above expression (3.14) never produces colour factors in the denominator as can be easily checked by expanding in ϵ for any given, positive ℓ.

3.3 Singularities of the amplitude

The main result of the previous section is that, in the soft approximation, the wavefunction reduces to a polynomial in $\left(p^2/k^2\right)^\epsilon$, given by eq. (3.14). Consequently, the calculation of the amplitude (3.7) is straightforward, because it only involves integrals of the type

$$\int_0^{p^2}\frac{{\rm d}k^2}{k^2}\left(\frac{p^2}{k^2}\right)^{n\epsilon} = -\frac{1}{n\epsilon}. \quad (3.15)$$

With eq. (3.14) we obtain

$$\hat{\mathcal{M}}_{\rm NLL}^{(+,\ell)} = i\pi\frac{1}{(2\epsilon)^\ell}\frac{B_0^\ell(\epsilon)}{\ell!}(1-\hat{B}_{-1}(\epsilon))(C_A-\mathbf{T}_t^2)^{\ell-1}\sum_{n=1}^{\ell}(-1)^{n+1}\binom{\ell}{n} \times\prod_{m=0}^{n-2}\left[1-\hat{B}_m(\epsilon)\frac{(2C_A-\mathbf{T}_t^2)}{(C_A-\mathbf{T}_t^2)}\right]\mathbf{T}_{s-u}^2\mathcal{M}^{(\rm tree)}+\mathcal{O}(\epsilon^0) \quad (3.16)$$

where the factor $(1-\hat{B}_{-1})$ follows from rewriting the factor $e^{\epsilon\gamma_{\rm E}}/\Gamma(1-\epsilon) = B_{-1}(\epsilon)$:

$$B_0^{\ell-1}(\epsilon)\frac{e^{\epsilon\gamma_{\rm E}}}{\Gamma(1-\epsilon)} = B_0^\ell(\epsilon)\frac{B_{-1}(\epsilon)}{B_0(\epsilon)} = B_0^\ell(\epsilon)(1-\hat{B}_{-1}(\epsilon)). \quad (3.17)$$

At this point we briefly return to the observations and assumptions discussed at the end of section 2.3. There, we stated that the ℓ-loop amplitude divided by B_0^ℓ (2.4) is both uniformly of weight ℓ and free of ζ_2. The above result clearly confirms this statement, if only for contributions that originate in the soft limit: Expanding eq. (3.16) (divided by B_0^ℓ) in ϵ amounts to expanding $\hat{B}_m(\epsilon)$ for different values of m which, according to eq. (3.12), yields a series that has both the aforementioned properties.[1] A similar discussion at the end of section 4.5 will show this to be true also for the "non-soft" contributions and thereby verify our conjecture.

We emphasise, once again, that the result in eq. (3.16) captures all singularities of the amplitude as well as finite terms that originate in the soft limit. We shall return to the finite terms in chapter 4. For the present chapter, however, we can safely ignore *any* finite contributions.

The overall factor of $1/(2\epsilon)^\ell$ in eq. (3.16) implies that all singularities are obtained by retaining only contributions up to $\epsilon^{\ell-1}$ in the subsequent factors. When this is taken into account a great simplification arises: indeed, as shown in appendix B, it is possible to prove that

$$\hat{\mathcal{M}}_{\text{NLL}}^{(+,\ell)} = i\pi \frac{1}{(2\epsilon)^\ell} \frac{B_0^\ell(\epsilon)}{\ell!} (1 - \hat{B}_{-1}(\epsilon)) \left(1 - \hat{B}_{-1}(\epsilon) \frac{(2C_A - \mathbf{T}_t^2)}{(C_A - \mathbf{T}_t^2)}\right)^{-1} \times (C_A - \mathbf{T}_t^2)^{\ell-1} \mathbf{T}_{s-u}^2 \mathcal{M}^{(\text{tree})} + \mathcal{O}(\epsilon^0). \quad (3.18)$$

It is remarkable that the complicated sum of products of bubble integrals weighed by a binomial factor collapses to a single factor which depends only on one bubble integral, namely $\hat{B}_{-1}(\epsilon)$. The main ingredient of the proof in appendix B is the fact that the wavefunction itself is finite.

Eq. (3.18) constitutes the main result of this section: by iterating the BFKL equation (which had not been diagonalised before in $4-2\epsilon$ dimensions) we obtained the singular part of the even amplitude at NLL accuracy, to all orders in the strong coupling constant.

Anticipating comparison with the structure of infrared divergences dictated by the soft anomalous dimension in section 5.1, it proves useful to rearrange eq. (3.18) in such a

[1] To avoid confusion, the above reasoning excludes terms proportional to ζ_2 and $\zeta_2\zeta_n$ with n odd. It does not rule out $\zeta_2^2 = \frac{5}{2}\zeta_4$, $\zeta_2\zeta_n$ with n even, etc. In other words, there may be occurrences of $(\pi^2)^a$ where $a \geq 2$ but not π^2 itself.

way to single out the colour structures C_A and $(C_A - \mathbf{T}_t^2)$. Indeed, as mentioned at the end of section 2.3, the dipole formula of infrared divergences fixes the singularities of the even amplitude in the high-energy limit to be proportional to the colour structure $(C_A - \mathbf{T}_t^2)^{\ell-1}\mathbf{T}_{s-u}^2$ at ℓ loops.

From eq. (3.18) we obtain

$$\hat{\mathcal{M}}_{\text{NLL}}^{(+,\ell)} = i\pi \frac{1}{(2\epsilon)^\ell} \frac{B_0^\ell(\epsilon)}{\ell!} \left(1 - R(\epsilon)\frac{C_A}{(C_A - \mathbf{T}_t^2)}\right)^{-1} \times (C_A - \mathbf{T}_t^2)^{\ell-1}\mathbf{T}_{s-u}^2 \mathcal{M}^{(\text{tree})} + \mathcal{O}(\epsilon^0), \quad (3.19)$$

where we have introduced the function

$$\begin{aligned} R(\epsilon) \equiv \frac{B_0(\epsilon)}{B_{-1}(\epsilon)} - 1 &= \frac{\Gamma^3(1-\epsilon)\Gamma(1+\epsilon)}{\Gamma(1-2\epsilon)} - 1 \\ &= -2\zeta_3\epsilon^3 - 3\zeta_4\epsilon^4 - 6\zeta_5\epsilon^5 - \left(10\zeta_6 - 2\zeta_3^2\right)\epsilon^6 + \mathcal{O}(\epsilon^7). \end{aligned} \quad (3.20)$$

In section 5.1 we show that it is possible to resum eq. (3.19), cf. eq. (5.18), and extract from it the high-energy limit of the soft anomalous dimension at NLL. Before addressing this topic, however, it proves useful to explore in more detail the implications of eq. (3.19) by writing explicitly a few orders in perturbation theory. Up to three loops eq. (3.19) reduces to

$$\hat{\mathcal{M}}_{\text{NLL}}^{(+,\ell=1,2,3)} = i\pi \frac{B_0^\ell(\epsilon)}{\ell!(2\epsilon)^\ell}(C_A - \mathbf{T}_t^2)^{\ell-1}\mathbf{T}_{s-u}^2 \mathcal{M}^{(\text{tree})} + \mathcal{O}(\epsilon^0), \quad (3.21)$$

i.e. only one colour structure contributes to the amplitude up to three loops, and the singularities are correctly reproduced by the dipole formula of infrared divergences.

Starting at four loops, and for the subsequent three orders, one gets an additional contribution proportional to a new colour structure:

$$\hat{\mathcal{M}}_{\text{NLL}}^{(+,\ell=4,5,6)} = i\pi \frac{B_0^\ell(\epsilon)}{\ell!(2\epsilon)^\ell} \left\{(C_A - \mathbf{T}_t^2)^{\ell-1} + R(\epsilon)C_A(C_A - \mathbf{T}_t^2)^{\ell-2}\right\} \times \mathbf{T}_{s-u}^2 \mathcal{M}^{(\text{tree})} + \mathcal{O}(\epsilon^0) \quad (3.22)$$

which matches with the infrared-divergent part of the result reported earlier in eq. (2.49). It can be easily verified (see section 5.1) that the infrared divergences associated with the first colour structure are predicted by the dipole formula, while the ones associated with the second are not.

Next, starting at seven loops, and for the subsequent three orders, yet another colour structure arises:

$$\hat{\mathcal{M}}_{\text{NLL}}^{(+,\ell=7,8,9)} = i\pi \frac{B_0^\ell(\epsilon)}{\ell!(2\epsilon)^\ell} \Big\{ (C_A - \mathbf{T}_t^2)^{\ell-1} + R(\epsilon) C_A (C_A - \mathbf{T}_t^2)^{\ell-2} + R^2(\epsilon) C_A^2 (C_A - \mathbf{T}_t^2)^{\ell-3} \Big\} \mathbf{T}_{s-u}^2 \mathcal{M}^{(\text{tree})} + \mathcal{O}(\epsilon^0) \quad (3.23)$$

Expanding eq. (3.19) for the next three orders in α_s we get

$$\hat{\mathcal{M}}_{\text{NLL}}^{(+,\ell=10,11,12)} = i\pi \frac{B_0^\ell(\epsilon)}{\ell!(2\epsilon)^\ell} \Big\{ (C_A - \mathbf{T}_t^2)^{\ell-1} + R(\epsilon) C_A (C_A - \mathbf{T}_t^2)^{\ell-2} + R^2(\epsilon) C_A^2 (C_A - \mathbf{T}_t^2)^{\ell-3} + R^3(\epsilon) C_A^3 (C_A - \mathbf{T}_t^2)^{\ell-4} \Big\} \mathbf{T}_{s-u}^2 \mathcal{M}^{(\text{tree})} + \mathcal{O}(\epsilon^0). \quad (3.24)$$

It is now easy to understand the pattern of singularities implied by eq. (3.19): at each order the first colour structure, proportional to $(C_A - \mathbf{T}_t^2)^{\ell-1}$, describes the singularities predicted by the dipole formula. Additional colour structures are generated by the expansion of the geometric series $1/\left(1 - R(\epsilon)\frac{C_A}{(C_A - \mathbf{T}_t^2)}\right)$ in eq. (3.19). Given that $R(\epsilon)$ (3.20) starts at $\mathcal{O}(\epsilon^3)$ this generates a new colour structure with an increasing power of C_A, replacing one of the factors of $(C_A - \mathbf{T}_t^2)$, every three loops. All these new structures introduce infrared divergences, which are not accounted for by the dipole formula.

Now that we have solved the BFKL equation in the soft limit two new questions arise.

1. Is it possible to simplify the evolution away from the soft limit, where neither of the reggeons has a small momentum, such that we recover the missing finite terms of the amplitude?

2. Using the results of this chapter, how can the infrared divergences not accounted for by the dipole formula be included in the soft anomalous dimension?

The answers to these questions will be given in chapters 4 and 5, respectively.

Chapter 4

Finite terms

Looking at the three- and four-loop amplitudes, cf. eqs. (2.47) and (2.49), it is obvious that there is more to the signature-even $2 \to 2$ amplitude than just singularities: Starting from three loops each loop order contributes a non-trivial finite term.

Finite terms originate both in the soft limit where one reggeon has a small momentum w.r.t. the other, cf. section 3.1, as well as its kinematic complement — which we will refer to as the *hard* region. The former soft-limit finite terms are readily computed with the methods developed in the previous chapter. To compute finite terms produced by hard kinematics on the other hand will require a rather different approach which will be set up in this chapter, starting in section 4.2.

We will proceed just as in the previous chapter and discuss the evolution of the wavefunction first. For reasons explained in section 4.2 this can be done considering the two-dimensional limit of the BFKL equation. Based on the simplified evolution we develop an algorithmic procedure to calculate the two-dimensional wavefunction to any loop order.

Consequently, we describe how to compute finite terms of the amplitude from the two-dimensional wavefunction in section 4.4. Particular attention is paid to the recombination of soft and hard contributions and results are presented in section 4.5.

4.1 Finite contributions from soft kinematics

Let us open this chapter by summarising what the soft-limit analysis in chapter 3 can tell us about finite contributions to the amplitude.

By means of the soft approximation we are able to describe the wavefunction and amplitude accurately as long as one of the reggeons has a small momentum w.r.t. the other, cf. section 3.1. For simplicity we focused on one limit ($k \to 0$) and found that the singular terms are given by a simple one-dimensional integral, cf. eq. (3.7). We argued that the UV cutoff necessary to compute such integrals would affect finite terms. Let us therefore briefly return to this issue and introduce an alternative, cutoff-independent method.

As a first step we symmetrise the soft wavefunction w.r.t. swapping $k \leftrightarrow p-k$, making manifest the invariance of the BFKL evolution under exchange of the two reggeons. The $k \to 0$ soft limit yields a wavefunction that is polynomial in $(p^2/k^2)^\epsilon$, cf. eq. (3.14). Because of said symmetry the $k \to p$ soft limit must give the *same* polynomial, with p^2/k^2 replaced by $p^2/(p-k)^2$. Besides invariance under $k \leftrightarrow p-k$ the symmetrised soft wavefunction has to reproduce the two aforementioned polynomials in the respective limits. In other words, we can infer that it is a polynomial in

$$\left(\frac{p^4}{k^2(p-k)^2}\right)^\epsilon \longrightarrow \begin{cases} \left(\frac{p^2}{k^2}\right)^\epsilon & \text{for } k \to 0 \\ \left(\frac{p^2}{(p-k)^2}\right)^\epsilon & \text{for } k \to p \end{cases} \tag{4.1}$$

and the sought-after symmetric wavefunction is readily constructed by replacing

$$\frac{p^2}{k^2} \longrightarrow \frac{p^4}{k^2(p-k)^2} \tag{4.2}$$

in eq. (3.14) giving

$$\tilde{\Omega}_{\mathrm{s}}^{(\ell-1)}(p,k) = \frac{(C_A - \mathbf{T}_t^2)^{\ell-1}}{(2\epsilon)^{\ell-1}} \sum_{n=0}^{\ell-1} (-1)^n \binom{\ell-1}{n} \left(\frac{p^4}{k^2(p-k)^2}\right)^{n\epsilon} \times \prod_{m=0}^{n-1} \left\{1 - \hat{B}_m(\epsilon) \frac{(2C_A - \mathbf{T}_t^2)}{(C_A - \mathbf{T}_t^2)}\right\}. \tag{4.3}$$

Note the "tilde" which was introduced to distinguish the symmetrised soft wavefunction from the asymmetric Ω_{s} used in chapter 3. For the remainder of this chapter we will exclusively work with $\tilde{\Omega}_{\mathrm{s}}$ and its loop coefficients $\tilde{\Omega}_{\mathrm{s}}^{(\ell)}$.

Importantly, the expression in eq. (4.3) contains *both* soft limits ($k \to 0$ and $k \to p$) and the last integral (2.25) can therefore *not* be simplified to the aforementioned one-dimensional integral (3.7). Instead eq. (2.25) generates bubble integrals when acting on the symmetrised soft wavefunction (4.3). Explicitly, one needs to compute integrals of the type

$$\int [\mathrm{D}k] \frac{(p^2)^{1+2\epsilon}}{(k^2)^{1+n\epsilon}((p-k)^2)^{1+n\epsilon}} \tag{4.4}$$

which is readily done with the formula in eq. (2.34). As expected they produce the same singular terms we found in section 3.3. On top of that, the results can be expanded to the finite order where the $\mathcal{O}(\epsilon^0)$ term is now independent of a cutoff. It is straightforward to derive an analytic expression for the associated ℓ-loop amplitude,

$$\begin{aligned}\hat{\mathcal{M}}^{(+,\ell)}_{\mathrm{NLL}} = i\pi \frac{1}{(2\epsilon)^\ell} \frac{B_0^{\ell-1}(\epsilon)}{(\ell-1)!} e^{\epsilon\gamma_{\mathrm{E}}} (C_A - \mathbf{T}_t^2)^{\ell-1} \sum_{n=0}^{\ell-1} (-1)^n \binom{\ell-1}{n} \\ \times \frac{\Gamma^2(1-(1+n)\epsilon)\Gamma(1+(1+2n)\epsilon)}{(1+n)\Gamma^2(1+n\epsilon)\Gamma(1-(2+2n)\epsilon)} \\ \times \prod_{m=0}^{n-2} \left[1 - \hat{B}_m(\epsilon) \frac{(2C_A - \mathbf{T}_t^2)}{(C_A - \mathbf{T}_t^2)}\right] \mathbf{T}^2_{s-u} \mathcal{M}^{(\mathrm{tree})} + \mathcal{O}(\epsilon^0),\end{aligned} \tag{4.5}$$

where the $\mathcal{O}(\epsilon^0)$ indicates that the provided expression does not contain all finite terms of the two-reggeon amplitude, as discussed in the previous chapter. The leading (i.e. finite) terms through five loops read

$$\left(B_0^{-1} \hat{\mathcal{M}}^{(+,1)}_{\mathrm{NLL}}\right)\Big|^{\mathrm{soft}}_{\mathcal{O}(\epsilon^0)} = 0 \tag{4.6a}$$

$$\left(2B_0^{-2} \hat{\mathcal{M}}^{(+,2)}_{\mathrm{NLL}}\right)\Big|^{\mathrm{soft}}_{\mathcal{O}(\epsilon^0)} = 0 \tag{4.6b}$$

$$\left(3!B_0^{-3} \hat{\mathcal{M}}^{(+,3)}_{\mathrm{NLL}}\right)\Big|^{\mathrm{soft}}_{\mathcal{O}(\epsilon^0)} = -\frac{7}{2}(C_A - \mathbf{T}_t^2)^2\zeta_3 - \frac{3}{4}C_A(C_A - \mathbf{T}_t^2)\zeta_3 \tag{4.6c}$$

$$\left(4!B_0^{-4} \hat{\mathcal{M}}^{(+,4)}_{\mathrm{NLL}}\right)\Big|^{\mathrm{soft}}_{\mathcal{O}(\epsilon^0)} = -\frac{3}{16}C_A(C_A - \mathbf{T}_t^2)^2\zeta_4 \tag{4.6d}$$

$$\left(5!B_0^{-5} \hat{\mathcal{M}}^{(+,5)}_{\mathrm{NLL}}\right)\Big|^{\mathrm{soft}}_{\mathcal{O}(\epsilon^0)} = -\frac{93}{2}(C_A - \mathbf{T}_t^2)^4\zeta_5 - \frac{27}{16}C_A(C_A - \mathbf{T}_t^2)^3\zeta_5 \tag{4.6e}$$

etc., where we have divided the ℓ-loop amplitude by $B_0^\ell/l!$ (2.4). These will have to be combined with contributions produced by hard kinematics to recover the finite part of the amplitude. The details of the reconstruction of the full amplitude will be dealt with at the end of this chapter.

4.2 BFKL evolution in two dimensions

As stated in chapter 1 much of the complication of solving the BFKL evolution stems from the D-dimensionality of the Hamiltonian. Recalling that the two-reggeon wavefunction is finite at any loop order and that singularities are exclusively created by integration near the soft limit it should be clear that no regularisation is required if we (a) only care about finite terms, and (b) remove any soft kinematics from the last integration.

In two dimensions, let us view the Euclidean momentum vectors k, k' and p as complex numbers

$$k = k_x + ik_y, \quad k' = k'_x + ik'_y \quad \text{and} \quad p = p_x + ip_y \tag{4.7}$$

where the real and imaginary parts are the components of the corresponding momenta and introduce new variables $z, w \in \mathbb{C}$ according to

$$\frac{k_x + ik_y}{p_x + ip_y} = \frac{z}{z-1} \qquad \text{and} \qquad \frac{k'_x + ik'_y}{p_x + ip_y} = \frac{w}{w-1}. \tag{4.8}$$

Since the wavefunction is a function of Lorentz scalars (i.e. squares of momenta) it will be symmetric under the exchange $z \leftrightarrow \bar{z}$ with $\bar{z}$ the complex conjugate of z.

In the new variables the BFKL kernel (2.11) reads

$$p^2 f(p,k,k') \longrightarrow (1-w)^2(1-\bar{w})^2 K(w,\bar{w},z,\bar{z}) \tag{4.9}$$

where

$$K(w,\bar{w},z,\bar{z}) = \frac{z\bar{w} + w\bar{z}}{w\bar{w}(z-w)(\bar{z}-\bar{w})} = \frac{1}{\bar{w}(z-w)} + \frac{2}{(z-w)(\bar{z}-\bar{w})} + \frac{1}{w(\bar{z}-\bar{w})}. \tag{4.10}$$

Furthermore, in the limit $\epsilon \to 0$, $J(p,k)$ (2.31) becomes

$$J(p,k) \longrightarrow j(z,\bar{z}) \equiv \frac{1}{2}\log\left[\frac{z}{(1-z)^2}\frac{\bar{z}}{(1-\bar{z})^2}\right] \tag{4.11}$$

and the measure

$$\frac{\mathrm{d}^2 k'}{p^2} \longrightarrow \frac{\mathrm{d}^2 w}{(1-w)^2(1-\bar{w})^2}. \tag{4.12}$$

We employ the same notation as in the D-dimensional case but add the subscript "2d" to avoid confusion. In accordance with section 2.2 this implies

$$\Omega^{(\ell)}_{2\mathrm{d}}(z,\bar{z}) = \hat{H}_{2\mathrm{d}}\Omega^{(\ell-1)}_{2\mathrm{d}}(z,\bar{z}) \tag{4.13}$$

where

$$\hat{H}_{2\mathrm{d}}\psi(z,\bar{z}) = (2C_A - \mathbf{T}_t^2)\hat{H}_{2\mathrm{d,i}}\psi(z,\bar{z}) + (C_A - \mathbf{T}_t^2)\hat{H}_{2\mathrm{d,m}}\psi(z,\bar{z}). \tag{4.14}$$

Plugging in the above expressions we find the two parts of the Hamiltonian to be

$$\hat{H}_{2\mathrm{d,i}}\psi(z,\bar{z}) = \frac{1}{4\pi}\int \mathrm{d}^2 w K(w,\bar{w},z,\bar{z})\left[\psi(w,\bar{w}) - \psi(z,\bar{z})\right] \tag{4.15}$$

$$\hat{H}_{2\mathrm{d,m}}\psi(z,\bar{z}) = j(z,\bar{z})\psi(z,\bar{z}) \tag{4.16}$$

where reader is reminded that $\Omega_{2\mathrm{d}}^{(0)}(z,\bar{z}) = \Omega^{(0)}(p,k) = 1$.

In the next section we proceed to solve for the wavefunction $\Omega_{2\mathrm{d}}$ by iterating the two-dimensional Hamiltonian (4.13).

4.3 Evolution of the two-dimensional wavefunction

It is useful to settle on a language before diving into the iteration of the two-dimensional wavefunction. To this end we introduce the class of iterated integrals dubbed *single-valued harmonic polylogarithms* (SVHPLs) which were first described by Brown in ref. [48]. Many applications of SVHPLs in high-energy calculations [27, 28, 49–52] and scattering amplitudes in general [38, 53, 54] have since been found.

As the name suggests, single-valued harmonic polylogarithms are single-valued functions which can be written as linear combinations of products of harmonic polylogarithms (HPLs) of z with HPLs of $\bar{z}$. We shall denote SVHPLs by $\mathcal{L}_\sigma(z,\bar{z})$ where σ is a sequence of *letters*, typically zeros and ones.[1] The *letters* are said to form an *alphabet*, $\{0,1\}$, and σ is, by analogy, referred to as a *word*. The length of a word is often called the *weight* of the SVHPL. Appendix C provides a summary of the definitions and properties of HPLs and SVHPLs that are used in the following.

SVHPLs are the natural choice for the two-dimensional BFKL evolution as $j(z,\bar{z})$ (4.11) belongs to this class,

$$j(z,\bar{z}) = \frac{1}{2}\mathcal{L}_0(z,\bar{z}) + \mathcal{L}_1(z,\bar{z}), \tag{4.17}$$

and the action of the Hamiltonian $\hat{H}_{2\mathrm{d,i}}$ preserves single-valuedness when acting on a single-valued function. This can be expected on general grounds: any complex pair $z,\bar{z}$

[1] For the most part of this chapter we will use the standard letters, 0 and 1. Only in section 4.3.2 we introduce a new alphabet to simplify the two-dimensional evolution.

identifies a point in the Euclidean transverse momentum plane. Physically there cannot be branch cuts in the Euclidean region which, by definition, guarantees single-valued results. Indeed, single-valuedness was confirmed at every step of the iteration.

The two-dimensional wavefunction is symmetric under $z \leftrightarrow \bar{z}$ as mentioned in section 4.2. Furthermore, we observe invariance under simultaneously swapping $z \leftrightarrow 1/z$ and $\bar{z} \leftrightarrow 1/\bar{z}$. Both these symmetries are easily verified by looking at eqs. (4.11) and (4.15) where, for the latter symmetry, one changes the integration variables $w \to 1/w$, $\bar{w} \to 1/\bar{w}$. We will use these properties to simplify the iteration of the wavefunction as well as its results in section 4.3.2.

The evolution of the wavefunction in strictly two dimensions inherits from the D-dimensional case the following characteristics. Firstly, iterating $\hat{H}_{\mathrm{2d,m}}$ amounts to multiplying by $j(z,\bar{z})$ and therefore evaluating shuffle products of SVHPLs. Secondly, each application of $\hat{H}_{\mathrm{2d,i}}$ adds one layer of integration such that $\Omega_{\mathrm{2d}}^{(\ell-1)}$ can be written as a linear combination of SVHPLs of weight $\ell - 1$.

To calculate these integrals we will translate the action of the Hamiltonian $\hat{H}_{\mathrm{2d,i}}$ to a set of differential equations and solve these in terms of SVHPLs. This, obviously, relies on the aforementioned fact that SVHPLs form a *basis* of the two-dimensional BFKL evolution. As the procedure is generally suited to calculate finite two-dimensional integrals that evaluate to iterated polylogarithms we think it is worthwhile to discuss it in some detail.

Suppose we would like to compute the action of a linear operator $\hat{O}$, which may involve integration, on a function ψ. Given the two-dimensional nature of the problem we choose the complex variable z and its complex conjugate $\bar{z}$ for the purpose of the calculation.

Assume now that we find a differential operator Δ with the following properties:

$$i.\ \Delta \text{ commutes with } \hat{O} \tag{4.18}$$

$$ii.\ \Delta\psi \text{ is a pure function which is of lower weight than } \psi. \tag{4.19}$$

Then,

$$\Delta\left[\hat{O}\psi(z,\bar{z})\right] = \hat{O}\left[\Delta\psi(z,\bar{z})\right] \tag{4.20}$$

and we can compute $\hat{O}\left[\psi(z,\bar{z})\right]$ by integrating the differential equation (4.20), assuming that the r.h.s. is known explicitly. If it is not the procedure can be applied recursively,

i.e.

$$\Delta\left[\hat{O}\left[\Delta\psi(z,\bar{z})\right]\right] = \hat{O}\left[\Delta^2\psi(z,\bar{z})\right] \tag{4.21}$$

until the r.h.s. is simple enough to be calculated. After each integration a constant has to be fixed, e.g. by matching to known boundary conditions.

Importantly, solving the differential equation amounts to computing a one-dimensional integral as opposed to the original two-dimensional one. With *ii.* above eq. (4.19) the former is readily performed on HPLs, according to eq. (C.1), and even more general iterated polylogarithms. For SVHPLs we integrate the holomorphic part (C.16) after which the full result is recovered by application of the single-valued map $\mathbf{s}$ defined in eq. (C.17).

For reasons that will become clear shortly the two-dimensional BFKL Hamiltonian requires us to find not one but a set of differential operators that commute with $\hat{H}_{2\mathrm{d,i}}$. The needed operators turn out to be logarithmic derivatives of the form $\Delta_i = f_i(z)\frac{\mathrm{d}}{\mathrm{d}z}$. Since not all of them commute with all parts of the Hamiltonian we will outline the procedure using the simplest example, $\Delta_1 = z\frac{\mathrm{d}}{\mathrm{d}z}$, and introduce the other operators as they are needed.

For generic values of w and z one finds using eq. (4.10)

$$z\frac{\mathrm{d}}{\mathrm{d}z}K(w,\bar{w},z,\bar{z}) = -\frac{\mathrm{d}}{\mathrm{d}w}wK(w,\bar{w},z,\bar{z}) \qquad \text{(for generic } w,z\text{)}. \tag{4.22}$$

This implies that $z\frac{\mathrm{d}}{\mathrm{d}z}$ exactly commutes with the Hamiltonian, namely

$$\begin{aligned} z\frac{\mathrm{d}}{\mathrm{d}z}\left[\hat{H}_{2\mathrm{d,i}}\Psi(z,\bar{z})\right] &= \frac{1}{4\pi}\int \mathrm{d}^2w \left\{\left(-\frac{\mathrm{d}}{\mathrm{d}w}wK(w,\bar{w},z,\bar{z})\right)\left[\Psi(w,\bar{w})-\Psi(z,\bar{z})\right]\right. \\ &\qquad \left. -K(w,\bar{w},z,\bar{z})\left(z\frac{\mathrm{d}}{\mathrm{d}z}\Psi(z,\bar{z})\right)\right\} \\ &= \frac{1}{4\pi}\int \mathrm{d}^2w K(w,\bar{w},z,\bar{z})\left[w\frac{\mathrm{d}}{\mathrm{d}w}\Psi(w,\bar{w}) - z\frac{\mathrm{d}}{\mathrm{d}z}\Psi(z,\bar{z})\right] \\ &= \hat{H}_{2\mathrm{d,i}}\left[z\frac{\mathrm{d}}{\mathrm{d}z}\Psi(z,\bar{z})\right] \qquad \text{(for generic } w,z\text{)}. \end{aligned} \tag{4.23}$$

However, the complex-conjugate pairs $w,\bar{w}$ and $z,\bar{z}$ cannot be treated as independent variables everywhere. Derivatives w.r.t. those variables receive additional contributions from the non-holomorphic/singular points of the function they act on. These "anomalies" are captured by the two-dimensional Poisson equation

$$\partial_w\partial_{\bar{w}}\log(w\bar{w}) = \pi\delta^2(w) \tag{4.24}$$

namely, by contributions of the form

$$\frac{\mathrm{d}}{\mathrm{d}w}\frac{1}{\bar{w}-\bar{c}} = \pi\delta^2(\bar{w}-\bar{c}) = \pi\delta^2(w-c) = \frac{\mathrm{d}}{\mathrm{d}\bar{w}}\frac{1}{w-c} \tag{4.25}$$

with c a complex number. In general, non-holomorphic appear at 0, at a finite complex value as in the above example (4.25), or at ∞.

For easy bookkeeping let us split a derivative into its *regular part* ("reg"), which is correct in the holomorphic regime, and its *contact terms* ("con"), governed by eq. (4.25). Eq. (4.22) therefore correctly reads

$$\begin{aligned} z\frac{\mathrm{d}}{\mathrm{d}z}K(w,\bar{w},z,\bar{z}) &= \left[z\frac{\mathrm{d}}{\mathrm{d}z}K(w,\bar{w},z,\bar{z})\right]_{\mathrm{reg}} + \left[z\frac{\mathrm{d}}{\mathrm{d}z}K(w,\bar{w},z,\bar{z})\right]_{\mathrm{con}} \\ &= -\left[\frac{\mathrm{d}}{\mathrm{d}w}wK(w,\bar{w},z,\bar{z})\right]_{\mathrm{reg}} + \left[z\frac{\mathrm{d}}{\mathrm{d}z}K(w,\bar{w},z,\bar{z})\right]_{\mathrm{con}} \\ &= -\frac{\mathrm{d}}{\mathrm{d}w}\left[wK(w,\bar{w},z,\bar{z})\right] + \left[\frac{\mathrm{d}}{\mathrm{d}w}wK(w,\bar{w},z,\bar{z})\right]_{\mathrm{con}} \\ &\qquad + \left[z\frac{\mathrm{d}}{\mathrm{d}z}K(w,\bar{w},z,\bar{z})\right]_{\mathrm{con}} \end{aligned} \tag{4.26}$$

which modifies eq. (4.23) to give

$$\begin{aligned} z\frac{\mathrm{d}}{\mathrm{d}z}\left[\hat{H}_{\mathrm{2d,i}}\Psi(z,\bar{z})\right] &= \hat{H}_{\mathrm{2d,i}}\left[z\frac{\mathrm{d}}{\mathrm{d}z}\Psi(z,\bar{z})\right] \\ &\quad + \frac{1}{4\pi}\int \mathrm{d}^2w \left\{\left[\frac{\mathrm{d}}{\mathrm{d}w}wK(w,\bar{w},z,\bar{z})\right]_{\mathrm{con}} + \left[z\frac{\mathrm{d}}{\mathrm{d}z}K(w,\bar{w},z,\bar{z})\right]_{\mathrm{con}}\right\} \\ &\qquad \times\left[\Psi(w,\bar{w}) - \Psi(z,\bar{z})\right]. \end{aligned} \tag{4.27}$$

A few last obstacles need to be overcome before we can derive the explicit form of the contact terms so we delay their derivation until the end of this section.

We shall continue to refer to the behaviour in eq. (4.27) as the commutativity of $z\frac{\mathrm{d}}{\mathrm{d}z}$ and $\hat{H}_{\mathrm{2d,i}}$ even though we implicitly mean commutativity *modulo contact terms*. Note, that the presence of the contact terms does not conflict with the strategy outlined above; each contact term contains a (two-dimensional) δ-function which makes the integral on the r.h.s. of eq. (4.27) easy to evaluate.

The operator $z\frac{\mathrm{d}}{\mathrm{d}z}$ is suited to calculate the action of $\hat{H}_{\mathrm{2d,i}}$ on any SVHPL of the form $\mathcal{L}_{0,\sigma}(z,\bar{z})$: After commuting with the Hamiltonian it lowers the weight of the SVHPL while the result remains a pure function.

$$z\frac{\mathrm{d}}{\mathrm{d}z}\left[\hat{H}_{\mathrm{2d,i}}\mathcal{L}_{0,\sigma}(z,\bar{z})\right] = \hat{H}_{\mathrm{2d,i}}\left[\mathcal{L}_{\sigma}(z,\bar{z})\right] + (\text{contact terms}), \tag{4.28}$$

where we have used eq. (C.8). On the other hand, $z\frac{\mathrm{d}}{\mathrm{d}z}$ does not have the same effect when acting on a SVHPL $\mathcal{L}_{1,\sigma}(z,\bar{z})$,

$$z\frac{\mathrm{d}}{\mathrm{d}z}\left[\hat{H}_{\mathrm{2d,i}}\mathcal{L}_{1,\sigma}(z,\bar{z})\right] = \hat{H}_{\mathrm{2d,i}}\left[\frac{z}{1-z}\mathcal{L}_{\sigma}(z,\bar{z})\right] + (\text{contact terms}), \tag{4.29}$$

and, in particular, does not fulfil the second criterion (4.19). One may be tempted to use $(1-z)\frac{\mathrm{d}}{\mathrm{d}z}$ instead but, unfortunately, such an operator does not commute with $\hat{H}_{\mathrm{2d,i}}$.

The solution is to split the Hamiltonian $\hat{H}_{\mathrm{2d,i}} = \hat{H}_{\mathrm{2d,i_1}} + \hat{H}_{\mathrm{2d,i_2}}$ with

$$\hat{H}_{\mathrm{2d,i}_n}\Psi(z,\bar{z}) = \frac{1}{4\pi}\int \mathrm{d}^2 w K_n(w,\bar{w},z,\bar{z})\left[\Psi(w,\bar{w}) - \Psi(z,\bar{z})\right] \tag{4.30}$$

and

$$K_1(w,\bar{w},z,\bar{z}) = \left(\frac{1}{w-z} - \frac{1}{w}\right)\frac{1}{\bar{w}-\bar{z}} \tag{4.31}$$

$$K_2(w,\bar{w},z,\bar{z}) = \frac{1}{w-z}\left(\frac{1}{\bar{w}-\bar{z}} - \frac{1}{\bar{w}}\right) \tag{4.32}$$

where $K_1(w,\bar{w},z,\bar{z}) + K_2(w,\bar{w},z,\bar{z}) = K(w,\bar{w},z,\bar{z})$, cf. eq. (4.10).

Repeating the above procedure it is straightforward to verify that

$$\left[z\frac{\mathrm{d}}{\mathrm{d}z}, \hat{H}_{\mathrm{2d,i_1}}\right] = (\text{contact terms}), \quad \left[z(1-z)\frac{\mathrm{d}}{\mathrm{d}z}, \hat{H}_{\mathrm{2d,i_1}}\right] = (\text{contact terms}) \tag{4.33a}$$

$$\left[z\frac{\mathrm{d}}{\mathrm{d}z}, \hat{H}_{\mathrm{2d,i_2}}\right] = (\text{contact terms}), \quad \left[(1-z)\frac{\mathrm{d}}{\mathrm{d}z}, \hat{H}_{\mathrm{2d,i_2}}\right] = (\text{contact terms}). \tag{4.33b}$$

In the notation introduced above the complete set of differential operators consists of $\Delta_i = f_i(z)\frac{\mathrm{d}}{\mathrm{d}z}$ where

$$f_1(z) = z, \qquad f_2(z) = 1-z, \qquad f_3(z) = z(1-z) \tag{4.34}$$

and we can calculate the action of $\hat{H}_{\mathrm{2d,i}}$ on $\mathcal{L}_{1,\sigma}$ as follows.

For the case of $\hat{H}_{\mathrm{2d,i_1}}$ we trivially split

$$\mathcal{L}_{1,\sigma}(z,\bar{z}) = \mathcal{L}_{1,\sigma}(z,\bar{z}) + \mathcal{L}_{0,\sigma}(z,\bar{z}) - \mathcal{L}_{0,\sigma}(z,\bar{z}) \tag{4.35}$$

and use the linearity of the Hamiltonian to act with it on $(\mathcal{L}_{1,\sigma} + \mathcal{L}_{0,\sigma})$ and $(-\mathcal{L}_{0,\sigma})$ separately. The differential operators Δ_3 and Δ_1 (4.34), respectively, are then applied to the resulting expressions. With eq. (4.33a) and (C.8) one can easily verify that they produce the desired lower-weight pure functions (4.19):

$$z(1-z)\frac{\mathrm{d}}{\mathrm{d}z}\left[\hat{H}_{\mathrm{i_1}}\left(\mathcal{L}_{0,\sigma}(z,\bar{z}) + \mathcal{L}_{1,\sigma}(z,\bar{z})\right)\right] = \hat{H}_{\mathrm{i_1}}\left[\mathcal{L}_{\sigma}(z,\bar{z})\right] + (\text{contact terms}) \tag{4.36a}$$

$$z\frac{\mathrm{d}}{\mathrm{d}z}\left[\hat{H}_{\mathrm{i_1}}\left(-\mathcal{L}_{0,\sigma}(z,\bar{z})\right)\right] = \hat{H}_{\mathrm{i_1}}\left[-\mathcal{L}_{\sigma}(z,\bar{z})\right] + (\text{contact terms}) \tag{4.36b}$$

For $\hat{H}_{2\mathrm{d},\mathrm{i}_2}$ there is no need to split the SVHPL and one simply uses eq. (4.34) to obtain

$$(1-z)\frac{\mathrm{d}}{\mathrm{d}z}\left[\hat{H}_{\mathrm{i}_2}\mathcal{L}_{1,\sigma}(z,\bar{z})\right] = \hat{H}_{\mathrm{i}_2}\left[\mathcal{L}_\sigma(z,\bar{z})\right] + (\text{contact terms}). \tag{4.37}$$

Having introduced K_1 and K_2 we can finally derive the explicit form of the contact terms. First, let us write eq. (4.27) for general $\Delta_i = f_i(z)\frac{\mathrm{d}}{\mathrm{d}z}$ and the two parts of the split Hamiltonian,

$$\begin{aligned} f_i(z)\frac{\mathrm{d}}{\mathrm{d}z}\left[\hat{H}_{2\mathrm{d},\mathrm{i}_n}\Psi(z,\bar{z})\right] &= \hat{H}_{2\mathrm{d},\mathrm{i}_n}\left[f_i(z)\frac{\mathrm{d}}{\mathrm{d}z}\Psi(z,\bar{z})\right] \\ &+ \frac{1}{4\pi}\int \mathrm{d}^2w \left\{\left[\frac{\mathrm{d}}{\mathrm{d}w}f_i(w)K_n(w,\bar{w},z,\bar{z})\right]_{\mathrm{con}} + \left[f_i(z)\frac{\mathrm{d}}{\mathrm{d}z}K_n(w,\bar{w},z,\bar{z})\right]_{\mathrm{con}}\right\} \\ &\times \left[\Psi(w,\bar{w}) - \Psi(z,\bar{z})\right] \end{aligned} \tag{4.38}$$

where the allowed combinations of i and n are

$$n = 1 \quad \longrightarrow \quad i = 1 \text{ or } 3 \tag{4.39}$$

$$n = 2 \quad \longrightarrow \quad i = 1 \text{ or } 2 \tag{4.40}$$

which should be obvious from eqs. (4.33a), (4.33b) and (4.34).

Before we act with the differential operators on the K_n we note that the f_i (4.34) only depend on one complex variable but not its complex conjugate. According to eq. (4.25) this implies that

$$\left[\frac{\mathrm{d}}{\mathrm{d}w}f_i(w)K_1(w,\bar{w},z,\bar{z})\right]_{\mathrm{con}} = f_i(w)\left[\frac{\mathrm{d}}{\mathrm{d}w}K_1(w,\bar{w},z,\bar{z})\right]_{\mathrm{con}} \tag{4.41}$$

since the contact terms of the derivative are only sensitive to non-holomorphic points in $\bar{w}$. Consequently, we only have to consider the following four cases,

$$\left[\frac{\mathrm{d}}{\mathrm{d}w}K_1(w,\bar{w},z,\bar{z})\right]_{\mathrm{con}} = \pi\left[\delta^2(w-z) - \delta^2(w-\infty)\right]\frac{z}{w(w-z)} \tag{4.42a}$$

$$\left[\frac{\mathrm{d}}{\mathrm{d}z}K_1(w,\bar{w},z,\bar{z})\right]_{\mathrm{con}} = -\pi\delta^2(z-w)\frac{z}{w(w-z)} \tag{4.42b}$$

$$\left[\frac{\mathrm{d}}{\mathrm{d}w}K_2(w,\bar{w},z,\bar{z})\right]_{\mathrm{con}} = \pi\left[\delta^2(w-z) - \delta^2(w)\right]\frac{1}{w-z} \tag{4.42c}$$

$$\left[\frac{\mathrm{d}}{\mathrm{d}z}K_2(w,\bar{w},z,\bar{z})\right]_{\mathrm{con}} = -\pi\delta^2(z-w)\frac{1}{w-z}, \tag{4.42d}$$

where in eqs. (4.42b) and (4.42d) we have dropped[2] terms proportional to $\delta^2(z)$. Eq. (4.25) was used to remove $\bar{w}$ and $\bar{z}$ from the δ functions in favour of their complex conjugates.

[2] In contrast to w, z is an external variable and we may choose $z \neq 0$.

The term $\delta^2(w-\infty) = \delta^2(\bar{w}-\infty)$ in eq. (4.42a) reflects the singular behaviour of K_1 where $1/\bar{w} \to 0$. Due to the sum of contact terms inside the curly brackets in eq. (4.38) (and, again, using eq. (4.41)) the terms proportional to $\delta^2(w-z) = \delta^2(z-w)$ in eqs. (4.42a)–(4.42d) cancel identically.

4.3.1 Differential equations

Finding the differential equations is now simply a matter of putting together the results of the previous section. Starting with the easiest case, $\Delta_1 \hat{H}_{2\mathrm{d,i}_n} \mathcal{L}_{0,\sigma}$, we notice that the contact terms (4.42a)–(4.42d) vanish and divide by $f_1(z) = z$ to arrive at

$$\frac{\mathrm{d}}{\mathrm{d}z} \hat{H}_{2\mathrm{d,i}_n} \mathcal{L}_{0,\sigma}(z,\bar{z}) = \frac{\hat{H}_{2\mathrm{d,i}_n} \mathcal{L}_{\sigma}(z,\bar{z})}{z} \tag{4.43}$$

The next-to-easiest case is eq. (4.37) which, after plugging in the contact terms and dividing by $f_2(z) = 1-z$ gives

$$\frac{\mathrm{d}}{\mathrm{d}z} \hat{H}_{2\mathrm{d,i}_2} \mathcal{L}_{1,\sigma}(z,\bar{z}) = \frac{\hat{H}_{2\mathrm{d,i}_2} \mathcal{L}_{\sigma}(z,\bar{z})}{1-z} - \frac{1}{4} \frac{\mathcal{L}_{1,\sigma}(z,\bar{z}) - [\mathcal{L}_{1,\sigma}(w,\bar{w})]_{w,\bar{w}\to 0}}{z(1-z)}. \tag{4.44}$$

where the shorthand $[\ldots]_{w,\bar{w}\to 0}$ denotes the $w, \bar{w} \to 0$ limit of the functions inside the square brackets. This term can, in fact, be dropped as it always contains a single SVHPL whose indices feature (at least) one "1" and, thus, is equal to zero in the limit.

The last case is governed by eqs. (4.36a) and (4.36b). We insert the corresponding contact terms and divide the equations by $f_3(z) = z(1-z)$ and $f_1(z) = z$, respectively. Next we add the two resulting expressions and combine their l.h.s. using the linearity of $\hat{H}_{2\mathrm{d,i}_1}$ and $\frac{\mathrm{d}}{\mathrm{d}z}$. The resulting differential equation reads

$$\begin{aligned} \frac{\mathrm{d}}{\mathrm{d}z} \hat{H}_{2\mathrm{d,i}_1} \mathcal{L}_{1,\sigma}(z,\bar{z}) = {} & \frac{\hat{H}_{2\mathrm{d,i}_1} \mathcal{L}_{\sigma}(z,\bar{z})}{1-z} \\ & - \frac{1}{4} \frac{\mathcal{L}_{0,\sigma}(z,\bar{z}) + \mathcal{L}_{1,\sigma}(z,\bar{z}) - [\mathcal{L}_{0,\sigma}(w,\bar{w}) + \mathcal{L}_{1,\sigma}(w,\bar{w})]_{w,\bar{w}\to\infty}}{1-z} \end{aligned} \tag{4.45}$$

with $[\ldots]_{w,\bar{w}\to\infty}$ the $w, \bar{w} \to \infty$ limit of the functions inside the square brackets. Taking this limit requires some careful analytic continuation of the involved HPLs to ensure that w and $\bar{w}$ stay complex-conjugate as they approach infinity.

$\hat{H}_{2\mathrm{d,i}}$ (and the $\hat{H}_{2\mathrm{d,i}_n}$) is a linear operator and so one can sum up the above equations (4.43)–(4.45) and recombine $\hat{H}_{2\mathrm{d,i}_1} + \hat{H}_{2\mathrm{d,i}_2} \to \hat{H}_{2\mathrm{d,i}}$ for a more compact expression:

$$\frac{\mathrm{d}}{\mathrm{d}z}\hat{H}_{2\mathrm{d,i}}\mathcal{L}_{0,\sigma}(z,\bar{z}) = \frac{\hat{H}_{2\mathrm{d,i}}\mathcal{L}_{\sigma}(z,\bar{z})}{z} \tag{4.46a}$$

$$\begin{aligned}\frac{\mathrm{d}}{\mathrm{d}z}\hat{H}_{2\mathrm{d,i}}\mathcal{L}_{1,\sigma}(z,\bar{z}) &= \frac{\hat{H}_{2\mathrm{d,i}}\mathcal{L}_{\sigma}(z,\bar{z})}{1-z} - \frac{1}{4}\frac{\mathcal{L}_{1,\sigma}(z,\bar{z})}{z} \\ &\quad - \frac{1}{4}\frac{\mathcal{L}_{0,\sigma}(z,\bar{z}) + 2\mathcal{L}_{1,\sigma}(z,\bar{z}) - [\mathcal{L}_{0,\sigma}(w,\bar{w}) + \mathcal{L}_{1,\sigma}(w,\bar{w})]_{w,\bar{w}\to\infty}}{1-z}\end{aligned} \tag{4.46b}$$

Since the differential equations only fix the z dependence of the (wave)function — which is a function of both z and $\bar{z}$ — a small detour is necessary to recover the action of $\hat{H}_{2\mathrm{d,i}}$ on SVHPLs: we take the holomorphic part of a given SVHPL, integrate it w.r.t. z (according to the differential equations) and afterwards reconstruct the functional dependence on $\bar{z}$ by requiring the result be single-valued. As a matter of fact, this simply amounts to replacing

$$\int_0^z \mathrm{d}t \frac{\mathcal{L}_{\sigma}(t,\bar{t})}{t} \longrightarrow \mathcal{L}_{0,\sigma}(z,\bar{z}) \qquad \text{and} \qquad \int_0^z \mathrm{d}t \frac{\mathcal{L}_{\sigma}(t,\bar{t})}{1-t} \longrightarrow \mathcal{L}_{1,\sigma}(z,\bar{z}) \tag{4.47}$$

For more details on this procedure see appendix C.2.1.

After each integration we need to fix an integration constant. We find that this is conveniently done by matching with the soft limit. For soft kinematics, i.e. small $z, \bar{z}$, only SVHPLs with all-zero indices can give non-zero contributions. They correspond to powers of logarithms

$$\mathcal{L}_{\vec{0}_n}(z,\bar{z}) = \frac{\log^n(z\bar{z})}{n!} \qquad \text{with} \qquad \vec{0}_n = \underbrace{0,\ldots,0}_{n \text{ zeros}} \tag{4.48}$$

where $z\bar{z} = k^2/p^2$ in the soft limit.

In eq. (3.10) we calculated the action of the small-k (or soft) Hamiltonian $\hat{H}_{\mathrm{s}}$ on powers of $\xi = (k^2/p^2)^{-\epsilon}$. The action of $\hat{H}_{\mathrm{i}}$ in the soft limit can be isolated by looking at the coefficient of $2C_A - \mathbf{T}_t^2$ and thus is

$$\hat{H}_{\mathrm{i}}|_{\mathrm{soft}} \left(\frac{k^2}{p^2}\right)^{-m\epsilon} = \frac{\hat{B}_m(\epsilon)}{2\epsilon}\left(\frac{k^2}{p^2}\right)^{-(m+1)\epsilon} \tag{4.49}$$

Expanding both sides in $\delta = m\epsilon$ lets us extract the power of $\log(k^2/p^2) = \log(z\bar{z})$ we are interested in after which we can take the limit $\epsilon \to 0$. For reference, we find

$$\hat{H}_{\mathrm{i}}|_{\mathrm{soft}}\mathcal{L}_0(z,\bar{z}) = \mathcal{O}(\epsilon) \tag{4.50a}$$

$$\hat{H}_{\mathrm{i}}|_{\mathrm{soft}}\mathcal{L}_{0,0}(z,\bar{z}) = \zeta_3 + \mathcal{O}(\epsilon) \tag{4.50b}$$

$$\hat{H}_{\mathrm{i}}|_{\mathrm{soft}}\mathcal{L}_{0,0,0}(z,\bar{z}) = \zeta_3\mathcal{L}_0(z,\bar{z}) + \mathcal{O}(\epsilon) \tag{4.50c}$$

$$\hat{H}_{\mathrm{i}}|_{\mathrm{soft}}\mathcal{L}_{0,0,0,0}(z,\bar{z}) = \zeta_3\mathcal{L}_{0,0}(z,\bar{z}) + \zeta_5 + \mathcal{O}(\epsilon) \tag{4.50d}$$

$$\hat{H}_{\mathrm{i}}|_{\mathrm{soft}}\mathcal{L}_{0,0,0,0,0}(z,\bar{z}) = \zeta_3\mathcal{L}_{0,0,0}(z,\bar{z}) + \zeta_5\mathcal{L}_0(z,\bar{z}) + \mathcal{O}(\epsilon) \tag{4.50e}$$

etc., from which we observe that the integration constants exhibit a very simple pattern. Moreover, these integration constants can only contribute ordinary zeta numbers (i.e. the values of the Riemann zeta function at integer arguments) because they are generated upon expanding $\hat{B}_m(\epsilon)$ (3.12) and thus gamma functions.

We can now calculate the action of $\hat{H}_{\mathrm{2d,i}}$ on any SVHPL by iteratively solving the differential equations (4.46a) and (4.46b), starting from the lowest-weight functions, $\mathcal{L}_0$ and $\mathcal{L}_1$. This is equivalent to saying we have set up an algorithm capable of calculating the two-dimensional wavefunction to any loop order. Due to the finiteness of the wavefunction it is straightforward to verify the results numerically: We integrate eq. (4.15) numerically and compare to the analytical result for a number of randomly generated pairs $z, \bar{z}$. Specifically, with $w = w_1 + iw_2$ and $z = z_1 + iz_2$ the action of $\hat{H}_{\mathrm{2d,i}}$ (4.15) can be written

$$\begin{aligned}\hat{H}_{\mathrm{2d,i}}\psi(z,\bar{z}) = \frac{1}{2\pi}\int_{-\infty}^{\infty}\mathrm{d}w_1\int_{-\infty}^{\infty}\mathrm{d}w_2\frac{w_1z_1 + w_2z_2}{(w_1^2+w_2^2)((w_1-z_1)^2+(w_2-z_2)^2)} \\ \times\left[\psi(w_1+iw_2, w_1-iw_2) - \psi(z_1+iz_2, z_1-iz_2)\right].\end{aligned} \tag{4.51}$$

where $\psi(z,\bar{z})$ is a (linear combination of) SVHPL(s). This type of integral is readily evaluated numerically in e.g. `Mathematica`.

For the wavefunction up to weight four we find

$$\Omega^{(1)}_{\text{2d}} = \frac{1}{2}C_2\left(\mathcal{L}_0 + 2\mathcal{L}_1\right) \tag{4.52a}$$

$$\Omega^{(2)}_{\text{2d}} = \frac{1}{2}C_2^2\left(\mathcal{L}_{0,0} + 2\mathcal{L}_{0,1} + 2\mathcal{L}_{1,0} + 4\mathcal{L}_{1,1}\right) + \frac{1}{4}C_1C_2\left(-\mathcal{L}_{0,1} - \mathcal{L}_{1,0} - 2\mathcal{L}_{1,1}\right) \tag{4.52b}$$

$$\begin{aligned}\Omega^{(3)}_{\text{2d}} = {}& \frac{1}{4}C_1C_2^2\left(-2\mathcal{L}_{0,0,1} - 3\mathcal{L}_{0,1,0} - 7\mathcal{L}_{0,1,1} - 2\mathcal{L}_{1,0,0} - 7\mathcal{L}_{1,0,1} - 7\mathcal{L}_{1,1,0}\right.\\ & \left.-14\mathcal{L}_{1,1,1} + 2\zeta_3\right) + \frac{3}{4}C_2^3\left(\mathcal{L}_{0,0,0} + 2\mathcal{L}_{0,0,1} + 2\mathcal{L}_{0,1,0} + 4\mathcal{L}_{0,1,1} + 2\mathcal{L}_{1,0,0}\right.\\ & \left.+4\mathcal{L}_{1,0,1} + 4\mathcal{L}_{1,1,0} + 8\mathcal{L}_{1,1,1}\right) + \frac{1}{16}C_1^2C_2\left(\mathcal{L}_{0,0,1} + 2\mathcal{L}_{0,1,0} + 4\mathcal{L}_{0,1,1}\right.\\ & \left.+\mathcal{L}_{1,0,0} + 4\mathcal{L}_{1,0,1} + 4\mathcal{L}_{1,1,0} + 8\mathcal{L}_{1,1,1}\right)\end{aligned} \tag{4.52c}$$

$$\begin{aligned}\Omega^{(4)}_{\text{2d}} = {}& \frac{1}{8}C_1C_2^3\left(-9\mathcal{L}_{0,0,0,1} - 14\mathcal{L}_{0,0,1,0} - 34\mathcal{L}_{0,0,1,1} - 14\mathcal{L}_{0,1,0,0} - 42\mathcal{L}_{0,1,0,1}\right.\\ & \left.-44\mathcal{L}_{0,1,1,0} - 92\mathcal{L}_{0,1,1,1} - 9\mathcal{L}_{1,0,0,0} - 34\mathcal{L}_{1,0,0,1} - 42\mathcal{L}_{1,0,1,0} - 92\mathcal{L}_{1,0,1,1}\right.\\ & \left.-34\mathcal{L}_{1,1,0,0} - 92\mathcal{L}_{1,1,0,1} - 92\mathcal{L}_{1,1,1,0} - 184\mathcal{L}_{1,1,1,1} + 8\mathcal{L}_0\zeta_3 + 28\mathcal{L}_1\zeta_3\right)\\ & + \frac{1}{32}C_1^2C_2^2\left(7\mathcal{L}_{0,0,0,1} + 15\mathcal{L}_{0,0,1,0} + 34\mathcal{L}_{0,0,1,1} + 15\mathcal{L}_{0,1,0,0} + 56\mathcal{L}_{0,1,0,1}\right.\\ & \left.+56\mathcal{L}_{0,1,1,0} + 116\mathcal{L}_{0,1,1,1} + 7\mathcal{L}_{1,0,0,0} + 40\mathcal{L}_{1,0,0,1} + 56\mathcal{L}_{1,0,1,0}\right.\\ & \left.+116\mathcal{L}_{1,0,1,1} + 34\mathcal{L}_{1,1,0,0} + 116\mathcal{L}_{1,1,0,1} + 116\mathcal{L}_{1,1,1,0} + 232\mathcal{L}_{1,1,1,1}\right.\\ & \left.-44\mathcal{L}_1\zeta_3\right) + \frac{1}{64}C_1^3C_2\left(-\mathcal{L}_{0,0,0,1} - 3\mathcal{L}_{0,0,1,0} - 6\mathcal{L}_{0,0,1,1} - 3\mathcal{L}_{0,1,0,0}\right.\\ & \left.-12\mathcal{L}_{0,1,0,1} - 12\mathcal{L}_{0,1,1,0} - 24\mathcal{L}_{0,1,1,1} - \mathcal{L}_{1,0,0,0} - 8\mathcal{L}_{1,0,0,1} - 12\mathcal{L}_{1,0,1,0}\right.\\ & \left.-24\mathcal{L}_{1,0,1,1} - 6\mathcal{L}_{1,1,0,0} - 24\mathcal{L}_{1,1,0,1} - 24\mathcal{L}_{1,1,1,0} - 48\mathcal{L}_{1,1,1,1} + 12\mathcal{L}_1\zeta_3\right)\\ & + \frac{3}{2}C_2^4\left(\mathcal{L}_{0,0,0,0} + 2\mathcal{L}_{0,0,0,1} + 2\mathcal{L}_{0,0,1,0} + 4\mathcal{L}_{0,0,1,1} + 2\mathcal{L}_{0,1,0,0} + 4\mathcal{L}_{0,1,0,1}\right.\\ & \left.+4\mathcal{L}_{0,1,1,0} + 8\mathcal{L}_{0,1,1,1} + 2\mathcal{L}_{1,0,0,0} + 4\mathcal{L}_{1,0,0,1} + 4\mathcal{L}_{1,0,1,0} + 8\mathcal{L}_{1,0,1,1}\right.\\ & \left.+4\mathcal{L}_{1,1,0,0} + 8\mathcal{L}_{1,1,0,1} + 8\mathcal{L}_{1,1,1,0} + 16\mathcal{L}_{1,1,1,1}\right)\end{aligned} \tag{4.52d}$$

where we introduced $C_1 = 2C_A - \mathbf{T}_t^2$, $C_2 = C_A - \mathbf{T}_t^2$ and write $\Omega^{(\ell)} \equiv \Omega^{(\ell)}(z,\bar{z})$, $\mathcal{L}_\sigma \equiv \mathcal{L}_\sigma(z,\bar{z})$ for brevity. Further results up to weight 13 can be found in the ancillary file `wavefunction_2dL_w13.txt`.

Interestingly, a new type of transcendental number appears for the first time in the twelve-loop wavefunction — a so-called multiple zeta value (MZV). While it is no surprise that MZVs do not appear at lower loop orders as we explain in the following two paragraphs the fact that they *do* appear starting at twelve loops is a non-trivial statement with number-theoretical implications.

MZVs are the values of HPLs evaluated at special points, typically their branch points $z = 1$ or $z \to \infty$, for example[3] $H_{0,0,0,0,1,0,0,1}(1) = H_{5,3}(1) = \zeta_{5,3}$. It turns out that SVHPLs only cover a subset of all MZVs when evaluated at $z = \bar{z} = 1$ or $z, \bar{z} \to \infty$ and we refer to this subset as single-valued multiple zeta values. They are discussed in detail in refs. [55, 56] where the authors show that, up to weight ten, the algebra of single-valued MZVs is generated by ordinary (odd) zeta numbers ζ_n. At weight eleven however a new type of number appears, alongside the expected ζ_{11}. We shall call it[4] $g_{5,3,3}$ and it is defined by

$$g_{5,3,3} = -\frac{4}{7}\zeta_2^3\zeta_5 + \frac{6}{5}\zeta_2^2\zeta_7 + 45\zeta_2\zeta_9 + \zeta_{5,3,3} \tag{4.53}$$

with $\zeta_{5,3,3} = H_{5,3,3}(1)$.

There are two sources that contribute (multiple) zeta values to the wavefuction: the integration constants fixed by the soft limit and the $w, \bar{w} \to \infty$ limit in eq. (4.46b). The former are generated by expanding gamma functions, cf. eq. (4.49) with eq. (3.12), and can therefore contribute only ordinary zeta numbers, see the examples in eqs. (4.50a)–(4.50e). The value of the large-$w, \bar{w}$ limit on the other hand is guaranteed to multiply the weight-one SVHPL $\mathcal{L}_1(z, \bar{z})$ which is generated by the denominator, $1 - z$, upon integrating the differential equation (4.46b). Being the sole source of (single-valued) MZVs this explains why $g_{5,3,3}$ cannot appear at loop orders $\ell < 12$. Indeed, we find that $g_{5,3,3}$ is accompanied by $\mathcal{L}_1$ in the twelve-loop wavefunction:

$$\begin{aligned}\Omega^{(12)}_{\text{2d}}(z, \bar{z}) \supset \Bigg(&\frac{88653C_2^2C_1^{10}}{163840} - \frac{1021171C_2^3C_1^9}{327680} - \frac{3517129C_2^4C_1^8}{81920} \\ &+ \frac{43378313C_2^5C_1^7}{81920} - \frac{1190279C_2^6C_1^6}{512} + \frac{1583033C_2^7C_1^5}{320} \\ &- \frac{6320709C_2^8C_1^4}{1280} + \frac{135513C_2^9C_1^3}{80}\Bigg) \times g_{5,3,3}\mathcal{L}_1(z, \bar{z})\end{aligned} \tag{4.54}$$

According to ref. [56] (cf. eq. (7.4) there) two more such numbers have to be introduced at weight 13 and, using the same logic, we anticipate that they make an appearance in the 14-loop wavefunction.

The observed term $g_{5,3,3}\mathcal{L}_1(z, \bar{z})$ at twelve loops immediately rules out the possibility to find a closed-form expresson for the two-dimensional wavefunction in terms of gamma

[3] MZVs use the collapsed notation, cf. eq. (C.4) in appendix C.1.

[4] Brown [56] refers to it as $\zeta^{\mathfrak{m}}_{\text{sv}}(3, 5, 3)$ while Schnetz [55] calls it g_{335}.

functions as was done in the soft limit (3.14). We will, in fact, encounter a contribution proportional to $g_{5,3,3}$ in the amplitude at eleven loops and choose to continue the discussion of single-valued MZVs when we interpret our results below eqs. (4.88a)–(4.88e) in section 4.5.

Before we go ahead and compute the associated terms of the amplitude it is worthwhile to explore the aforementioned symmetries of the wavefunction in some more detail and we do so in the next section. This will ultimately lead to a better understanding of the iteration in two dimensions and enable us to calculate it to even higher loop orders.

4.3.2 Alphabets and symmetries

Throughout this work we have tried to exploit the symmetries of the BFKL evolution to aide calculations and simplify expressions. In this section we explore to what extent symmetries can guide us in the two-dimensional limit. As mentioned in section 4.3, in two dimensions, the wavefunction is invariant under two transformations: complex conjugation and inversion of the arguments.

The latter, i.e. the fact that $\Omega_{2\mathrm{d}}(z,\bar{z}) = \Omega_{2\mathrm{d}}(1/z, 1/\bar{z})$, corresponds to the swapping the two reggeons and was used, for example, to identify the two soft limits in chapter 3. In the present context, it inspired us to introduce a new alphabet for SVHPLs. Instead of 0 and 1, corresponding to integration over $\mathrm{d}\log z$ and $\mathrm{d}\log(1-z)$, respectively, we shall use a and s. They are associated with integration over $\mathrm{d}\log z$ and $\mathrm{d}\log z/(1-z)^2$ and thus behave antisymmetrically and symmetrically, respectively, under $z \to 1/z$.

Using the letters a and s simplifies $j(z,\bar{z}) = \mathcal{L}_s(z,\bar{z})/2$ (4.11) and hence the action of $\hat{H}_{2\mathrm{d,m}}$ (4.16) which now amounts to shuffling an s into the indices of the function it acts on, for example

$$\hat{H}_{2\mathrm{d,m}}\mathcal{L}_{a,s,a,s}(z,\bar{z}) = \frac{1}{2}\mathcal{L}_{s,a,s,a,s}(z,\bar{z}) + \mathcal{L}_{a,s,s,a,s}(z,\bar{z}) + \mathcal{L}_{a,s,a,s,s}(z,\bar{z}). \tag{4.55}$$

The action of $\hat{H}_{2\mathrm{d,i}}$ (4.15) in the new alphabet has a much richer and more complicated structure. However, we notice that at symbol level, i.e. keeping only the highest-weight SVHPLs, it simply amounts to replacing $s \to ss - aa$ and multiplying by $-\frac{1}{4}$. To give

an example,

$$\hat{H}_{\text{2d,i}}\mathcal{L}_{a,s,a,s}(z,\bar{z}) = -\frac{1}{4}\left(\mathcal{L}_{a,s,s,a,s}(z,\bar{z}) - \mathcal{L}_{a,a,a,a,s}(z,\bar{z})\right.$$
$$\left. + \mathcal{L}_{a,s,a,s,s}(z,\bar{z}) - \mathcal{L}_{a,s,a,a,a}(z,\bar{z})\right) + \Sigma_{\text{sub}} \quad (4.56)$$

where Σ_{sub} contains products of subleading-weight SVHPLs and zeta numbers, i.e. terms like $\mathcal{L}_\sigma \zeta_{n_1} \cdots \zeta_{n_m}$ with $|\sigma| + n_1 + \cdots + n_m = 5$ and $|\sigma| < 5$ in the above example. It can be derived from the differential equations (4.46a) and (4.46b) and we need to consider the two cases $\hat{H}_{\text{2d,i}}\mathcal{L}_{a,\sigma}$ and $\hat{H}_{\text{2d,i}}\mathcal{L}_{s,\sigma}$. Due to the equivalence of the letters 0 and a eq. (4.46a) immediately gives the action on $\mathcal{L}_{a,\sigma}$

$$\frac{\mathrm{d}}{\mathrm{d}z}\hat{H}_{\text{2d,i}}\mathcal{L}_{a,\sigma}(z,\bar{z}) = \frac{\hat{H}_{\text{2d,i}}\mathcal{L}_\sigma(z,\bar{z})}{z}. \quad (4.57)$$

The simple recursive nature of this equation shows that $\hat{H}_{\text{2d,i}}$ (4.15) does not "touch" the a indices of a SVHPL and can, at most, generate subleading terms Σ_{sub} through integration constants, cf. eqs. (4.50a)–(4.50e).

Using Σ_{sub} as a "bin" to throw subleading terms into, the action on $\mathcal{L}_{s,\sigma}$ can be written

$$\begin{aligned}
\frac{\mathrm{d}}{\mathrm{d}z}\hat{H}_{\text{2d,i}}\mathcal{L}_{s,\sigma}(z,\bar{z}) &= \frac{\mathrm{d}}{\mathrm{d}z}\hat{H}_{\text{2d,i}}\left[\mathcal{L}_{0,\sigma}(z,\bar{z}) + 2\mathcal{L}_{1,\sigma}(z,\bar{z})\right] \\
&= \frac{1+z}{z(1-z)}\hat{H}_{\text{2d,i}}\mathcal{L}_\sigma(z,\bar{z}) \\
&\quad - \frac{1}{2}\left(\frac{\mathcal{L}_{0,\sigma}(z,\bar{z}) + 2\mathcal{L}_{1,\sigma}(z,\bar{z})}{1-z} + \frac{\mathcal{L}_{1,\sigma}(z,\bar{z})}{z}\right) + \Sigma_{\text{sub}} \\
&= \frac{1+z}{z(1-z)}\hat{H}_{\text{2d,i}}\mathcal{L}_\sigma(z,\bar{z}) \\
&\quad - \frac{1}{4}\frac{1+z}{z(1-z)}\left(\mathcal{L}_{0,\sigma}(z,\bar{z}) + 2\mathcal{L}_{1,\sigma}(z,\bar{z})\right) + \frac{1}{4}\frac{\mathcal{L}_{0,\sigma}(z,\bar{z})}{z} + \Sigma_{\text{sub}} \\
&= \frac{1+z}{z(1-z)}\hat{H}_{\text{2d,i}}\mathcal{L}_\sigma(z,\bar{z}) \\
&\quad - \frac{1}{4}\left(\frac{1+z}{z(1-z)}\mathcal{L}_{s,\sigma}(z,\bar{z}) - \frac{\mathcal{L}_{a,\sigma}(z,\bar{z})}{z}\right) + \Sigma_{\text{sub}} \quad (4.58)
\end{aligned}$$

where the first term in the final expression is again a "passive" term, like the one encountered in eq. (4.57). The following term however, creates two leading-weight terms which, upon integration, yield $-\frac{1}{4}(\mathcal{L}_{s,s,\sigma} - \mathcal{L}_{a,a,\sigma})$ and hence confirm the pattern described above eq. (4.56). Note that by the recursive nature of the differential equation this applies to *every* letter s in the word (s,σ), not just the first one.

In the following we show that it is possible to unravel the recursive definition of $\hat{H}_{\text{2d,i}}$ (4.15) beyond symbol level. The Σ_{sub} in the above equations are generated by two

independent and additive sources: the $w, \bar{w} \to \infty$ limit in eq. (4.46b) and the constants of integration as shown in eqs. (4.50a)–(4.50e). Let us denote them $\Sigma_{\text{sub}(\infty)}$ and $\Sigma_{\text{sub}(0)}$, respectively, with their sum equalling Σ_{sub}. Empirically we observe that $\Sigma_{\text{sub}(0)}$ follows a simple pattern when using the $\{a, s\}$ alphabet:

$$\hat{H}_{\text{i}}\mathcal{L}_{w_1,\ldots,w_{\ell-1}}(z,\bar{z}) = \Sigma_{\text{lead}} + \Sigma_{\text{sub}(\infty)} + \sum_{j\geq 3,\ \text{odd}}^{\ell} \zeta_j \mathcal{L}_{w_1,\ldots,w_{\ell-j}}(z,\bar{z}). \tag{4.59}$$

with Σ_{lead} now the leading-weight SVHPLs governed by eq. (4.58). $\Sigma_{\text{sub}(\infty)}$ in turn can be summarised by

$$\begin{aligned}\hat{H}_{\text{i}}\mathcal{L}_{w_1,\ldots,w_{\ell-1}}(z,\bar{z}) = \Sigma_{\text{lead}} + \Sigma_{\text{sub}(0)} + \sum_{j=1}^{\ell} \frac{1}{8} \left(\mathcal{L}_{w_1,\ldots,w_j}(z,\bar{z}) - \mathcal{L}_{w_1,\ldots,w_{j-1},a}(z,\bar{z})\right) \\ \times \left[\mathcal{L}_{a,w_{j+1},\ldots,w_\ell}(z,\bar{z}) + \mathcal{L}_{s,w_{j+1},\ldots,w_\ell}(z,\bar{z})\right]_{z,\bar{z}\to\infty}. \end{aligned} \tag{4.60}$$

Observe that $w_j = s$ in the equation above is a necessary yet not sufficient requirement for a non-zero contribution. Being based on observations the patterns described in eqs. (4.60) and (4.59) need to be verified against the wavefunctions computed in the previous section. We find perfect agreement with the data available at the time of writing (i.e. the wavefunction up to and including 13 loops) and are thus very confident that the above description is correct.

By introducing the $\{a, s\}$ alphabet we have accounted for the symmetry of the wavefunction under inversion, $z \to 1/z$, at symbol level, i.e. as far as leading-weight terms are concerned. Our basis of SVHPLs respects neither this nor the invariance under complex conjugation at function level: in general $\mathcal{L}_\sigma(z,\bar{z}) \neq \mathcal{L}_\sigma(1/z, 1/\bar{z})$ and $\mathcal{L}_\sigma(z,\bar{z}) \neq \mathcal{L}_\sigma(\bar{z}, z)$. Expecting further simplifications we will therefore construct a set of symmetrised functions in the remainder of this section.

In the following we heavily use relations between SVHPLs under a standard set of variable transformations. As we find this to be quite poorly described in the literature we summarise the most important aspects in appendix C.2.2. Quintessentially, these relations determine the coefficients c_w in $\mathcal{L}_\sigma(g(z), g(\bar{z})) = \sum_w c_w \mathcal{L}_w(z,\bar{z})$ where the sum runs over all words up to weight $|\sigma|$ and, in the present case, $g(x) = 1/x$ or $g(x) = \bar{x}$.

Let us define[5]

$$\mathcal{F}_\sigma(z,\bar{z}) = \frac{1}{4}\left(\mathcal{L}_\sigma(z,\bar{z}) + \mathcal{L}_\sigma(\bar{z},z) + \mathcal{L}_\sigma(1/z,1/\bar{z}) + \mathcal{L}_\sigma(1/\bar{z},1/z)\right) \tag{4.61}$$

with σ a word belonging to an alphabet of one's choosing. In the following we stick with the $\{a,s\}$ alphabet.

Due to the symmetries of the wavefunction

$$\Omega_{2\mathrm{d}}(z,\bar{z}) = \Omega_{2\mathrm{d}}(\bar{z},z) = \Omega_{2\mathrm{d}}(1/z,1/\bar{z}) = \Omega_{2\mathrm{d}}(1/\bar{z},1/z) \tag{4.62}$$

and thus

$$\Omega_{2\mathrm{d}}(z,\bar{z}) = \frac{1}{4}\left(\Omega_{2\mathrm{d}}(z,\bar{z}) + \Omega_{2\mathrm{d}}(\bar{z},z) + \Omega_{2\mathrm{d}}(1/z,1/\bar{z}) + \Omega_{2\mathrm{d}}(1/\bar{z},1/z)\right) \tag{4.63}$$

one can simply replace $\mathcal{L}_\sigma(z,\bar{z}) \to \mathcal{F}_\sigma(z,\bar{z})$ to go from the $\mathcal{L}$ to the $\mathcal{F}$ basis. It may therefore not be immediately obvious how eq. (4.61) simplifies the results. Indeed, it requires a few more steps to showcase the advantages of a symmetrised basis.

Firstly, the wavefunction in the $\mathcal{L}$ basis contains functions whose indices feature an odd number of the letter a. Their leading-weight components are antisymmetric under $z \to 1/z$ because

$$\mathrm{d}\log z = -\mathrm{d}\log 1/z \tag{4.64}$$

Converted to $\mathcal{F}$ functions they are hence zero at symbol level or, in other words, equal to products of lower-weight SVHPLs and zeta numbers. This can be turned into a recursive algorithm that successively removes all odd-a functions. Schematically,

1. Take wavefunction and replace $\mathcal{L}_\sigma(z,\bar{z}) \to \mathcal{F}_\sigma(z,\bar{z})$
2. Choose an $\mathcal{F}_\sigma(z,\bar{z})$ where σ contains an odd number of a letters. Plug in definition (4.61) and rewrite SVHPLs as functions of $z,\bar{z}$ using the rules in appendix C.2.2. The resulting SVHPLs will be of lower weight than the original $\mathcal{F}_\sigma$.
3. Replace again $\mathcal{L}_\sigma(z,\bar{z}) \to \mathcal{F}_\sigma(z,\bar{z})$
4. Repeat step 2 & 3 until a fixed point is reached and only functions with an even number of a letters remain.

[5]The set of $\mathcal{F}$s does evidently not span the space of SVHPLs but it does cover the entire space of wavefunctions.

Note that step 3 is valid for the same reason it was legitimate to replace $\mathcal{L}_\sigma(z,\bar{z}) \to \mathcal{F}_\sigma(z,\bar{z})$ in the wavefunction, cf. eqs. (4.62) and (4.63). To give a few examples for odd-a functions,

$$\mathcal{F}_a(z,\bar{z}) = 0 \tag{4.65a}$$

$$\mathcal{F}_{a,s}(z,\bar{z}) = \mathcal{F}_{s,a}(z,\bar{z}) = 0 \tag{4.65b}$$

$$\mathcal{F}_{a,s,s}(z,\bar{z}) = \mathcal{F}_{s,s,a}(z,\bar{z}) = 4\zeta_3 \tag{4.65c}$$

$$\mathcal{F}_{s,a,s}(z,\bar{z}) = -8\zeta_3 \tag{4.65d}$$

$$\mathcal{F}_{s,s,s,a}(z,\bar{z}) = \mathcal{F}_{s,a,s,s}(z,\bar{z}) = 4\zeta_3\mathcal{F}_s(z,\bar{z}). \tag{4.65e}$$

Secondly, we may combine $\mathcal{F}_\sigma(z,\bar{z})$ and $\mathcal{F}_{\tilde{\sigma}}(z,\bar{z})$ with $\tilde{\sigma}$ the word σ reversed, at the cost of generating subleading terms. This is due to the following identity of SVHPLs:

$$\mathcal{L}_\sigma(z,\bar{z}) = \mathcal{L}_{\tilde{\sigma}}(\bar{z},z) + \Sigma_{\text{sub}} \tag{4.66}$$

For a function $\mathcal{F}_\sigma$ this entails

$$\mathcal{F}_\sigma(z,\bar{z}) = \mathcal{F}_{\tilde{\sigma}}(z,\bar{z}) + \Sigma_{\text{sub}} \tag{4.67}$$

due to the invariance under complex conjugation. Besides removing nearly half of the $\mathcal{F}$ functions we find the generated subleading terms to sometimes reduce but never increase the complexity of a given expression. For the procedure to be algorithmic one chooses which letter to cumulate in the left (or right) half of a word.

Using eq. (4.67) in favour of words that start rather then end with the letter s and with the same abbreviations as in eqs. (4.52a)–(4.52d) we find the wavefunction up to four loops is given by

$$\Omega^{(1)}_{\text{2d}} = \frac{1}{2}C_2\mathcal{F}_s \tag{4.68a}$$

$$\Omega^{(2)}_{\text{2d}} = \frac{1}{8}C_1C_2\left(\mathcal{F}_{a,a} - \mathcal{F}_{s,s}\right) + \frac{1}{2}C_2^2\mathcal{F}_{s,s} \tag{4.68b}$$

$$\begin{aligned}\Omega^{(3)}_{\text{2d}} = {}& \frac{1}{16}C_1C_2^2\left(\mathcal{F}_{a,s,a} + 6\mathcal{F}_{s,a,a} - 7\mathcal{F}_{s,s,s} + 8\zeta_3\right) \\ & + \frac{1}{16}C_1^2C_2\left(\mathcal{F}_{s,s,s} - \mathcal{F}_{s,a,a}\right) + \frac{3}{4}C_2^3\mathcal{F}_{s,s,s}\end{aligned} \tag{4.68c}$$

$$\Omega_{\text{2d}}^{(4)} = \frac{1}{16}C_1C_2^3\left(\mathcal{F}_{a,s,s,a} + 6\mathcal{F}_{s,a,a,s} + 4\mathcal{F}_{s,a,s,a} + 12\mathcal{F}_{s,s,a,a} - 23\mathcal{F}_{s,s,s,s}\right.$$
$$\left.+20\zeta_3\mathcal{F}_s\right) + \frac{1}{64}C_1^2C_2^2\left(-\mathcal{F}_{a,s,s,a} - 9\mathcal{F}_{s,a,a,s} - 2\mathcal{F}_{s,a,s,a} - 24\mathcal{F}_{s,s,a,a}\right.$$
$$\left.+7\mathcal{F}_{a,a,a,a} + 29\mathcal{F}_{s,s,s,s} - 4\zeta_3\mathcal{F}_s\right) + \frac{1}{64}C_1^3C_2\left(\mathcal{F}_{s,a,a,s} + 3\mathcal{F}_{s,s,a,a}\right.$$
$$\left.-\mathcal{F}_{a,a,a,a} - 3\mathcal{F}_{s,s,s,s}\right) + \frac{3}{2}C_2^4\mathcal{F}_{s,s,s,s}. \tag{4.68d}$$

Indeed, comparing the results in eqs. (4.68a)–(4.68d) to the wavefunction in terms of standard SVHPLs (and the standard $\{0,1\}$ alphabet) in eqs. (4.52a)–(4.52d) shows the benefits of the new basis. In terms of $\mathcal{F}$ functions the wavefunction takes not only a very compact form and is expressed in terms of fewer functions it also removes subleading terms in some cases, like the $-\frac{3}{16}\mathcal{L}_1\zeta_3$ in the coefficient of $C_1^3C_2$ at four loops (4.52d).

4.4 Finite contributions from hard kinematics

Having set up an algorithm to calculate the two-dimensional wavefunction to any number of loops let us remind ourselves of the main question we try to answer in this chapter: What are the finite terms of the signature-even amplitude at NLL? As demonstrated in section 4.1, the soft limit discussed in chapter 3 gives a partial answer by providing finite terms that originate in kinematic configurations where one of the two reggeons has a small momentum. We then argued that the two-dimensional calculation in turn is suited to describe the BFKL evolution in the complementary kinematic regime, the hard region.

As we are about to compute the missing finite terms by integrating the two-dimensional wavefunction a clear distinction between the two regions is crucial, to avoid both double counting and overlooking terms. Only then will the combined results equal the finite amplitude as predicted by the BFKL equation.

A first important observation is that simply adding the integrated two-dimensional wavefunction to the leading terms of eq. (4.5) will not give the correct result. This is because, at the level of the wavefunction, the two-dimensional approach does not impose any kinematic restrictions and therefore *contains* (the two-dimensional limit of) the soft wavefunction. A naive addition would inevitably induce double counting. The

observation hence motivates the definition of a two-dimensional *hard* wavefunction

$$\Omega_{\text{2d,h}}(z,\bar{z}) = \Omega_{\text{2d}}(z,\bar{z}) - \tilde{\Omega}_{\text{2d,s}}(z,\bar{z}) \tag{4.69}$$

as the difference of the two-dimensional wavefunction calculated in the previous section and the two-dimensional limit of the symmetrised soft wavefunction (4.3),

$$\tilde{\Omega}_{\text{2d,s}}(z,\bar{z}) \equiv \lim_{\epsilon\to 0} \tilde{\Omega}_{\text{s}}(k,p)\big|_{\log(k^2(p-k)^2/p^4)\to\mathcal{L}_s(z,\bar{z})}. \tag{4.70}$$

Taking the limit $\epsilon \to 0$ in eq. (4.70) amounts to isolating the leading $\mathcal{O}(\epsilon^0)$ terms of Ω_{s}; having taken the limit, we switch to the two-dimensional variables z and $\bar{z}$ (4.8), and the SVHPL $\mathcal{L}_s(z,\bar{z}) = \log\frac{z\bar{z}}{(1-z)^2(1-\bar{z})^2}$ introduced in section 4.3.2. In other words, $\tilde{\Omega}_{\text{2d,s}}(z,\bar{z})$ is naturally expressed in terms of the *same* SVHPLs used in the previous sections ensuring the compatibility of the two terms on the r.h.s. of eq. (4.69). We will return to $\tilde{\Omega}_{\text{2d,s}}$ in section 5.2.1 where we derive a resummed all-order expression by means of exponentiation, cf. eq. (5.48).

Because we subtracted the two-dimensional limit of the *symmetrised* soft wavefunction (4.3) $\Omega_{\text{2d,h}}$ vanishes in both soft limits, i.e. at $z,\bar{z} \to 0$ and $z,\bar{z} \to \infty$. This behaviour acts as a sanity check that we have successfully disentangled soft and hard finite terms. Moreover, it is easy to verify that $\Omega_{\text{2d,h}}$ does not contain powers of $\log z\bar{z}$ thus rendering the "last integral" (2.25) finite, as expected.

In two dimensions this "last integral", defined in eq. (2.25), becomes

$$\int [\mathrm{D}k] \frac{p^2}{k^2(p-k)^2}\psi(p,k) \quad \overset{\epsilon\to 0}{\longrightarrow} \quad \frac{1}{4\pi}\int \frac{\mathrm{d}^2 z}{z\bar{z}}\psi(z,\bar{z}). \tag{4.71}$$

The missing finite terms, to which the rest of this section is dedicated, are consequently governed by the integral

$$\hat{\mathcal{M}}^{(+)}_{\text{NLL}}\big|^{\text{hard}}_{\mathcal{O}(\epsilon^0)} = -i\pi\frac{1}{4\pi}\int \frac{\mathrm{d}^2 z}{z\bar{z}}\Omega_{\text{2d,h}}(z,\bar{z})\mathbf{T}^2_{s-u}\mathcal{M}^{(\text{tree})}_{ij\to ij}. \tag{4.72}$$

For a lighter notation we define

$$I \equiv \frac{1}{4\pi}\int \frac{\mathrm{d}^2 z}{z\bar{z}}\Omega_{\text{2d,h}}(z,\bar{z}) \tag{4.73}$$

and develop two independent methods in the following to compute such integrals. The first method, see section 4.4.1, is based on the idea that we can write two-dimensional integrals of a function as one-dimensional integrals of the discontinuity of said function.

It uses a contour deformation in radial coordinates and was inspired by the calculations described in section 7.1 of ref. [57]. The second method, see section 4.4.2, relies on the symmetry of the wavefunction under inversion, $z \to 1/z$, $\bar{z} \to 1/\bar{z}$, and the action of $\hat{H}_{\rm 2d,i}$ at fixed external points.

4.4.1 Method I: Integrating discontinuity

Let us define a regularised version of the integral I in eq. (4.73),

$$I_{\rm reg} = \frac{1}{4\pi} \int_{\delta^2 < z\bar{z} < 1/\delta^2} \frac{{\rm d}^2 z}{z\bar{z}} \Omega_{\rm 2d,h}(z,\bar{z}), \tag{4.74}$$

where the cutoff δ is assumed to be small, $\delta \ll 1$. The introduction of δ may seem superfluous at this point as $\lim_{z,\bar{z}\to 0} \Omega_{\rm 2d} = \lim_{z,\bar{z}\to\infty} \Omega_{\rm 2d} = \lim_{\epsilon\to 0} \tilde{\Omega}_{\rm s}$ and thus, using eq. (4.69), $\lim_{z,\bar{z}\to 0} \Omega_{\rm 2d,h} = \lim_{z,\bar{z}\to\infty} \Omega_{\rm 2d,h} = 0$; more precisely, up to logarithms, $\Omega_{\rm 2d,h}$ vanishes linearly in $z\bar{z}$ in both soft limits, rendering the integral in eq. (4.73) convergent, and the difference $I - I_{\rm reg} = \mathcal{O}(\delta^2)$ (up to logarithms). The necessity of this cutoff despite this good convergence will become clear shortly.

The exclusion of the points $\{0, \infty\}$ in eq. (4.74) enables us to introduce polar coordinates such that $z\bar{z} = r^2$ and $z/\bar{z} = e^{2i\theta}$, as now all points in the integration region have a non-vanishing Jacobian:

$$I_{\rm reg} = \frac{1}{4\pi} \int_\delta^{1/\delta} \frac{\rm d}{{\rm d}r} \int_0^{2\pi} {\rm d}\theta \Omega_{\rm 2d,h} \left(re^{i\theta}, re^{-i\theta} \right). \tag{4.75}$$

To proceed we express the angular integral in the latter as an integration in the complex y plane with $y \equiv e^{i\theta}$, getting

$$I_{\rm reg} = \frac{1}{4\pi i} \int_\delta^{1/\delta} \frac{\rm d}{{\rm d}r} \oint_{|y|=1} \frac{\rm d}{{\rm d}y} \Omega_{\rm 2d,h}(ry, r/y), \tag{4.76}$$

where the contour runs along the unit circle.

The method outlined in the following is based on the deformation of this contour. Essential to it is the fact that the integrand, at any order, is expressed in terms of SVHPLs, whose analytic structure is well understood. These functions are single-valued as long as their arguments are complex conjugates of one another, namely as long as the contour in eq. (4.76) runs along the unit circle. Outside of this region, i.e. upon deformation the contour, the HPLs in $\Omega_{\rm 2d,h}(z,\bar{z})$ exhibit branch cuts[6] where $z \in [1, \infty]$

[6] This is in line with what we know about the hard wavefunction, in particular, that $\Omega_{\rm 2d,h}(z,\bar{z})$ does now contain powers of $\log z\bar{z}$ which have branch cuts on the negative z and $\bar{z}$ axes.

and $\bar{z} \in [1, \infty]$, with no other singularities present. In the r, y coordinates of eq. (4.76) they correspond to cuts along the real axis in the complex y plane where $y \in [1/r, \infty]$ and $y \in [0, r]$, respectively.

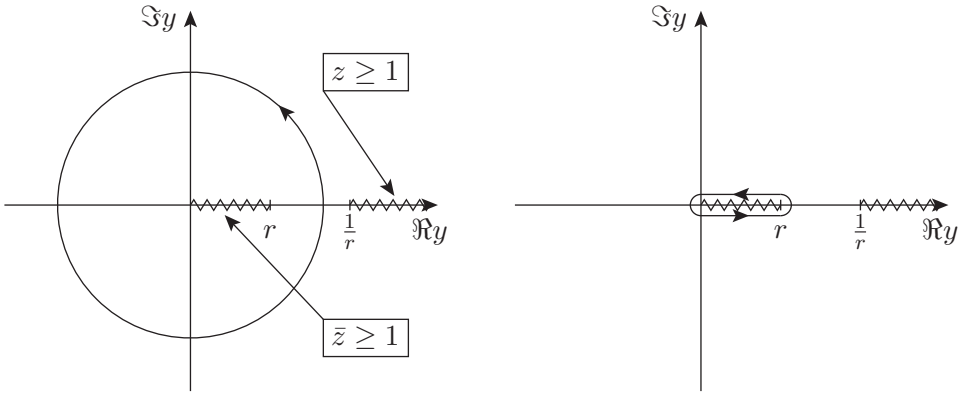

Figure 4.1: Position of the branch cuts in z and $\bar{z}$ in the complex y-plane for $r < 1$ (l.h.s.). The contour along the unit circle in eq. (4.76) can be deformed and, consequently, identified with the integral of the $\bar{z}$-discontinuity in eq. (4.77) (r.h.s.).

For $r < 1$ there is a branch cut-free interval $(r, 1/r)$ through which the contour along the unit circle passes, cf. the l.h.s. of figure 4.1. The contour can consequently be shrunk until it corresponds to integrating the $\bar{z}$-discontinuity of the wavefunction over y from 0 to r, cf. the r.h.s. of figure 4.1. We can now understand why it is necessary to work with the regularised integral I_{reg} (4.74) instead of the original I (4.73): while the hard wavefunction $\Omega_{\text{2d,h}}(z, \bar{z})$ vanishes at 0 and ∞ its discontinuity, in general, does not. In other words, the contour deformation introduces spurious divergent terms and the cutoff introduced in eq. (4.74) regularises them.

For $r > 1$ the branch cuts of z and $\bar{z}$ overlap. However, since $\Omega_{\text{2d,h}}(z, \bar{z})$ is guaranteed to be single-valued they must cancel identically in the interval $(1/r, r)$. Repeating the procedure, we again identify the contour integration with integrating the $\bar{z}$-discontinuity of $\Omega_{\text{2d,h}}(z, \bar{z})$ over y, this time, from 0 to $1/r$.

After modifying the contour in eq. (4.76) we find

$$I_{\text{reg}} = \frac{1}{4\pi i}\left(\int_\delta^1 \frac{\mathrm{d}r}{r}\int_0^r \frac{\mathrm{d}y}{y}\mathrm{disc}_{\bar{z}}[\Omega_{\text{2d,h}}(ry, r/y)] + \int_1^{1/\delta}\frac{\mathrm{d}r}{r}\int_0^{1/r}\frac{\mathrm{d}y}{y}\mathrm{disc}_{\bar{z}}[\Omega_{\text{2d,h}}(ry, r/y)]\right).$$

Changing variables then gives

$$
\begin{aligned}
I_{\rm reg} &= \frac{1}{4\pi i}\left(\int_\delta^1 \frac{{\rm d}r}{r}\int_1^\infty \frac{{\rm d}\bar z}{\bar z}{\rm disc}_{\bar z}[\Omega_{\rm 2d,h}(r^2/\bar z,\bar z)]\right.\\
&\qquad\left.+\int_1^{1/\delta}\frac{{\rm d}r}{r}\int_0^1\frac{{\rm d}z}{z}{\rm disc}_{\bar z}[\Omega_{\rm 2d,h}(z,r^2/z)]\right)\\
&= \frac{1}{8\pi i}\left(\int_1^\infty \frac{{\rm d}\bar z}{\bar z}\int_{\delta^2/\bar z}^{1/\bar z}\frac{{\rm d}z}{z}{\rm disc}_{\bar z}[\Omega_{\rm 2d,h}(z,\bar z)]\right.\\
&\qquad\left.+\int_0^1\frac{{\rm d}z}{z}\int_{1/z}^{1/(\delta^2 z)}\frac{{\rm d}\bar z}{\bar z}{\rm disc}_{\bar z}[\Omega_{\rm 2d,h}(z,\bar z)]\right)\\
&= \frac{1}{8\pi i}\left(\int_0^1 \frac{{\rm d}x}{x}\int_{\delta^2 x}^{x}\frac{{\rm d}z}{z}{\rm disc}_{\bar z}[\Omega_{\rm 2d,h}(z,1/x)]\right.\\
&\qquad\left.+\int_0^1\frac{{\rm d}z}{z}\int_{\delta^2 z}^{z}\frac{{\rm d}x}{x}{\rm disc}_{\bar z}[\Omega_{\rm 2d,h}(z,1/x)]\right). \qquad (4.77)
\end{aligned}
$$

The two terms correspond respectively to $r<1$ and $r>1$. Note that the two are equal owing to the symmetry of $\Omega_{\rm 2d,h}$ under inversion $z\leftrightarrow 1/z$, $\bar z\leftrightarrow 1/\bar z$.

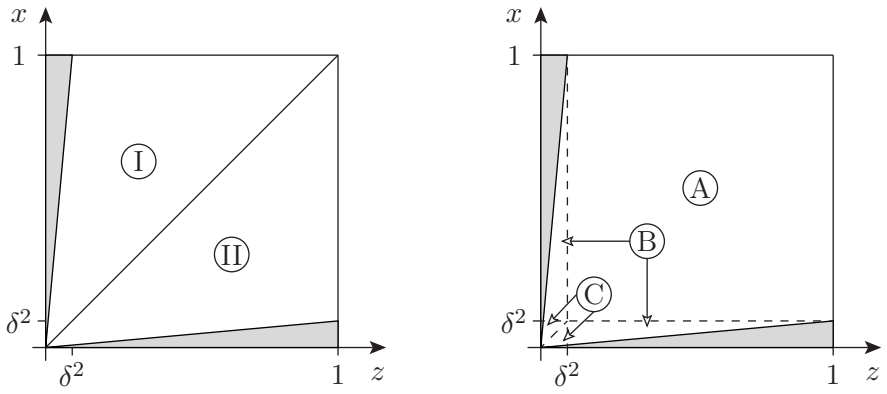

Figure 4.2: Illustration of the integrations in the $r<1$ (I) and $r>1$ (II) contribution to $I_{\rm reg}$ (4.76) (white triangles, l.h.s.). They can be viewed as the integral over a square (A) plus two wedges (B) minus two small triangles (C) (delimited by dashed lines, r.h.s.).

Let us now discuss the evaluation of the final expression in eq. (4.77), where the integration region of the two terms is depicted as the white area in figure 4.2. In order to perform the integration it is useful to view the integrals as the integral over a square

$$
I_A(\delta)=\frac{1}{8\pi i}\int_{\delta^2}^1\frac{{\rm d}z}{z}\int_{\delta^2}^1\frac{{\rm d}x}{x}{\rm disc}_{\bar z}[\Omega_{\rm 2d,h}(z,1/x)] \qquad (4.78)
$$

plus (the integrals over) two wedges

$$I_B(\delta) = \frac{1}{8\pi i}\left(\int_0^1 \frac{\mathrm{d}x}{x}\int_{\delta^2 x}^{\delta^2}\frac{\mathrm{d}z}{z}\mathrm{disc}_{\bar{z}}[\Omega_{\mathrm{2d,h}}(z,1/x)] + \int_0^1 \frac{\mathrm{d}z}{z}\int_{\delta^2 z}^{\delta^2}\frac{\mathrm{d}x}{x}\mathrm{disc}_{\bar{z}}[\Omega_{\mathrm{2d,h}}(z,1/x)]\right) \quad (4.79)$$

minus two small triangles

$$I_C(\delta) = \frac{1}{8\pi i}\left(\int_0^{\delta^2} \frac{\mathrm{d}x}{x}\int_{\delta^2 x}^{x}\frac{\mathrm{d}z}{z}\mathrm{disc}_{\bar{z}}[\Omega_{\mathrm{2d,h}}(z,1/x)] + \int_0^{\delta^2} \frac{\mathrm{d}z}{z}\int_{\delta^2 z}^{z}\frac{\mathrm{d}x}{x}\mathrm{disc}_{\bar{z}}[\Omega_{\mathrm{2d,h}}(z,1/x)]\right), \quad (4.80)$$

cf. the r.h.s. of figure 4.2. Next we would like to evaluate each of these contributions, distinguishing between finite δ-independent terms, and logarithmically-divergent, cutoff-dependent ones.

To do so we remind the reader that the discontinuity w.r.t. $\bar{z}$ of $\Omega_{\mathrm{2d,h}}(z,1/x)$ evaluates to HPLs of z and x. $I_A(\delta)$ of eq. (4.78) thus generates HPLs at 1, giving rise to MZVs, and at δ^2; the latter contain logarithmically-divergent terms in δ. The first (second) integral in the expression of $I_B(\delta)$ in eq. (4.79) is calculated close to $z = 0$ ($x = 0$), cf. figure 4.2. One can therefore expand the discontinuity function in the integrand and discard terms suppressed by powers of z (x) keeping only powers of $\log z$ ($\log x$). The inner integrals then yield powers of $\log\delta^2$, $\log\delta^2 x = \log x + \log\delta^2$ and $\log\delta^2 z = \log z + \log\delta^2$, respectively. The outer integrals thereupon generate MZVs from their upper limits; in addition they produce logarithmically-divergent terms in δ. Contributions from the lower integration limits are dropped according to the (standard) regularisation of HPLs:

$$\lim_{z\to 0}\log z = 0. \quad (4.81)$$

A similar analysis of $I_C(\delta)$ in eq. (4.80) reveals that only powers of $\log\delta^2$ are generated by the integrations over the two small triangles in figure 4.2.

Since the original integral I in eq. (4.73) is finite and $I_{\mathrm{reg}} \to I$ for $\delta \to 0$ all terms proportional to $\log\delta^2$ have to cancel between the three contributions $I_A(\delta)$, $I_B(\delta)$ and $I_C(\delta)$. This enables us to derive a simplified integral in which the logarithmically-

divergent terms are absent altogether whilst giving the same finite terms:

$$I_{\text{reg}} = \frac{1}{8\pi i}\int_0^1 \frac{\mathrm{d}z}{z}\int_0^1 \frac{\mathrm{d}x}{x}\text{disc}_{\bar{z}}[\Omega_{\text{2d,h}}(z,1/x)] + \frac{1}{8\pi i}\left(-\int_0^1 \frac{\mathrm{d}x}{x}\int_0^x \frac{\mathrm{d}z}{z}\text{disc}_{\bar{z}=1}[\Omega_{\text{2d,h}}(z,1/x)]\Big|_{z\ll 1} - \int_0^1 \frac{\mathrm{d}z}{z}\int_0^z \frac{\mathrm{d}x}{x}\text{disc}_{\bar{z}=1}[\Omega_{\text{2d,h}}(z,1/x)]\Big|_{x\ll 1}\right) \quad (4.82)$$

where all integrals are regulated according to eq. (4.81) and $\text{disc}_{\bar{z}=1}[\Omega_{\text{2d,h}}(z,1/x)]\big|_{z\ll 1}$ and $\text{disc}_{\bar{z}=1}[\Omega_{\text{2d,h}}(z,1/x)]\big|_{x\ll 1}$ refer to the aforementioned expansion of the integrand around small z and x, respectively. The first integral in eq. (4.82) reproduces all finite, cut-off independent terms in $I_A(\delta)$ (4.78), while the second and third ones reproduce, respectively, the finite terms in the two integral in $I_B(\delta)$ (4.79); finally, given that no cutoff-independent terms are produce by $I_C(\delta)$, it is absent in eq. (4.82).

The above calculation is biased towards the discontinuity w.r.t. $\bar{z}$ which is purely a matter of choice. A similar calculation can be performed to get an answer in terms of the discontinuity w.r.t. z or a mixed expression that features both discontinuities.

This integration method was further checked as follows. Given a wavefunction (or SVHPL) we expand around $z = \bar{z} = 0$ and change variables to the polar coordinates introduced above in eq. (4.76). The result is a sum of terms of the form $r^a y^b \log^c(r^2)$ with rational constant coefficients and $a, c \geq 0$ and b are integer powers. Integrating the azimuth over $[0, 2\pi]$ then removes all terms that explicitly depend on y, i.e. that have $b \neq 0$. Next, we determine the rational coefficients in terms of harmonic numbers[7]. This enables us to perform the sum ad infinitum after we integrate term-by-term w.r.t. r.

4.4.2 Method II: Iterating shifted wavefunction

The previous method, albeit straightforward on paper, is computationally demanding at high loop orders as it requires extensive use of analytic continuations of HPLs to calculate discontinuities. It turns out there is an easier way to perform the final integration, which lets us make use of our knowledge about the action of the Hamiltonian, established upon computing the wavefunction in section 4.3.

[7]This step requires some amount of creativity but is greatly helped by The On-Line Encyclopedia of Integer Sequences (OEIS), `https://oeis.org`.

Consider the action of $\hat{H}_{\rm 2d,i}$ (4.15) on the wavefunction $\Omega_{\rm 2d,h}(1-z,1-\bar{z})$

$$\hat{H}_{\rm 2d,i}\Omega_{\rm 2d,h}(1-z,1-\bar{z}) = \frac{1}{4\pi}\int \mathrm{d}^2 w K(w,\bar{w},z,\bar{z})\left[\Omega_{\rm 2d,h}(1-w,1-\bar{w})-\Omega_{\rm 2d,h}(1-z,1-\bar{z})\right] \quad (4.83)$$

and set $z=\bar{z}=1$ under the integral. Using $\Omega_{\rm 2d,h}(0,0)=0$ one gets on the right-hand side:

$$\lim_{z,\bar{z}\to 1} K(w,\bar{w},z,\bar{z})\left[\Omega_{\rm 2d,h}(1-w,1-\bar{w})-\Omega_{\rm 2d,h}(1-z,1-\bar{z})\right] = K(w,\bar{w},1,1)\Omega_{\rm 2d,h}(1-w,1-\bar{w}) \quad (4.84)$$

with the kernel

$$K(w,\bar{w},1,1) = \frac{1}{w\bar{w}(1-w)(1-\bar{w})} + \frac{1}{(1-w)(1-\bar{w})} - \frac{1}{w\bar{w}}, \quad (4.85)$$

cf. eq. (4.10). It thus follows that eq. (4.83), taken in the limit $z,\bar{z}\to 1$, yields:

$$\int \mathrm{d}^2 w K(w,\bar{w},1,1)\Omega_{\rm 2d,h}(1-w,1-\bar{w}) = \int \frac{\mathrm{d}^2 w}{w\bar{w}}\left[\Omega_{\rm 2d,h}\left(\frac{1}{1-w},\frac{1}{1-w}\right)+\Omega_{\rm 2d,h}(w,\bar{w})-\Omega_{\rm 2d,h}(1-w,1-\bar{w})\right] \quad (4.86)$$

where we changed the integration variables in the first two terms on the r.h.s. — in the first using $w\to w/(w-1)$, and in the second using $w\to 1-w$, and then factored out a common denominator. Given that the wavefunction is symmetric under inversion, $\Omega_{\rm 2d,h}(1/w,1/\bar{w})=\Omega_{\rm 2d,h}(w,\bar{w})$, the first and third terms in the last equation cancel and we find

$$\hat{H}_{\rm 2d,i}\Omega_{\rm 2d,h}(1-z,1-\bar{z})\big|_{z,\bar{z}\to 1} = \frac{1}{4\pi}\int \frac{\mathrm{d}^2 w}{w\bar{w}}\Omega_{\rm 2d,h}(w,\bar{w}) = I, \quad (4.87)$$

which is readily identified with the integral in eq. (4.73), i.e. the one we would like to compute.

We thus conclude that the integral in eq. (4.72), representing the hard wavefunction contribution to the amplitude, may be calculated with the methods we developed for the computation of the two-dimensional wavefunction itself, described in section 4.3. In practice one rewrites the wavefunction $\Omega_{\rm 2d,h}(1-z,1-\bar{z})$ in terms of SVHPLs of z and $\bar{z}$, then applies the Hamiltonian by solving the corresponding differential equations, and finally evaluates the resulting expression at $z,\bar{z}=1$. The last step produces the anticipated MZVs.

While method I, described in section 4.4.1), and method II show perfect agreement when applied to the wavefunction, we emphasise that while former may be applied on individual SVHPLs, the latter can only be applied to expressions which are symmetric under inversion of their arguments, cf. eqs. (4.86) and (4.87).

4.5 Finite terms of the amplitude

With the methods described in the previous sections it is straightforward to integrate the two-dimensional wavefunction and thereby compute the hard contribution to the amplitude, namely the finite terms not captured by the soft limit. Before we present our results let us, for the last time, review the assumptions made about the amplitude at the end of section 2.3. There, we claimed the ℓ-loop amplitude (divided by B_0^ℓ (2.4)) has two important properties: all of its terms have weight ℓ and there are no terms proportional to ζ_2. We proved the correctness of this statement for contributions from the soft limit in section 3.3, see below eq. (3.16). In the following we argue that this is true for the just-calculated hard contributions, too.

First, we note that both methods for the last integral, cf. sections 4.4.1 and 4.4.2, increase the weight of the functions they act on by one, before evaluating the result at $z = \bar{z} = 1$. In method I the action of the discontinuity first lowers the weight of its argument by one which is then compensated by two consecutive integrations which each raise the weight by one. Method II on the other hand applies the Hamiltonian $\hat{H}_{2\mathrm{d,i}}$ on the wavefunction after a variable transformation $z \to 1 - z$. Changing the variables of a SVHPL does obviously not change its weight and the action of the Hamiltonian corresponds to integrating a first-order differential equation which raises the weight of the operand by one.

SVHPLs at $z = \bar{z} = 1$ evaluate to multiple zeta values (MZVs) of the same weight, cf. the discussion below eqs. (4.52a)–(4.52d). We remind the reader that the $(\ell - 1)$-loop wavefunction consists of weight-$(\ell-1)$ SVHPLs and weight-$(\ell-1)$ products of SVHPLs and zeta numbers and conclude that the hard contributions to the ℓ-loop amplitude therefore have uniform weight ℓ. The absence of ζ_2 is readily explained by the fact that SVHPLs can, by construction, only ever evaluate to odd zeta numbers, for any argument.

We start the discussion of the results by presenting the contributions that originate in the hard region. They are the immediate result of the previous sections and, through five loops, read

$$\left(B_0^{-1}\hat{\mathcal{M}}^{(+,1)}_{\text{NLL}}\right)\Big|^{\text{hard}}_{\mathcal{O}(\epsilon^0)} = 0 \tag{4.88a}$$

$$\left(2B_0^{-2}\hat{\mathcal{M}}^{(+,2)}_{\text{NLL}}\right)\Big|^{\text{hard}}_{\mathcal{O}(\epsilon^0)} = 0 \tag{4.88b}$$

$$\left(3!B_0^{-3}\hat{\mathcal{M}}^{(+,3)}_{\text{NLL}}\right)\Big|^{\text{hard}}_{\mathcal{O}(\epsilon^0)} = -\frac{9}{4}(C_A-\mathbf{T}_t^2)^2\zeta_3+\frac{3}{4}C_A(C_A-\mathbf{T}_t^2)\zeta_3 \tag{4.88c}$$

$$\left(4!B_0^{-4}\hat{\mathcal{M}}^{(+,4)}_{\text{NLL}}\right)\Big|^{\text{hard}}_{\mathcal{O}(\epsilon^0)} = 0 \tag{4.88d}$$

$$\begin{aligned}\left(5!B_0^{-5}\hat{\mathcal{M}}^{(+,5)}_{\text{NLL}}\right)\Big|^{\text{hard}}_{\mathcal{O}(\epsilon^0)} &= -25(C_A-\mathbf{T}_t^2)^4\zeta_5+\frac{35}{2}C_A(C_A-\mathbf{T}_t^2)^3\zeta_5\\ &\quad-\frac{5}{2}C_A^2(C_A-\mathbf{T}_t^2)^2\zeta_5\end{aligned} \tag{4.88e}$$

where one can observe the aforementioned homogeneous weight property and absence of even zeta numbers. Similar to the wavefunction, at twelve loops (and above), these hard contributions to the amplitude cannot be expressed in terms of ordinary zeta numbers beyond a certain loop order. In fact, most of what we discussed in the context of the wavefunction below eqs. (4.52a)–(4.52d) applies to the amplitude as well: Either of the two methods presented in section 4.4.1 and 4.4.2 requires us to evaluate SVHPLs at $z=\bar{z}=1$ and we hence have to anticipate the presence of (single-valued) MZVs starting from weight eleven. Indeed, the eleven-loop amplitude features a term proportional to $g_{5,3,3}$ (4.53):

$$\begin{aligned}11!B_0^{-11}\hat{\mathcal{M}}^{(+,11)}_{\text{NLL}} \supset \Bigg(&\frac{1094181C_2^{10}}{2560}+\frac{6979863C_AC_2^9}{5120}-\frac{2158233C_A^2C_2^8}{5120}\\ &-\frac{1668513C_A^3C_2^7}{1024}+\frac{716859C_A^4C_2^6}{1024}+\frac{2393589C_A^5C_2^5}{5120}\\ &-\frac{2028411C_A^6C_2^4}{5120}+\frac{510873C_A^7C_2^3}{5120}-\frac{44253C_A^8C_2^2}{5120}\Bigg)\times g_{5,3,3}\end{aligned} \tag{4.89}$$

$\hat{\mathcal{M}}^{(+,11)}_{\text{NLL}}$ is the highest loop order available to us at the time of writing but there are a few things we can say about higher-order contributions. First, the twelve-loop hard amplitude will again be comprised of ordinary zeta numbers ζ_n or, more precisely, of weight-twelve products of odd zeta numbers. At the next order, $\ell=13$, the next two single-valued MZVs, which we mentioned below eq. (4.53), can appear. In Brown's notation they are called $\zeta^{\mathbf{m}}_{\text{sv}}(5,3,5)$ and $\zeta^{\mathbf{m}}_{\text{sv}}(3,7,3)$ and can be found in eq. (7.4) of ref. [56].

Speculations aside, the fact that the term in eq. (4.89) *does* appear in the eleven-loop amplitude already excludes that there exists a simple all-order formula in terms of gamma functions for these terms as it was the case for the singular contributions from the soft limit. In general, trying to infer whether or not resummation in the hard region is possible from the results alone is rather difficult. More insights might be gained from solving the evolution equation for the *purely-hard* which we derive in section 5.2.2.

Most importantly, combining eqs. (4.6a)–(4.6e) and eqs. (4.88a)–(4.88e) recovers the finite terms of the one- to four-loop results of ref. [25] and of our numerical five-loop result in eq. (2.51). For reference,

$$\left(B_0^{-1}\hat{\mathcal{M}}_{\text{NLL}}^{(+,1)}\right)\Big|_{\mathcal{O}(\epsilon^0)} = 0 \tag{4.90a}$$

$$\left(2B_0^{-2}\hat{\mathcal{M}}_{\text{NLL}}^{(+,2)}\right)\Big|_{\mathcal{O}(\epsilon^0)} = 0 \tag{4.90b}$$

$$\left(3!B_0^{-3}\hat{\mathcal{M}}_{\text{NLL}}^{(+,3)}\right)\Big|_{\mathcal{O}(\epsilon^0)} = -\frac{11}{4}(C_A - \mathbf{T}_t^2)^2\zeta_3 \tag{4.90c}$$

$$\left(4!B_0^{-4}\hat{\mathcal{M}}_{\text{NLL}}^{(+,4)}\right)\Big|_{\mathcal{O}(\epsilon^0)} = -\frac{3}{16}C_A(C_A - \mathbf{T}_t^2)^2\zeta_4 \tag{4.90d}$$

$$\begin{aligned}\left(5!B_0^{-5}\hat{\mathcal{M}}_{\text{NLL}}^{(+,5)}\right)\Big|_{\mathcal{O}(\epsilon^0)} = &-\frac{53}{2}(C_A - \mathbf{T}_t^2)^4\zeta_5 + \frac{253}{16}C_A(C_A - \mathbf{T}_t^2)^3\zeta_5 \\ &- \frac{5}{2}C_A^2(C_A - \mathbf{T}_t^2)^2\zeta_5\end{aligned} \tag{4.90e}$$

These finite terms can be added to the infrared-singular ones of eq. (3.18) to recover the full signature-even amplitude at NLL. The combined results up to eight loops can be found in eqs. (6.1a)–(6.1g), and up to eleven loops in the provided ancillary file `amplitude_w11.txt`. Previously know to the four-loop order, it can now be calculated to any number of loops with the methods presented in chapters 3 and 4.

Chapter 5

Resummation

5.1 The soft anomalous dimension

It is well known that infrared divergences in gauge-theory scattering amplitudes are multiplicatively "renormalisable": finite hard-scattering amplitudes may be obtained by multiplying the original infrared-divergent amplitude by a renormalisation factor $\mathbf{Z}(\{p_i\}, \mu, \alpha_s(\mu))$, which is matrix-valued in colour-flow space. This factor solves a renormalisation group equation, and hence can be written as a path-ordered exponential of a soft anomalous dimension $\mathbf{\Gamma}(\{p_i\}, \mu, \alpha_s(\mu))$, integrated over the scale μ. As such, the soft anomalous dimension constitutes a fundamental ingredient for the calculation of scattering processes at any given order in perturbation theory, and much effort has been devoted to its determination. It has been shown that the soft anomalous dimension has a simple dipole structure up to two loops [34]. Corrections involving three and four partons arise starting at three loops, and a series of analyses has been performed in order to constrain their structure at three loops and beyond [35–37,58–60]; the complete correction at three loops was calculated recently [32, 33].

The general structure of the soft anomalous dimension is fixed by the factorisation properties of soft and collinear radiation, along with symmetry properties, such as rescaling invariance of soft corrections with respect to the momenta of the hard partons. The latter properties link dipole terms to the cusp anomalous dimension and dictate the structure of corrections to the soft anomalous dimension that correlate more than two partons [35–37,58]. In particular, they imply that at three loops, non-dipole corrections

can only depend on the kinematics via rescaling-invariant cross ratios. The soft anomalous dimension can be further constrained by the behaviour of scattering amplitudes in special kinematic limits, such as the Regge limit [23, 24, 26] and collinear limits [36, 59]. Furthermore, it was recently shown [38] that the space of functions in terms of which the non-dipole correction is expressed (single-valued multiple polylogarithms) can, in fact, be deduced from general considerations. A bootstrap procedure was then set up, which remarkably completely fixes the functional form of the non-dipole correction at three loops (up to an overall rational numerical factor) based on known information from the kinematic limits mentioned above, reproducing the result of the Feynman-diagram computation of ref. [32, 33]. The prospects of extending this bootstrap procedure to higher loops provides an additional motivation to determining the soft anomalous dimension in the high-energy limit.

As discussed above, ref. [25] determined the next-to-leading high-energy logarithms (NLL) of $2 \to 2$ scattering amplitudes at four loops. With the methods described in chapter 3 we have been able to extend this and compute the infrared singularities at NLL in the high-energy limit to all orders in perturbation theory. We are therefore able to determine the soft anomalous dimension in this approximation to all orders.

We start this section by briefly reviewing the structure of the soft anomalous dimension in the high-energy limit, and then determine it to all orders by extracting the $\mathcal{O}(1/\epsilon)$ coefficient from the amplitude obtained in section 3.3, which we then analyse numerically in detail. Finally we show that the singularity structure we deduced from the high-energy limit computation, consisting of poles of $\mathcal{O}(1/\epsilon)$ through to $\mathcal{O}(1/\epsilon^\ell)$ at ℓ loops, is consistent with infrared factorisation, namely it is exactly reproduced by the expansion of the path-ordered exponential of the integral of the soft anomalous dimension.

5.1.1 Infrared factorisation in the high-energy limit

The infrared divergences of scattering amplitudes can be factorised as

$$\mathcal{M}\left(\{p_i\}, \mu, \alpha_s(\mu)\right) = \mathbf{Z}\left(\{p_i\}, \mu, \alpha_s(\mu)\right) \mathcal{H}\left(\{p_i\}, \mu, \alpha_s(\mu)\right) \tag{5.1}$$

where $\mathcal{H}$ is a finite hard-scattering amplitude while $\mathbf{Z}$ captures all singularities. $\mathbf{Z}$ admits a renormalisation group equation whose solution (in the minimal-subtraction scheme)

can be written as a path-ordered exponential of the soft anomalous dimension:

$$\mathbf{Z}\left(\{p_i\},\mu,\alpha_s(\mu)\right)=\mathcal{P}\exp\left\{-\int_0^{\mu}\frac{\mathrm{d}\lambda}{\lambda}\mathbf{\Gamma}\left(\{p_i\},\lambda,\alpha_s(\lambda)\right)\right\}. \tag{5.2}$$

The scale dependence of the soft anomalous dimension $\mathbf{\Gamma}\left(\{p_i\},\lambda,\alpha_s\right)$ for *massless-parton* ($p_i^2=0$) scattering is both explicit and via the $4-2\epsilon$ dimensional coupling. In QCD (with n_f light quark flavours) the latter obeys the renormalisation group equation

$$\beta(\alpha_s,\epsilon)\equiv\frac{\mathrm{d}\alpha_s}{\mathrm{d}\log\mu}=-2\epsilon\alpha_s-\frac{\alpha_s^2}{2\pi}\sum_{n=0}^{\infty}b_n\left(\frac{\alpha_s}{\pi}\right)^n\qquad\text{with}\qquad b_0=\frac{11}{3}C_A-\frac{2}{3}n_f. \tag{5.3}$$

For our purposes only the zeroth order solution will be needed: $\alpha_s(\mu)=\alpha_s(p)\left(p^2/\mu^2\right)^{\epsilon}$. The explicit dependence on the scale ($\mathbf{\Gamma}$ is linear in $\log\lambda$) reflects the presence of double poles due to overlapping soft and collinear divergences.

The soft anomalous dimension in multileg scattering of massless partons is an operator in colour space given by [32, 35–37, 58]

$$\mathbf{\Gamma}\left(\{p_i\},\lambda,\alpha_s(\lambda)\right)=\mathbf{\Gamma}^{\text{dip.}}\left(\{p_i\},\lambda,\alpha_s(\lambda)\right)+\sum_{n=3}^{\infty}\mathbf{\Delta}^{(n)}\left(\frac{\alpha_s}{\pi}\right)^n\quad\text{with} \tag{5.4}$$

$$\mathbf{\Gamma}^{\text{dip.}}\left(\{p_i\},\lambda,\alpha_s(\lambda)\right)=-\frac{\gamma_K(\alpha_s)}{2}\sum_{i<j}\log\left(\frac{-s_{ij}}{\lambda^2}\right)\mathbf{T}_i\cdot\mathbf{T}_j+\sum_i\gamma_i(\alpha_s) \tag{5.5}$$

where $\mathbf{\Gamma}^{\text{dip.}}$ involves only pairwise interactions amongst the hard partons and is therefore referred to as the "dipole formula". The kinematic variables are $-s_{ij}=2|p_i\cdot p_j|e^{-i\pi\lambda_{ij}}$ with $\lambda_{ij}=1$ if partons i and j both belong to either the initial or the final state and $\lambda_{ij}=0$ otherwise. The function $\gamma_K(\alpha_s)$ in eq. (5.4) is the (lightlike) cusp anomalous dimension [61–63], *divided* by the quadratic Casimir of the corresponding Wilson lines. The functions $\gamma_i(\alpha_s)$ represent the field anomalous dimension corresponding to the parton i, which governs hard collinear singularities. Both $\gamma_K(\alpha_s)$ and $\gamma_i(\alpha_s)$ are known through three loops in QCD and their values are summarised in Appendix A of ref. [26]. In eq. (5.4) $\Delta^{(n)}$ for $n\geq 3$ accounts for multi-parton correlations. The three-loop correction $\Delta^{(3)}$, correlating up to four hard partons, was calculated recently [32,33] for any number of partons in general kinematics. Specialising to $2\to 2$ parton scattering in the high-energy limit, ref. [26] showed that $\Delta^{(3)}$ contributes starting from NNLL accuracy in the imaginary (even) part of the amplitude, and starting from N^{3}LL accuracy in the real (odd) part; we refer the interested reader to eq. (4.11) in ref. [26] for an expression for $\Delta^{(3)}$ in this limit. Given our focus here on NLL accuracy, we shall not discuss it further.

While it is known that $\mathbf{\Gamma}^{\text{dip.}}$ fully describes the infrared singularities associated with Regge pole factorisation [23, 24] — meaning it is exact at leading and NLL accuracy for the real part the amplitude — it does not fully capture the structure of the two-reggeon cut [25] at NLL accuracy, where $\Delta^{(n)}$ at four loops and beyond, are relevant. To identify the contribution of the soft anomalous dimension in two-parton scattering, $ij \to ij$, at increasing logarithmic accuracy, let us expand $\mathbf{\Gamma}$ in powers of α_s, keeping the product $\alpha_s L$ fixed, as follows:

$$\mathbf{\Gamma}\left(\alpha_s(\lambda)\right) = \mathbf{\Gamma}_{\text{LL}}\left(\alpha_s(\lambda), L\right) + \mathbf{\Gamma}_{\text{NLL}}\left(\alpha_s(\lambda), L\right) + \mathbf{\Gamma}_{\text{NNLL}}\left(\alpha_s(\lambda), L\right) + \dots \tag{5.6}$$

The N^kLL term in eq. (5.6) can be written as an expansion in $\alpha_s^m L^{m-k}$ for $m \geq k$. Using Regge-pole factorisation it can be shown [23, 24] that the leading logarithmic contribution $\mathbf{\Gamma}_{\text{LL}}$ takes the one-loop exact form,

$$\mathbf{\Gamma}_{\text{LL}}\left(\alpha_s(\lambda)\right) = \frac{\alpha_s(\lambda)}{\pi}\frac{\gamma_K^{(1)}}{2} L \mathbf{T}_t^2 = \frac{\alpha_s(\lambda)}{\pi} L \mathbf{T}_t^2 \tag{5.7}$$

This exactly corresponds to the infrared-divergent part of the one-loop gluon Regge trajectory in eq. (2.13). Note that the LL anomalous dimension has even signature $\mathbf{\Gamma}_{\text{LL}} = \mathbf{\Gamma}_{\text{LL}}^{(+)}$. At NLL the anomalous dimension can be divided into signature-even and odd parts:

$$\mathbf{\Gamma}_{\text{NLL}} = \mathbf{\Gamma}_{\text{NLL}}^{(+)} + \mathbf{\Gamma}_{\text{NLL}}^{(-)} \tag{5.8}$$

The even part[1], which is governed by the Regge pole, is two-loop exact. Referring to eq. (5.4), it contains the terms in the one-loop anomalous dimension that are not enhanced by L, as well as the infrared-divergent part of the two-loop gluon Regge trajectory:

$$\mathbf{\Gamma}_{\text{NLL}}^{(+)} = \frac{\alpha_s(\lambda)}{\pi}\sum_{i=1}^{2}\left(\frac{\gamma_K^{(1)}}{2} C_i \log\frac{-t}{\lambda^2} + 2\gamma_i^{(1)}\right) + \left(\frac{\alpha_s(\lambda)}{\pi}\right)^2 \frac{\gamma_K^{(2)}}{2} L \mathbf{T}_t^2 \tag{5.9}$$

The odd part is however sensitive to the two-reggeon cut. At one-loop it can be obtained from the dipole formula [23, 24],

$$\mathbf{\Gamma}_{\text{NLL}}^{(-)} = i\pi\frac{\alpha_s(\lambda)}{\pi}\mathbf{T}_{s-u}^2 + \mathcal{O}(\alpha_s^4 L^3) \tag{5.10}$$

[1]Note that the even part of the NLL anomalous dimension, $\mathbf{\Gamma}_{\text{NLL}}^{(+)}$, contributes to the *odd* NLL amplitude, $\mathcal{M}_{\text{NLL}}^{(-)}$, since it acts on the LL part of $\mathcal{H}$ in eq. (5.1), which is itself odd.

while higher-order terms have so far been unknown. The reduced amplitude obtained in section 3.1 contains information on the infrared divergences of next-to-leading high-energy logarithms to all orders in α_s, and hence allows us to determine $\mathbf{\Gamma}^{(-)}_{\rm NLL}$ to all orders.

In order to make contact with section 3.1 we need to express the reduced amplitude defined in eq. (2.18) in its infrared-factorised form. Focusing on the even component, we substitute eq. (5.1) there and expand it to NLL accuracy:

$$\hat{\mathcal{M}}^{(+)}_{\rm NLL} = \exp\left\{-\frac{B_0(\epsilon)}{2\epsilon}\frac{\alpha_s(\mu)}{\pi}L\mathbf{T}_t^2\right\}\left[\mathbf{Z}^{(-)}_{\rm NLL}\left(\frac{s}{t},\mu,\alpha_s(\mu)\right)\mathcal{H}^{(-)}_{\rm LL}\left(\{p_i\},\mu,\alpha_s(\mu)\right)\right.$$
$$\left.+\,\mathbf{Z}^{(+)}_{\rm LL}\left(\frac{s}{t},\mu,\alpha_s(\mu)\right)\mathcal{H}^{(+)}_{\rm NLL}\left(\{p_i\},\mu,\alpha_s(\mu)\right)\right] \quad (5.11)$$

where we have written the Regge trajectory explicitly according to eq. (2.13). Substituting $\mathbf{\Gamma}_{\rm LL}$ of eq. (5.7) into eq. (5.2) and integrating over the scale (using the zeroth-order scale dependence of α_s) we obtain:

$$\mathbf{Z}^{(+)}_{\rm LL}\left(\frac{s}{t},\mu,\alpha_s(\mu)\right) = \exp\left\{\frac{1}{2\epsilon}\frac{\alpha_s}{\pi}L\mathbf{T}_t^2\right\} \quad (5.12)$$

Considering the second term in the square brackets of eq. (5.11) we note that $\mathbf{Z}^{(+)}_{\rm LL}$ can be combined with the exponential of the Regge trajectory, and this combination gives rise to an exponent proportional to $(B_0(\epsilon)-1)/(2\epsilon) \sim \mathcal{O}(\epsilon)$. Given that the hard function is finite by definition, $\mathcal{H}^{(+)}_{\rm NLL} \sim \mathcal{O}(\epsilon^0)$, we conclude that the second term in eq. (5.11) only contributes to finite terms in $\hat{\mathcal{M}}^{(+)}_{\rm NLL}$. This implies that the infrared-singular part of the reduced amplitude is insensitive to $\mathcal{H}^{(+)}_{\rm NLL}$ [25] and is given by:

$$\hat{\mathcal{M}}^{(+)}_{\rm NLL} = \exp\left\{-\frac{B_0(\epsilon)}{2\epsilon}\frac{\alpha_s}{\pi}L\mathbf{T}_t^2\right\}$$
$$\times\,\mathbf{Z}^{(-)}_{\rm NLL}\left(\frac{s}{t},\mu,\alpha_s(\mu)\right)\mathcal{H}^{(-)}_{\rm LL}\left(\{p_i\},\mu,\alpha_s(\mu)\right)+\mathcal{O}(\epsilon^0) \quad (5.13)$$

Equation (5.13) can be further simplified by noticing that the hard function at LL accuracy is fixed by Regge factorisation: it is simply the exponential of the finite part of the gluon Regge trajectory, i.e. we have

$$\mathcal{H}^{(-)}_{\rm LL}\left(\{p_i\},\mu,\alpha_s(\mu)\right) = \exp\left\{\frac{B_0(\epsilon)-1}{2\epsilon}\frac{\alpha_s}{\pi}LC_A\right\}\mathcal{M}^{(\rm tree)} \quad (5.14)$$

where we used the fact that $\mathbf{T}_t^2 = C_A$ when acting on the Regge limit of the tree level amplitude. Moving this (finite) exponential to the left, this result allows us to write

eq. (5.13) more explicitly as

$$\exp\left\{\frac{1-B_0(\epsilon)}{2\epsilon}\frac{\alpha_s}{\pi}L(C_A-\mathbf{T}_t^2)\right\}\hat{\mathcal{M}}_{\rm NLL}=\exp\left\{-\frac{1}{2\epsilon}\frac{\alpha_s}{\pi}L\mathbf{T}_t^2\right\}$$
$$\times\,\mathcal{P}\exp\left\{-\int_0^p\frac{\mathrm{d}\lambda}{\lambda}\left[\mathbf{\Gamma}_{\rm LL}\left(\alpha_s(\lambda)\right)+\mathbf{\Gamma}_{\rm NLL}\left(\alpha_s(\lambda)\right)\right]\right\}\mathcal{M}^{(\rm tree)}+\mathcal{O}(\epsilon^0)\quad(5.15)$$

where it is understood that both sides of this equality are to be projected onto even signature. Below we will abbreviate the l.h.s. as $\bar{\mathcal{M}}_{\rm NLL}$. The NLL contribution to the path-ordered exponential on the second line can be written out fully as

$$-\int_0^p\frac{\mathrm{d}\lambda}{\lambda}\left[\mathcal{P}\exp\left\{-\int_0^\lambda\frac{\mathrm{d}\lambda'}{\lambda'}\mathbf{\Gamma}_{\rm LL}\left(\alpha_s(\lambda')\right)\right\}\right]$$
$$\times\,\mathbf{\Gamma}_{\rm NLL}\left(\alpha_s(\lambda)\right)\left[\mathcal{P}\exp\left\{-\int_\lambda^p\frac{\mathrm{d}\lambda'}{\lambda'}\mathbf{\Gamma}_{\rm LL}\left(\alpha_s(\lambda')\right)\right\}\right]\quad(5.16)$$

Finally, integrating the exponents in each of the two brackets as in eq. (5.12) and using again that $\mathbf{T}_t^2=C_A$ in the right factor upon acting on $\mathcal{M}^{(\rm tree)}$, we obtain, projecting onto the even amplitude:

$$\bar{\mathcal{M}}^{(+)}_{\rm NLL}=-\int_0^p\frac{\mathrm{d}\lambda}{\lambda}\exp\left\{\frac{1}{2\epsilon}\frac{\alpha_s(p)}{\pi}L(C_A-\mathbf{T}_t^2)\left[1-\left(\frac{p^2}{\lambda^2}\right)^\epsilon\right]\right\}$$
$$\times\,\mathbf{\Gamma}^{(-)}_{\rm NLL}\left(\alpha_s(\lambda)\right)\mathcal{M}^{(\rm tree)}+\mathcal{O}(\epsilon^0)\quad(5.17)$$

In order to compare this all-order expression to the results of the soft-limit BFKL analysis we need to resum the ℓ-loop amplitude (3.19) obtained in section 3.3 according to eq. (2.24). This is readily done and we find

$$\hat{\mathcal{M}}^{(+)}_{\rm NLL}=\frac{i\pi}{L(C_A-\mathbf{T}_t^2)}\left(1-R(\epsilon)\frac{C_A}{(C_A-\mathbf{T}_t^2)}\right)^{-1}$$
$$\times\left[\exp\left\{\frac{B_0(\epsilon)}{2\epsilon}\frac{\alpha_s}{\pi}L(C_A-\mathbf{T}_t^2)\right\}-1\right]\mathbf{T}^2_{s-u}\mathcal{M}^{(\rm tree)}+\mathcal{O}(\epsilon^0).\quad(5.18)$$

Exploiting now the fact that the exponential on the l.h.s. of eq. (5.15) is finite (and that $R(\epsilon)$ is finite), the BFKL prediction can be written as

$$\bar{\mathcal{M}}^{(+)}_{\rm NLL}=i\pi\left[\frac{\exp\left\{\frac{1}{2\epsilon}\frac{\alpha_s}{\pi}L(C_A-\mathbf{T}_t^2)\right\}-1}{L(C_A-\mathbf{T}_t^2)}\right]$$
$$\times\left(1-R(\epsilon)\frac{C_A}{(C_A-\mathbf{T}_t^2)}\right)^{-1}\mathbf{T}^2_{s-u}\mathcal{M}^{(\rm tree)}+\mathcal{O}(\epsilon^0)\quad(5.19)$$

with $R(\epsilon)$ defined in eq. (3.20). We now have two expressions for the infrared singularities of the reduced amplitude — an expression in terms of the soft anomalous

dimension, eq. (5.17), and the all-order result of BFKL evolution in the soft approximation, eq. (5.19). In the next section we equate them and extract $\mathbf{\Gamma}^{(-)}_{\text{NLL}}$.

5.1.2 Extraction of the soft anomalous dimension at NLL

In minimal subtraction schemes, anomalous dimensions can be extracted by taking the coefficient of pure $1/\epsilon$ single poles. Indeed, to get the coefficient of the single poles in eq. (5.17) we can drop the exponentials to get

$$\left[\bar{\mathcal{M}}^{(+)}_{\text{NLL}}\right]_{\text{single poles}} = -\int_0^p \frac{\mathrm{d}\lambda}{\lambda}\mathbf{\Gamma}^{(-)}_{\text{NLL}}\left(\alpha_s(\lambda)\right)\mathcal{M}^{(\text{tree})} \tag{5.20}$$

$$= \frac{1}{2\epsilon}\sum_{\ell=1}^{\infty}\left(\frac{\alpha_s(p)}{\pi}\right)^{\ell} L^{\ell-1}\frac{1}{\ell}\mathbf{\Gamma}^{(-,\ell)}_{\text{NLL}}\mathcal{M}^{(\text{tree})} \tag{5.21}$$

This result must be set equal to the single poles obtained from eq. (5.19), whose ℓ-loop coefficient is

$$\bar{\mathcal{M}}^{(+,\ell)}_{\text{NLL}} = \frac{i\pi}{2\epsilon\ell!}\left[\frac{(C_A-\mathbf{T}_t^2)}{2\epsilon}\right]^{\ell-1}\left(1-R(\epsilon)\frac{C_A}{(C_A-\mathbf{T}_t^2)}\right)^{-1}\mathbf{T}^2_{s-u}\mathcal{M}^{(\text{tree})}+\mathcal{O}(\epsilon^0) \tag{5.22}$$

Comparing with eq. (5.21) then gives

$$\mathbf{\Gamma}^{(-,\ell)}_{\text{NLL}} = i\pi G^{(\ell)}\mathbf{T}^2_{s-u} \tag{5.23}$$

with

$$G^{(\ell)} \equiv \frac{1}{(\ell-1)!}\left[\frac{(C_A-\mathbf{T}_t^2)}{2}\right]^{\ell-1}\left(1-R(\epsilon)\frac{C_A}{(C_A-\mathbf{T}_t^2)}\right)^{-1}\Bigg|_{\epsilon^{\ell-1}} \tag{5.24}$$

where the subscript indicates that one should extract the coefficient of $\epsilon^{\ell-1}$. Although the notation does not manifest this, the end result is always a polynomial in colour operators C_A and $\mathbf{T}_t^2$, since $R(\epsilon)$ has a regular series as $\epsilon\to 0$. Rescaling ϵ, this can also be written as

$$\mathbf{\Gamma}^{(-,\ell)}_{\text{NLL}} = \frac{i\pi}{(\ell-1)!}\left(1-R\left(\frac{x}{2}(C_A-\mathbf{T}_t^2)\right)\frac{C_A}{(C_A-\mathbf{T}_t^2)}\right)^{-1}\Bigg|_{x^{\ell-1}}\mathbf{T}^2_{s-u} \tag{5.25}$$

where the function $R(\epsilon) = -2\zeta_3\epsilon^3+\ldots$ is defined in eq. (3.20).

Eq. (5.25) is the main result of section 5.1: it gives the soft anomalous dimension in the Regge limit to any loop order at next-to-leading logarithmic accuracy (i.e. all terms of the form $\alpha_s^\ell L^{\ell-1}$); the even contribution $\mathbf{\Gamma}^{(+,\ell)}_{\text{NLL}}$ was given in eqs. (5.7) and (5.9). In other words, we now know eq. (5.10) to all orders:

$$\mathbf{\Gamma}^{(-)}_{\text{NLL}} = \sum_{\ell=1}^{\infty}\mathbf{\Gamma}^{(-,\ell)}_{\text{NLL}}\left(\frac{\alpha_s(\lambda)}{\pi}\right)^{\ell} L^{\ell-1} \tag{5.26}$$

Expanding the above formula explicitly to eight loops:

$$\mathbf{\Gamma}^{(-,1)}_{\rm NLL} = i\pi \mathbf{T}^2_{s-u} \tag{5.27a}$$

$$\mathbf{\Gamma}^{(-,2)}_{\rm NLL} = 0 \tag{5.27b}$$

$$\mathbf{\Gamma}^{(-,3)}_{\rm NLL} = 0 \tag{5.27c}$$

$$\mathbf{\Gamma}^{(-,4)}_{\rm NLL} = -i\pi \frac{\zeta_3}{24} C_A (C_A - \mathbf{T}_t^2)^2 \mathbf{T}^2_{s-u} \tag{5.27d}$$

$$\mathbf{\Gamma}^{(-,5)}_{\rm NLL} = -i\pi \frac{\zeta_4}{128} C_A (C_A - \mathbf{T}_t^2)^3 \mathbf{T}^2_{s-u} \tag{5.27e}$$

$$\mathbf{\Gamma}^{(-,6)}_{\rm NLL} = -i\pi \frac{\zeta_5}{640} C_A (C_A - \mathbf{T}_t^2)^4 \mathbf{T}^2_{s-u} \tag{5.27f}$$

$$\mathbf{\Gamma}^{(-,7)}_{\rm NLL} = i\pi \frac{1}{720} \left[\frac{\zeta_3^2}{16} C_A^2 (C_A - \mathbf{T}_t^2)^4 + \frac{1}{32} \left(\zeta_3^2 - 5\zeta_6 \right) C_A (C_A - \mathbf{T}_t^2)^5 \right] \mathbf{T}^2_{s-u} \tag{5.27g}$$

$$\begin{aligned} \mathbf{\Gamma}^{(-,8)}_{\rm NLL} = i\pi \frac{1}{5040} \Bigg[& \frac{3\zeta_3\zeta_4}{32} C_A^2 (C_A - \mathbf{T}_t^2)^5 \\ & + \frac{3}{64} \left(\zeta_3\zeta_4 - 3\zeta_7 \right) C_A (C_A - \mathbf{T}_t^2)^6 \Bigg] \mathbf{T}^2_{s-u} \end{aligned} \tag{5.27h}$$

These results are valid in any gauge theory, and hold modulo colour operators which vanish when acting on the Regge limit of the tree amplitude (which is given by the colour structure of the t-channel tree amplitude).

5.1.3 Properties of the soft anomalous dimension in the Regge limit

In the previous section we computed $\mathbf{\Gamma}^{(-)}_{\rm NLL}$, the imaginary part of the soft anomalous dimension in the Regge limit, to all orders. Let us briefly explore its properties addressing the colour structure, the convergence of the expansion, and finally its asymptotic high-energy behaviour.

Considering eq. (5.27a), our first observation is that colour structures of increasing complexity emerge every three loops, as dictated by the expansion of $R(\epsilon)$ in eq. (3.20): corrections going beyond the dipole formula start at four loops, where the colour structure is proportional to C_A to a single power. This correction reproduces precisely that found previously in ref. [25]. Proceeding to five and six loops $\mathbf{\Gamma}_{\rm NLL}$ only incurs extra powers of $(C_A - \mathbf{T}_t^2)$. Starting at seven loops, however terms with two powers of C_A appear as well. Similarly, a cubic power of C_A would emerge at ten loops, and so on. We also note that the zeta values appearing in $\mathbf{\Gamma}_{\rm NLL}$ are of uniform weight, which is, of course, again a mere consequence of the Taylor series of $R(\epsilon)$.

To proceed it would be useful to specify the relevant colour charge exchanged in the t channel, $\mathbf{T}_t^2$. To this end consider for example gluon-gluon scattering, where the t channel colour flow can be any of the SU(N_c) representations appearing in the decomposition

$$8 \otimes 8 = 1 \oplus 8_s \oplus 8_a \oplus 10 \oplus \overline{10} \oplus 27 \oplus 0 \tag{5.28}$$

where the labels refer to their dimensions[2] for $N_c = 3$. Because of Bose symmetry, the symmetry of the colour structure mirrors the signature of the corresponding amplitudes under $s \leftrightarrow u$ exchange. Thus, only even representations are relevant for the two-reggeon amplitude discussed here; these are the singlet, where $\mathbf{T}_t^2 = 0$, the symmetric octet with $\mathbf{T}_t^2 = C_A = N_c$, the 27 representation with $\mathbf{T}_t^2 = 2(N_c + 1)$, and the "0" representation, where $\mathbf{T}_t^2 = 2(N_c - 1)$. In the following we restrict the discussion to the first three cases, which are all relevant for QCD with $N_c = 3$ (the latter has a vanishing dimension, and hence it does not contribute).

The next observation, already mentioned in section 3.2, is that the symmetric octet representation with $\mathbf{T}_t^2 = C_A$, corresponds to a constant wavefunction, and thus a trivial solution to eq. (2.27), with no corrections to the reduced amplitude beyond one loop (as can be verified for example in the explicit results in eqs. (3.21) through (3.24) upon considering $\mathbf{T}_t^2 = C_A$). The reduced amplitude for the symmetric octet state is thus one-loop exact, corresponding to a simple Regge-pole behaviour with a gluon Regge trajectory for the original amplitude according to eq. (2.18). This of course reproduces the known behaviour of the symmetric-octet exchange used in the original derivation of the BFKL equation. In turn, for the singlet — the famous pomeron — and 27 representation, we find non-trivial radiative corrections associated with a Regge cut. We will thus use these two examples in the discussion that follows.

Let us consider the convergence properties of the perturbative series representing the soft anomalous dimension in eq. (5.23). One immediately notes that this series is highly convergent due to the $1/(\ell-1)!$ prefactor in eq. (5.24). Figure 5.1 illustrates this factorial suppression of the coefficients $G^{(\ell)}$ as a function of the order ℓ for $C_A = N_c = 3$ and for the two relevant representations, the singlet and the 27.

[2]The dimensions for general N_c are: $\dim(8) = N_c^2 - 1$, $\dim(10) = (N_c^2 - 4)(N_c^2 - 1)/4$, $\dim(27) = N_c^2(N_c + 3)(N_c - 1)/4$ and $\dim(0) = N_c^2(N_c - 3)(N_c + 1)/4$. Note that the latter vanishes for $N_c = 3$. A more complete exposition of the t-channel colour flow basis can be found in refs. [22, 26].

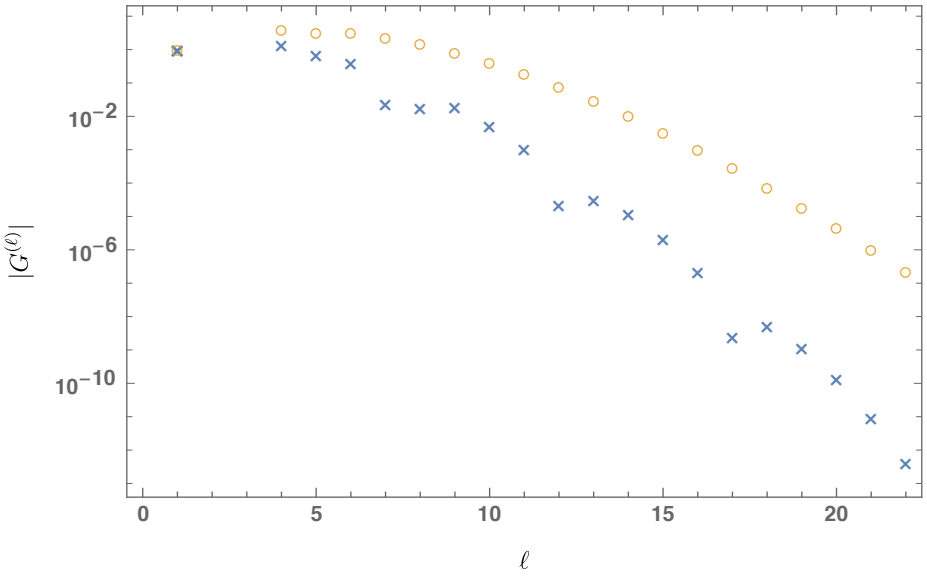

Figure 5.1: Logarithmic plot of the absolute value of the coefficients $G^{(\ell)}$ (5.30), for $\ell = 1, \ldots, 22$. The $|G^{(\ell)}|$ quickly become very small suggesting good convergence of the series. Shown is the singlet (crosses) and 27 exchange (circles).

Furthermore, we can establish that the anomalous dimension (5.25) has *an infinite radius of convergence* as a function of $x \equiv L\alpha_s/\pi$. To see this we write the resummed soft anomalous dimension as:

$$\mathbf{\Gamma}^{(-)}_{\rm NLL} = i\pi \frac{\alpha_s}{\pi} G\left(\frac{\alpha_s}{\pi} L\right) \mathbf{T}^2_{s-u} \tag{5.29}$$

where the generating function for the expansion coefficients is defined by

$$G(x) = \sum_{\ell=1}^{\infty} x^{\ell-1} G^{(\ell)} \tag{5.30}$$

It is convenient to further identify $G(x)$ as the Borel transform of some function

$$g(y) \equiv \int_0^\infty \mathrm{d}x G(x) e^{-x/y} = \sum_{\ell=1}^{\infty} G^{(\ell)} y^\ell (\ell-1)! \tag{5.31}$$

which upon using eq. (5.24), simply evaluates to

$$g(y) = y\left(1 - R\left(\frac{y}{2}(C_A - \mathbf{T}_t^2)\right) \frac{C_A}{(C_A - \mathbf{T}_t^2)}\right)^{-1}. \tag{5.32}$$

We may now recover the original $G(x)$ via the integral

$$G(x) = \frac{1}{2\pi i} \int_{w-i\infty}^{w+i\infty} \mathrm{d}\eta g\left(\frac{1}{\eta}\right) e^{\eta x} \tag{5.33}$$

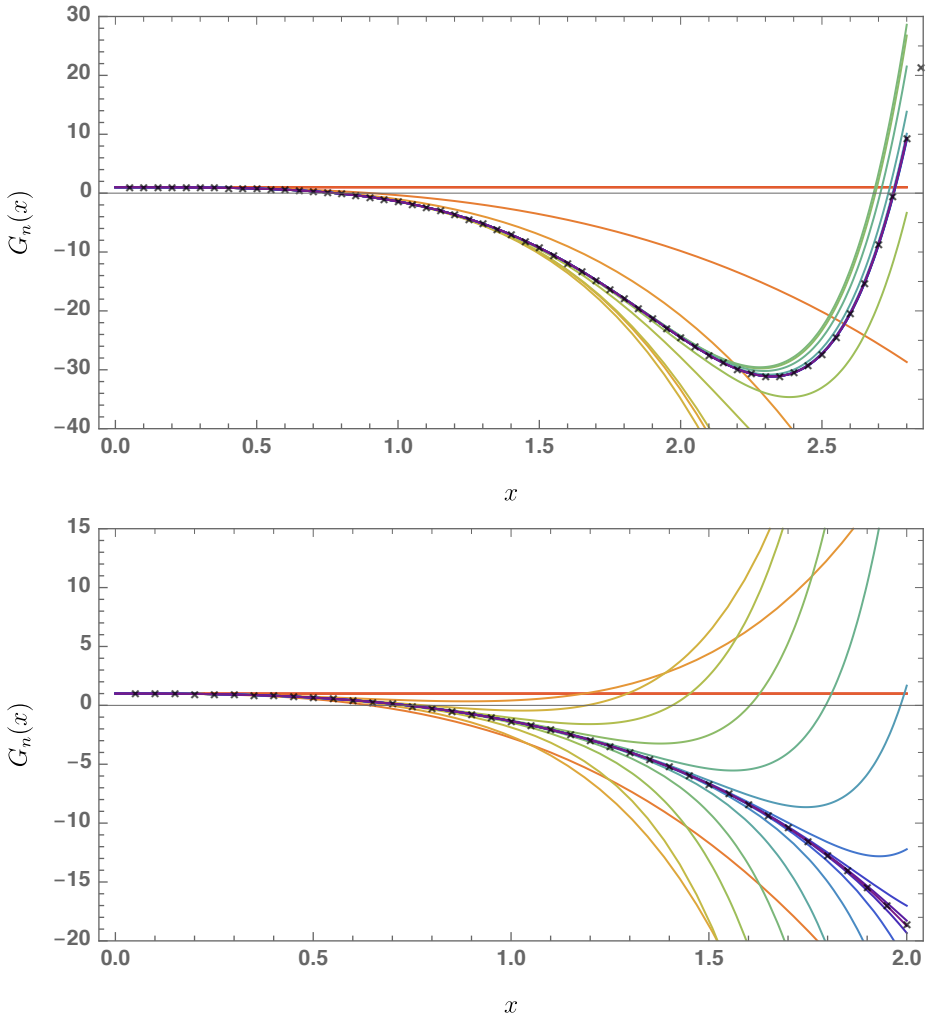

Figure 5.2: Partial sums $G_n(x) = \sum_{\ell=1}^{n} G^{(\ell)} x^{\ell-1}$ for $n = 1, \ldots, 22$ (rainbow, red through violet) and numerical results for $G(x)$ (black crosses). The plot illustrates convergence in that increasing the order n extends the range of x for which the partial sum matches the numerical result. The figure shows the singlet (top) as well as the 27 exchange (bottom).

where the integration contour runs parallel to the imaginary axis, to the right of all singularities of the integrand.

The function $g(y)$ in eq. (5.31) only has isolated poles away from the origin and has a finite radius of convergence: it is well-defined in a disc around the origin. It then follows that $G(x)$ has an infinite radius of convergence, hence this function — and the soft anomalous dimension $\mathbf{\Gamma}^{(-)}_{\text{NLL}}$ in eq. (5.29) — is *an entire function*, free of singularities for any finite $x = \alpha_s L/\pi$.

We stress that our use of the Borel transform is opposite to the usual application of Borel summation (which is ordinarily used to sum asymptotic series): the function $G(x)$, in which we are interested, is an entire function; we make use of its *inverse* Borel transform, $g(y)$, which has *worse* behaviour by having merely a finite radius of convergence. Nonetheless we find that numerically integrating eq. (5.33) is a particularly convenient way to evaluate the anomalous dimension. This numerical integration is compared to the partial sums

$$G_n(x) \equiv \sum_{\ell=1}^{n} G^{(\ell)} x^{\ell-1} \tag{5.34}$$

in figure 5.2, where we find good agreement for the given values of x. While it becomes challenging to efficiently compute the coefficients $G^{(\ell)}$ at high orders (here we only evaluated them for $\ell \leq 22$), we find the numerical integration of eq. (5.33) to be very stable, even for larger values of x. Thus, the remarkable convergence properties of $G(x)$ along with the Borel technique, presents us with the possibility of computing $\Gamma^{(-)}_{\text{NLL}}$ for $x = \alpha_s L/\pi \gg 1$, i.e. at asymptotically high energies. This is a rather unique situation in a perturbative setting — in other circumstances resummation techniques are limited to the region $x = \alpha_s L/\pi \lesssim 1$.

Evaluating the integral (5.33) and plotting $G(x)$ for larger values of x reveals oscillations with a constant period and an exponentially growing amplitude. Since this behaviour is difficult to capture graphically we instead show the logarithm of $|G(x)|$ weighted by the sign of $G(x)$ in figure 5.3. This observation suggests to approximate $G(x)$ in eq. (5.33) by

$$G(x) \longrightarrow c e^{ax} \cos(bx + d) \tag{5.35}$$

for sufficiently large values of x. By means of eq. (5.31), this model is equivalent to

$$g\left(\frac{1}{\eta}\right) \longrightarrow c\Re\left[\frac{e^{id}}{\eta - a - ib}\right] = \frac{c}{2}\left(\frac{e^{id}}{\eta - a - ib} + \frac{e^{-id}}{\eta - a + ib}\right) \tag{5.36}$$

which is to be integrated as in eq. (5.33) with a contour to the right of the poles. We thus find that to capture the behaviour $G(x)$ at large x it is sufficient to simply consider $g\left(\frac{1}{\eta}\right)$ as a pair of complex-conjugated poles at $\eta = a \pm ib$. Indeed, numerically extracting the rightmost poles of $g\left(\frac{1}{\eta}\right)$ of eq. (5.32) to identify the parameters a and b in eq. (5.36), and dividing the full, numerically-evaluated, $G(x)$ by e^{ax} leaves us with almost pure cosine-like behaviour for any $x \gg 1$. The rather impressive agreement

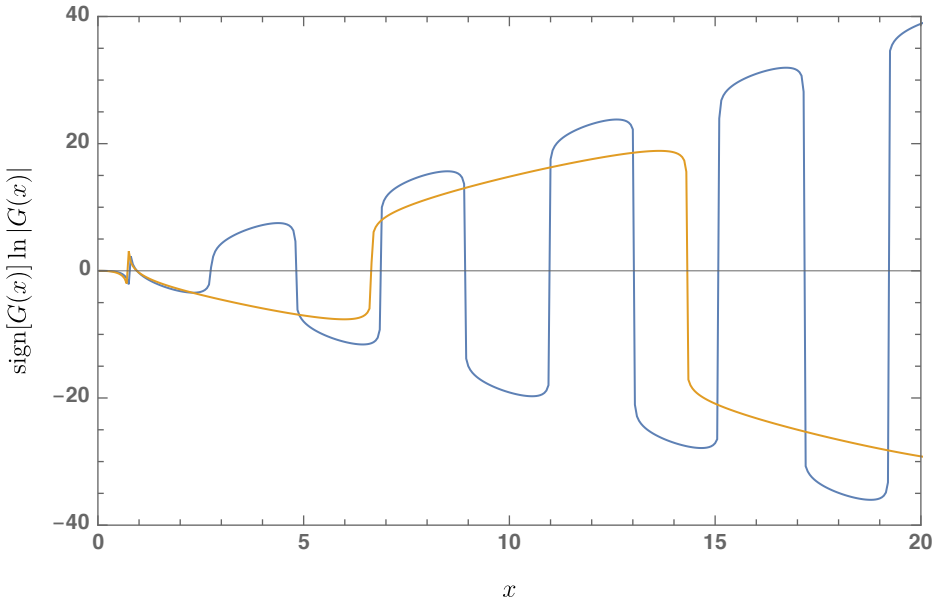

Figure 5.3: Numerical results for $\mathrm{sign}\,[G(x)]\log|G(x)|$ for the singlet (blue) and 27 exchange (orange). The "heartbeat" at small x reflects the logarithmic divergence of $\log|G(x)|$ where $G(x)$ changes its sign for the first time (similar divergences occur every oscillation but are not visible due to the finite resolution of the plot).

	a	b	c	d
1	1.97	1.52	0.25	0.48
27	1.46	0.41	0.58	2.01

Table 5.1: Numerical results for a, b, c and d, cf. eq. (5.35), for the singlet (1) and 27 representation.

between the simple model (5.35) and the numerical results can be seen in figure 5.4. For reference, we quote our numerical results for a, b, c and d in table 5.1.

5.1.4 Exponentiation check for higher-order infrared poles

As a final step we confirm the agreement between the BFKL prediction and the soft factorisation theorem. Thus far we have only used the single poles as predicted by the BFKL evolution to extract the NLL soft anomalous dimension $\mathbf{\Gamma}^{(-)}_{\mathrm{NLL}}$. As explained in section 5.1.1, higher-order poles of the amplitude are generated upon expansion of the path-ordered exponential in eq. (5.17). They have to match the BFKL computation and therefore provide an independent and non-trivial check of our results.

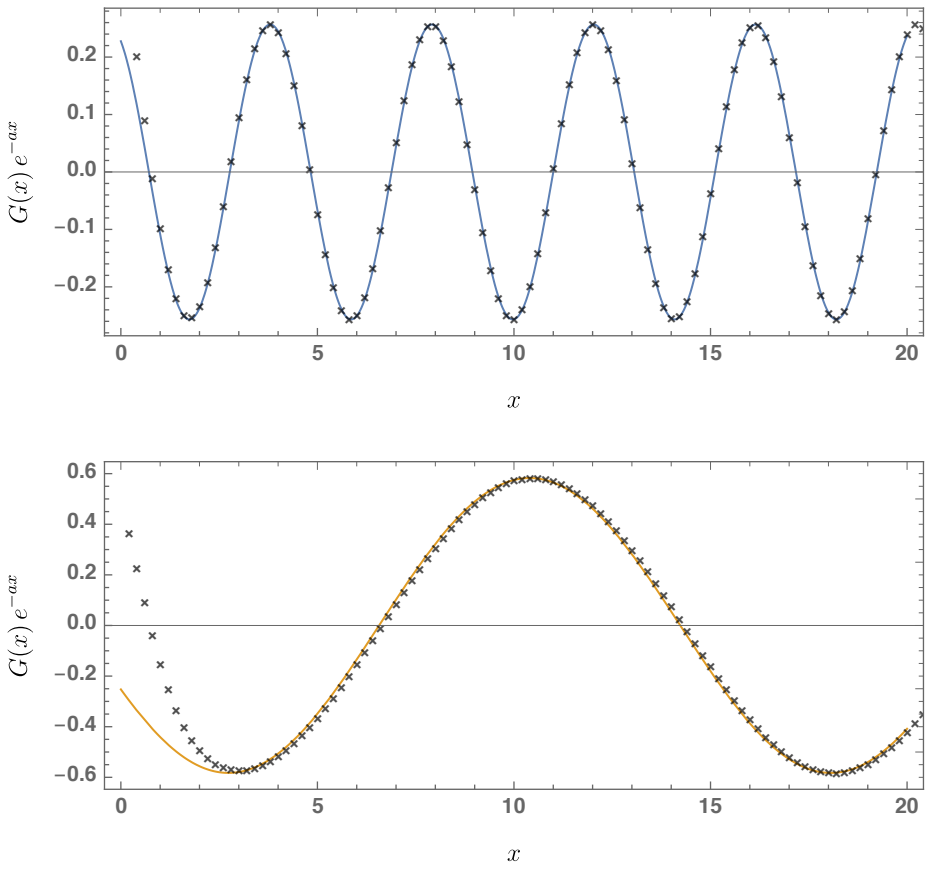

Figure 5.4: The approximation of eq. (5.35) for $G(x)$ for $x \gg 1$, divided by e^{ax} (solid line) contrasted with numerical results (crosses). The coefficients a and b were extracted from the poles of $g(1/\eta)$ while c and d were fitted after dividing the full, numerically evaluated, $G(x)$ by e^{ax}. Already for moderate values of x we observe excellent agreement. The singlet exchange is shown at the top and the 27 is at the bottom.

To see how this works, let us expand the BFKL result (5.19) to the first few orders, namely

$$\bar{\mathcal{M}}^{(+)}_{\text{NLL}}\left(\frac{s}{-t}\right) = \sum_{\ell=1}^{\infty}\left(\frac{\alpha_s}{\pi}\right)^{\ell} L^{\ell-1}\bar{\mathcal{M}}^{(+,\ell)}_{\text{NLL}} \tag{5.37}$$

with

$$\bar{\mathcal{M}}^{(+,1)}_{\text{NLL}} = i\pi\left[\frac{1}{2\epsilon} + \mathcal{O}(\epsilon^0)\right]\mathbf{T}^2_{s-u}\mathcal{M}^{(\text{tree})} \tag{5.38a}$$

$$\bar{\mathcal{M}}^{(+,2)}_{\text{NLL}} = i\pi\frac{(C_A - \mathbf{T}_t^2)}{2!}\left[\frac{1}{(2\epsilon)^2} + \mathcal{O}(\epsilon^0)\right]\mathbf{T}^2_{s-u}\mathcal{M}^{(\text{tree})} \tag{5.38b}$$

$$\bar{\mathcal{M}}^{(+,3)}_{\text{NLL}} = i\pi\frac{(C_A - \mathbf{T}_t^2)^2}{3!}\left[\frac{1}{(2\epsilon)^3} + \mathcal{O}(\epsilon^0)\right]\mathbf{T}^2_{s-u}\mathcal{M}^{(\text{tree})} \tag{5.38c}$$

$$\bar{\mathcal{M}}^{(+,4)}_{\rm NLL} = i\pi\frac{(C_A-\mathbf{T}_t^2)^3}{4!}\left[\frac{1}{(2\epsilon)^4}-\frac{1}{2\epsilon}\frac{\zeta_3 C_A}{4(C_A-\mathbf{T}_t^2)}+\mathcal{O}(\epsilon^0)\right]\mathbf{T}^2_{s-u}\mathcal{M}^{(\rm tree)} \tag{5.38d}$$

$$\bar{\mathcal{M}}^{(+,5)}_{\rm NLL} = i\pi\frac{(C_A-\mathbf{T}_t^2)^4}{5!}\left[\frac{1}{(2\epsilon)^5}-\frac{1}{(2\epsilon)^2}\frac{\zeta_3 C_A}{4(C_A-\mathbf{T}_t^2)}\right.$$
$$\left.-\frac{1}{2\epsilon}\frac{3\zeta_4 C_A}{16(C_A-\mathbf{T}_t^2)}+\mathcal{O}(\epsilon^0)\right]\mathbf{T}^2_{s-u}\mathcal{M}^{(\rm tree)} \tag{5.38e}$$

Let us begin with the leading pole. One can see a simple pattern in its ℓ-th order coefficient, which is proportional to $(C_A-\mathbf{T}_t^2)^{\ell-1}/(\ell!(2\epsilon)^\ell)$. This should be compared with the prediction (5.17) from infrared exponentiation, which we reproduce here for convenience:

$$\bar{\mathcal{M}}^{(+)}_{\rm NLL} = -\int_0^p\frac{\mathrm{d}\lambda}{\lambda}\exp\left\{\frac{1}{2\epsilon}\frac{\alpha_s(p)}{\pi}L(C_A-\mathbf{T}_t^2)\left[1-\left(\frac{p^2}{\lambda^2}\right)^\epsilon\right]\right\}$$
$$\times\,\mathbf{\Gamma}^{(-)}_{\rm NLL}\left(\alpha_s(\lambda)\right)\mathcal{M}^{(\rm tree)}+\mathcal{O}(\epsilon^0) \tag{5.39}$$

Substituting $\mathbf{\Gamma}^{(-)}_{\rm NLL}$ using eqs. (5.26) and (5.23), and taking into account that the running coupling $\alpha_s(\mu)=\alpha_s(p)\left(p^2/\mu^2\right)^\epsilon$, one gets

$$\bar{\mathcal{M}}^{(+)}_{\rm NLL} = -i\pi\sum_{k=1}^{\infty}G^{(k)}\left(\frac{\alpha_s(p)}{\pi}\right)^k L^{k-1}\int_0^p\frac{\mathrm{d}\lambda}{\lambda}\left(\frac{p^2}{\lambda^2}\right)^{\epsilon k}$$
$$\times\exp\left\{\frac{1}{2\epsilon}\frac{\alpha_s(p)}{\pi}L(C_A-\mathbf{T}_t^2)\left[1-\left(\frac{p^2}{\lambda^2}\right)^\epsilon\right]\right\}\mathbf{T}^2_{s-u}\mathcal{M}^{(\rm tree)}+\mathcal{O}(\epsilon^0) \tag{5.40}$$

For the leading pole it is clear that only the $G^{(1)}$ terms contribute, corresponding to the one-loop contribution to the soft anomalous dimension (5.10), and we then get:

$$\left[\bar{\mathcal{M}}^{(+)}_{\rm NLL}\right]_{\text{leading poles}} = -i\pi\frac{\alpha_s(p)}{\pi}\int_0^p\frac{\mathrm{d}}{\mathrm{d}\lambda}\left(\frac{p}{\lambda}\right)^\epsilon$$
$$\times\exp\left\{\frac{1}{2\epsilon}\frac{\alpha_s(p)}{\pi}L(C_A-\mathbf{T}_t^2)\left[1-\left(\frac{p}{\lambda}\right)^\epsilon\right]\right\}\mathbf{T}^2_{s-u}\mathcal{M}^{(\rm tree)}$$
$$=-i\pi\left[\frac{\exp\left\{\frac{1}{2\epsilon}\frac{\alpha_s(p)}{\pi}L(C_A-\mathbf{T}_t^2)\right\}-1}{L(C_A-\mathbf{T}_t^2)}\right]\mathbf{T}^2_{s-u}\mathcal{M}^{(\rm tree)}. \tag{5.41}$$

Expanding in α_s this matches precisely the $1/(\ell!(2\epsilon)^\ell)$ terms in eqs. (5.38a)–(5.38e), with the correct prefactor. This exponentiation of leading poles had been verified previously in ref. [25]. Moving on to the first subleading pole, the Regge prediction reveals a four-loop single pole in eq. (5.38d), as well as a five-loop double pole in eq. (5.38e) and so on, all proportional to ζ_3. In general, expanding the BFKL result (5.19) to higher orders one finds a tower of such terms going like $1/(\ell!(2\epsilon)^{\ell-3})$. In the infrared

exponentiation formula, these should be generated by a single parameter, the four-loop anomalous dimension, $\mathbf{\Gamma}^{(-,4)}_{\text{NLL}}$, which is indeed proportional to ζ_3 (see eq. (5.27a)). It can be traced back to the leading-order term in the expansion of $R(\epsilon)$ in eq. (3.20), contributing to $G^{(4)}$ in eq. (5.24). Similarly, a k-loop anomalous dimension $\mathbf{\Gamma}^{(-,k)}_{\text{NLL}}$, in general, contributes in proportion to $G^{(k)}$. Indeed, integrating eq. (5.40) we find that

$$\bar{\mathcal{M}}^{(+)}_{\text{NLL}} = \frac{i\pi}{2\epsilon}\sum_{k=1}^{\infty} G^{(k)}(k-1)!\sum_{\ell=k}^{\infty}\frac{1}{\ell!}\left(\frac{\alpha_s(p)}{\pi}\right)^{\ell} L^{\ell-1}\left(\frac{(C_A-\mathbf{T}_t^2)}{2\epsilon}\right)^{\ell-k} \times \mathbf{T}^2_{s-u}\mathcal{M}^{(\text{tree})} + \mathcal{O}(\epsilon^0) \quad (5.42)$$

Next we note that given k, all contributions with $\ell < k$ are either constant or vanish for $\epsilon \to 0$, and so in as far as the singularities are concerned the sum over ℓ can be performed over all positive integers, independently of k. This yields

$$\bar{\mathcal{M}}^{(+)}_{\text{NLL}} = i\pi\sum_{k=1}^{\infty}\frac{G^{(k)}(k-1)!(2\epsilon)^{k-1}}{L(C_A-\mathbf{T}_t^2)^k}\left[\exp\left\{\frac{1}{2\epsilon}\frac{\alpha_s}{\pi}L(C_A-\mathbf{T}_t^2)\right\}-1\right] \times \mathbf{T}^2_{s-u}\mathcal{M}^{(\text{tree})} + \mathcal{O}(\epsilon^0). \quad (5.43)$$

This shows that infrared exponentiation works out *if*, and *only if*, all the poles in the NLL amplitude can be written as a function of ϵ only (i.e. independent of α_s), times the quantity in the square bracket. With hindsight, infrared exponentiation thus explains the compact form of the BFKL result in eq. (5.19). Finally, it is straightforward to substitute in the definition of $G^{(k)}$ from eq. (5.24) and sum up the series over k, recovering the full result for the singularities of the amplitudes in eq. (5.19). This completes the proof that the BFKL result we obtained is consistent with infrared factorisation.

5.2 Resummation in two dimensions

At the time of writing the fully-resummed amplitude remains elusive. The crux of the matter is the intricate structure of the BFKL evolution in two dimensions which was discussed in chapter 4. In this limit, the wavefunction is a complicated linear combination of SVHPLs that, even after a number of simplifications, cf. section 4.3.2, we were not able to find a closed form for.[3]

[3]In fact, some of the terms of the wavefunction follow a very simple pattern, e.g. the coefficients of $(C_A-\mathbf{T}_t^2)^\ell$ at ℓ loops. For an in-depth discussion, see section 5.3.

Moreover, the computation of the "last integral" (2.25) in two dimensions is rather involved compared to its equivalent in the soft limit, cf. eq. (4.71) vs. eq. (3.7) with eq. (3.14). In other words, even if the two-dimensional wavefunction was known to any loop order it would be difficult to infer from it the corresponding amplitude.

Nonetheless, there are cases of resummation in two dimensions that are worth mentioning and we shall do so in the following sections 5.2.1–5.3. Through the following discussion we aim to share our insights and especially hope to inspire future research in this area.

5.2.1 Exponentiation of the two-dimensional soft wavefunction

The $\epsilon \to 0$ limit of the soft wavefunction (3.14) exponentiates. For this purpose define

$$\Omega_{\text{2d,s}}(p,k) \equiv \sum_{\ell=1}^{\infty} \left(\frac{\alpha_s}{\pi}\right)^{\ell} L^{\ell-1} \frac{\Omega_{\text{s}}^{(\ell-1)}(p,k)\big|_{\mathcal{O}(\epsilon^0)}}{(\ell-1)!} \tag{5.44}$$

by analogy with eq. (2.22). Here, the coefficients $\Omega_{\text{s}}^{(\ell-1)}(p,k)\big|_{\mathcal{O}(\epsilon^0)}$ are the $\mathcal{O}(\epsilon^0)$ terms in the expansion of eq. (3.14) for a given ℓ.

One observes a simple pattern on the r.h.s. of eq. (5.44), especially when using the colour factors $C_1 = 2C_A - \mathbf{T}_t^2$, $\tilde{C}_2 = \frac{1}{2}(C_A - \mathbf{T}_t^2)$ and rescaled zeta numbers $\tilde{\zeta}_n = \zeta_n/n$.

$$\Omega_{\text{s}}^{(0)}(p,k)\big|_{\mathcal{O}(\epsilon^0)} = 1 \tag{5.45a}$$

$$\Omega_{\text{s}}^{(1)}(p,k)\big|_{\mathcal{O}(\epsilon^0)} = \tilde{C}_2 \log\left(\frac{k^2}{p^2}\right) \tag{5.45b}$$

$$\frac{1}{2}\Omega_{\text{s}}^{(2)}(p,k)\big|_{\mathcal{O}(\epsilon^0)} = \frac{\tilde{C}_2^2}{2} \log^2\left(\frac{k^2}{p^2}\right) \tag{5.45c}$$

$$\frac{1}{3!}\Omega_{\text{s}}^{(3)}(p,k)\big|_{\mathcal{O}(\epsilon^0)} = \frac{\tilde{C}_2^3}{3!} \log^3\left(\frac{k^2}{p^2}\right) + C_1\tilde{C}_2^2\tilde{\zeta}_3 \tag{5.45d}$$

$$\frac{1}{4!}\Omega_{\text{s}}^{(4)}(p,k)\big|_{\mathcal{O}(\epsilon^0)} = \frac{\tilde{C}_2^4}{4!} \log^4\left(\frac{k^2}{p^2}\right) + C_1\tilde{C}_2^3\tilde{\zeta}_3 \log\left(\frac{k^2}{p^2}\right) \tag{5.45e}$$

$$\frac{1}{5!}\Omega_{\text{s}}^{(5)}(p,k)\big|_{\mathcal{O}(\epsilon^0)} = \frac{\tilde{C}_2^5}{5!} \log^5\left(\frac{k^2}{p^2}\right) + C_1\tilde{C}_2^4\left(\frac{\tilde{\zeta}_3}{2} \log^2\left(\frac{k^2}{p^2}\right) + \tilde{\zeta}_5\right) \tag{5.45f}$$

$$\begin{aligned}\frac{1}{6!}\Omega_{\text{s}}^{(6)}(p,k)\big|_{\mathcal{O}(\epsilon^0)} = {} & \frac{\tilde{C}_2^6}{5!} \log^6\left(\frac{k^2}{p^2}\right) + C_1^2\tilde{C}_2^4\frac{\tilde{\zeta}_3^2}{2} \\ & + C_1\tilde{C}_2^5\left(\frac{\tilde{\zeta}_3}{2} \log^3\left(\frac{k^2}{p^2}\right) + \tilde{\zeta}_5 \log\left(\frac{k^2}{p^2}\right)\right)\end{aligned} \tag{5.45g}$$

It suggests that the two-dimensional soft wavefunction can be resummed and, indeed, we find

$$\Omega_{\rm 2d,s}(p,k) = \frac{\alpha_s}{\pi}\left[e^{-x\gamma_{\rm E}(C_A-\mathbf{T}_t^2)}\frac{\Gamma\left(1-\frac{x}{2}(C_A-\mathbf{T}_t^2)\right)}{\Gamma\left(1+\frac{x}{2}(C_A-\mathbf{T}_t^2)\right)}\right]^{\frac{2C_A-\mathbf{T}_t^2}{C_A-\mathbf{T}_t^2}} e^{\frac{x}{2}(C_A-\mathbf{T}_t^2)\log\left(\frac{k^2}{p^2}\right)}. \quad (5.46)$$

where $x = \alpha_s L/\pi$.

We stress that eq. (5.46) only governs contributions from the limit $k \to 0$. We also know that contributions arise from $k \to p$, the other soft limit. These can be obtained from eq. (5.46) upon replacing $\log(k^2/p^2) \to \log((k-p)^2/p^2)$, see chapter 3. In the two-dimensional variables introduced in section 4.2, cf. eq. (4.8), these logarithms correspond to $\log(|z|^2/|z-1|^2)$ and $\log 1/|z-1|^2$, respectively. It is natural to sum the two limits at this point and restore the symmetry of the two-dimensional wavefunction under $z \leftrightarrow 1/z$, see e.g. section 4.3. In the language of section 4.3.2 we thus have

$$\log\left(\frac{k^2}{p^2}\right) + \log\left(\frac{(p-k)^2}{p^2}\right) \longrightarrow \log\left(\frac{z\bar{z}}{(1-z)^2(1-\bar{z})^2}\right) = \mathcal{L}_s(z,\bar{z}). \quad (5.47)$$

This is precisely what was done to symmetrise the D-dimensional soft wavefunction under $k \leftrightarrow k-p$ in section 4.1. With the "tilde" notation introduced there the resummed symmetric soft wavefunction is given by

$$\tilde{\Omega}_{\rm 2d,s}(z,\bar{z}) = \frac{\alpha_s}{\pi}\left[e^{-x\gamma_{\rm E}(C_A-\mathbf{T}_t^2)}\frac{\Gamma\left(1-\frac{x}{2}(C_A-\mathbf{T}_t^2)\right)}{\Gamma\left(1+\frac{x}{2}(C_A-\mathbf{T}_t^2)\right)}\right]^{\frac{2C_A-\mathbf{T}_t^2}{C_A-\mathbf{T}_t^2}} e^{\frac{x}{2}(C_A-\mathbf{T}_t^2)\mathcal{L}_s(z,\bar{z})}. \quad (5.48)$$

5.2.2 Evolution of the two-dimensional hard wavefunction

In order to separate soft and hard finite contributions to the amplitude we introduced the two-dimensional hard wavefunction $\Omega_{\rm 2d,h}$ in section 4.4, cf. eq. (4.69). The additive definition used there facilitated the transition from the wavefunction to the amplitude and recombination of finite terms. It is, however, not the only way to define a hard wavefunction.

To describe the evolution of the wavefunction in two dimensions it turns out a multiplicative definition is more appropriate. To this end let us define the *purely-hard* wavefunction $\tilde{\Omega}_{\rm 2d,h}$ (note the "tilde") according to

$$\Omega_{\rm 2d}(z,\bar{z}) = \tilde{\Omega}_{\rm 2d,h}(z,\bar{z})\tilde{\Omega}_{\rm 2d,s}(z,\bar{z}) \quad (5.49)$$

with $\Omega_{\rm 2d,s}(z,\bar{z})$ as given in eq. (5.48). Both $\Omega_{\rm 2d}$ and $\tilde{\Omega}_{\rm 2d,h}$ have loop expansions analogous to eq. (5.44).

The two-dimensional purely-hard wavefunction $\tilde{\Omega}_{\rm 2d,h}$ has interesting properties. First of all it has zero boundary conditions — it tends to 1 in both the $z \to 0$ and the $z \to \infty$ limit, i.e. all its perturbative corrections $\tilde{\Omega}^{(\ell)}_{\rm 2d,h}$ for $l \geq 1$ vanish. Second, it is generated by a modified BFKL evolution that we shall derive in the following.

To begin note that $\hat{H}_{\rm 2d}\Omega^{(\ell-1)}_{\rm 2d} = \Omega^{(\ell)}_{\rm 2d}$ is consistent with $\frac{\rm d}{{\rm d}x}\Omega_{\rm 2d} = \hat{H}_{\rm 2d}\Omega_{\rm 2d}$ and the loop expansion of $\Omega_{\rm 2d}$ (2.22) where $x = \alpha_s L/\pi$. Hence,

$$\begin{aligned}\hat{H}_{\rm 2d}\Omega_{\rm 2d}(z,\bar{z}) &= \frac{\rm d}{{\rm d}x}\left[\tilde{\Omega}_{\rm 2d,h}(z,\bar{z})\tilde{\Omega}_{\rm 2d,s}(z,\bar{z})\right] \\ &= \frac{\rm d}{{\rm d}x}\left[\tilde{\Omega}_{\rm 2d,h}(z,\bar{z})\right]\tilde{\Omega}_{\rm 2d,s}(z,\bar{z}) + \tilde{\Omega}_{\rm 2d,h}(z,\bar{z})\frac{\rm d}{{\rm d}x}\left[\tilde{\Omega}_{\rm 2d,s}(z,\bar{z})\right] \quad (5.50)\end{aligned}$$

which we solve for $\frac{\rm d}{{\rm d}x}\tilde{\Omega}_{\rm 2d,h}$ and replace the remaining derivatives by the actions of the corresponding Hamiltonians.

$$\frac{\rm d}{{\rm d}x}\tilde{\Omega}_{\rm 2d,h}(z,\bar{z}) = \tilde{\Omega}^{-1}_{\rm 2d,s}(z,\bar{z})\left(\hat{H}_{\rm 2d}\tilde{\Omega}_{\rm 2d,h}(z,\bar{z}) - \tilde{\Omega}_{\rm 2d,s}(z,\bar{z})\hat{H}_{\rm s}\right)\tilde{\Omega}_{\rm 2d,s}(z,\bar{z}) \quad (5.51)$$

According to eq. (5.47) we add the $k \to p$ (i.e. $z \to \infty$) contribution to the definition of $J_{\rm s}$ (3.3) inside $\hat{H}_{\rm s}$ (3.5). In two dimensions this amounts to $J_{\rm s}(p,k) \to j(z,\bar{z}) = \mathcal{L}_s(z,\bar{z})/2$, cf. eqs. (4.11) and (5.47). Since the action of $j(z,\bar{z})$ is multiplicative its contribution immediately cancels between the two terms in the parentheses in the above equation.

Likewise, the integral in $\hat{H}_{\rm s}$ (3.5) in two dimensions becomes nothing but the action of $\hat{H}_{\rm 2d,i}$ as can be easily verified. Therefore, eq. (5.51) can be written

$$\begin{aligned}\frac{\rm d}{{\rm d}x}\tilde{\Omega}_{\rm 2d,h}(z,\bar{z}) &= \tilde{\Omega}^{-1}_{\rm 2d,s}(z,\bar{z})\left(\hat{H}_{\rm 2d,i}\tilde{\Omega}_{\rm 2d,h}(z,\bar{z}) - \tilde{\Omega}_{\rm 2d,s}(z,\bar{z})\hat{H}_{\rm 2d,i}\right)\tilde{\Omega}_{\rm 2d,s}(z,\bar{z}) \quad (5.52)\\ &= e^{-\frac{x}{2}(C_A-\mathbf{T}_t^2)\mathcal{L}_s(z,\bar{z})}\Big(\hat{H}_{\rm 2d,i}\tilde{\Omega}_{\rm 2d,h}(z,\bar{z}) \\ &\qquad -\tilde{\Omega}_{\rm 2d,s}(z,\bar{z})\hat{H}_{\rm 2d,i}\Big)\, e^{\frac{x}{2}(C_A-\mathbf{T}_t^2)\mathcal{L}_s(z,\bar{z})} \quad (5.53)\end{aligned}$$

where we have plugged in the symmetrised resummed $\tilde{\Omega}_{\rm 2d,s}$ (5.48) and cancelled z-independent terms which commute with the parentheses. Lastly, we use the action of $\hat{H}_{\rm 2d,i}$ to arrive at

$$\frac{\rm d}{{\rm d}x}\tilde{\Omega}_{\rm 2d,h}(z,\bar{z}) = \frac{1}{4\pi}\int {\rm d}^2w\tilde{K}(w,\bar{w},z,\bar{z})\left[\tilde{\Omega}_{\rm 2d,h}(w,\bar{w}) - \tilde{\Omega}_{\rm 2d,h}(z,\bar{z})\right] \quad (5.54)$$

with

$$\tilde{K}(w,\bar{w},z,\bar{z}) = \exp\left\{\frac{x}{2}(C_A - \mathbf{T}_t^2)\left(\mathcal{L}_s(w,\bar{w}) - \mathcal{L}_s(z,\bar{z})\right)\right\} K(w,\bar{w},z,\bar{z}) \tag{5.55}$$

and $K(w,\bar{w},z,\bar{z})$ as defined in eq. (4.10). We notice that the effective Hamiltonian becomes x dependent. It may be solved using the initial condition $\tilde{\Omega}_{\mathrm{2d,h}} = 1$ in which case it could help to understand the systematics of the hard contributions to the amplitude, cf. eqs. (4.88a)–(4.88e).

5.3 The "all-m" wavefunction and its resummed amplitude

The D-dimensional BFKL evolution shows signs of exponentiation as well. The best example for this is the wavefunction generated by repeated application of $\hat{H}_{\mathrm{m}}$ (2.29). We call this the "all-m" amplitude owing to the chain of "m"s in the indices of the wavefunction, cf. eq. (2.38). Explicitly, we have

$$\Omega_{\mathrm{m}}(p,k) = J(p,k) = \frac{1}{2\epsilon}\left[2 - \left(\frac{p^2}{k^2}\right)^{\epsilon} - \left(\frac{p^2}{(p-k)^2}\right)^{\epsilon}\right] \tag{5.56}$$

and hence

$$\begin{aligned}\Omega_{\underbrace{\mathrm{m},\ldots,\mathrm{m}}_{n\text{ times}}}(p,k) = J^n(p,k) &= \frac{1}{(2\epsilon)^n}\left[2 - \left(\frac{p^2}{k^2}\right)^{\epsilon} - \left(\frac{p^2}{(p-k)^2}\right)^{\epsilon}\right]^n \\ &= \frac{1}{(2\epsilon)^n}\sum_{i,j,k=0}^{i+j+k=n}\binom{n}{i,j,k}2^i\left[-\left(\frac{p^2}{k^2}\right)^{\epsilon}\right]^j\left[-\left(\frac{p^2}{(p-k)^2}\right)^{\epsilon}\right]^k\end{aligned} \tag{5.57}$$

with the trinomial coefficients $\binom{n}{i,j,k} = n!/(i!j!k!)$. Upon integration according to eq. (2.25) one is confronted with only bubble integrals, cf. eq. (2.34) with $q = p$. The associated amplitude has colour coefficients $(C_A - \mathbf{T}_t^2)^{\ell-1}$ at ℓ loops and is readily computed by setting $n \to \ell - 1$ in eq. (5.57). The resulting expression

$$\begin{aligned}\hat{\mathcal{M}}^{(+,\ell)}_{\mathrm{NLL}}\Big|_{(C_A-\mathbf{T}_t^2)^{\ell-1}} &= -i\pi\frac{e^{\epsilon\gamma_{\mathrm{E}}}B_0^{\ell-1}}{(\ell-1)!} \\ &\quad\times\sum_{i,j,k=0}^{i+j+k=\ell-1}2^{i-2}(-)^{j+k}\binom{\ell-1}{i,j,k}B_{1+j\epsilon,1+k\epsilon}(\epsilon)\mathbf{T}^2_{s-u}\mathcal{M}^{(\mathrm{tree})}\end{aligned} \tag{5.58}$$

is not particularly enlightening per se. At the level of the all-order amplitude (2.24) however one notices that eq. (5.58) is generated by expansion in $x = \alpha_s L/\pi$ of

$$\begin{aligned}\hat{\mathcal{M}}^{(+)}_{\mathrm{NLL}}|_{(C_A-\mathbf{T}_t^2)^{\ell-1}} = \frac{i\pi}{(C_A-\mathbf{T}_t^2)L}\Bigg\{&\frac{B_{-1}(\epsilon)}{B_0(\epsilon)}\left(e^{x\frac{B_0(\epsilon)}{2\epsilon}(C_A-\mathbf{T}_t^2)}-1\right) \\ &+\left(\frac{\Gamma(1-x(C_A-\mathbf{T}_t^2))}{\Gamma(1+x(C_A-\mathbf{T}_t^2))}\frac{\Gamma^2(1+\frac{x}{2}(C_A-\mathbf{T}_t^2))}{\Gamma^2(1-\frac{x}{2}(C_A-\mathbf{T}_t^2))}-1\right)\Bigg\}\mathbf{T}^2_{s-u}\mathcal{M}^{(\mathrm{tree})}.\end{aligned} \tag{5.59}$$

Voilà another example of resummation in the context of BFKL evolution.

Chapter 6

Conclusion and outlook

6.1 Conclusion

In this work we have demonstrated how the BFKL evolution equation that governs the imaginary part of the signature-even $2 \to 2$ scattering amplitude can be solved to all orders by considering two special limits: the soft limit and the two-dimensional limit. In both of these limits the evolution can be simplified considerably which enabled us to derive algorithmic methods to calculate the wavefunction and amplitude to any loop order.

The soft limit, i.e. configurations where one of the two exchanged reggeons has a small momentum, controls the singular behaviour of the amplitude. The divergent terms can be resummed and we presented the all-order singular amplitude, which is correct up to $\mathcal{O}(\epsilon^0)$ terms, in eq. (5.18). Subsequently we extracted from this result the soft anomalous dimension in the high-energy limit at NLL, cf. eq. (5.25). Conversely, the soft factorisation theorem indirectly confirmed the singular amplitude to all loop orders as was discussed in section 5.1.4. The soft limit also provided the finite contributions to the amplitude that originate in soft configurations, see section 4.1

To compute the remaining finite terms it is sufficient to evolve the wavefunction in strictly two dimensions and stay clear of soft kinematics when calculating the corresponding two-dimensional amplitude. Using single-valued harmonic polylogarithms (SVHPLs) and differential equations we were able to iterate the wavefunction freely and analyse its properties at high loop orders, cf. eqs. (4.52a)–(4.52d) and the ancillary

files `wavefunction_2dL_w13.txt` and `wavefunction_2dF_w10.txt`. At twelve loops a single-valued multiple zeta value (MZV) appears indicating that there is no simple closed form in terms of gamma functions for the two-dimensional wavefunction. At the same time the absence of MZVs up to eleven loops serves as an additional sanity check of our methods.

The two-dimensional wavefunction can be expressed in a compact way in terms of $\mathcal{F}$ functions (4.61) which are symmetric under inversion as well as complex conjugation at function level. Moreover, the introduction of a new alphabet enables us to unravel the recursion of the BFKL evolution and thus facilitates faster, higher-order computations, cf. section 4.3.2.

The wavefunction can be integrated by means of either of the two methods discussed in section 4.4 which yields the hard finite terms. The results agree with the conjectured homogeneous weight property, cf. eqs. (4.88a)–(4.88e) and `amplitude_w11.txt`, and contain the aforementioned single-valued MZV as soon as the weight allows for it, i.e. at eleven loops. This, again, rules out any form of resummation in terms of gamma functions for these terms.

The finite contributions from the soft limit on the other hand exponentiate to give a simple all-order result (5.46). It can be used to derive an effective Hamiltonian which governs the iteration of the purely-hard wavefunction in two dimensions, cf. sections 5.2.1 and 5.2.2. At the level of the amplitude, the contributions generated upon integration of the "all-m" wavefunction can be computed exactly as it involves only bubble integrals. Because of its simple colour dependence, $(C_A - \mathbf{T}_t^2)^{\ell-1}$ at ℓ loops, we were able to resum it to all loop orders (5.59).

The sum of the above soft ($k \to 0$) and two-dimensional ($\epsilon \to 0$) limit recovers the result of the D-dimensional BFKL evolution at the level of the amplitude. The results were verified against the analytic results of ref. [25] and numerical calculations beyond four loops. Up to seven loops the signature-even amplitude at NLL receives the contributions

$$\left(B_0^{-1}\hat{\mathcal{M}}_{\text{NLL}}^{(+,1)}\right) = \frac{1}{2\epsilon} \tag{6.1a}$$

$$\left(2B_0^{-2}\hat{\mathcal{M}}_{\text{NLL}}^{(+,2)}\right) = \frac{C_2}{4\epsilon^2} \tag{6.1b}$$

$$\left(3!B_0^{-3}\hat{\mathcal{M}}_{\text{NLL}}^{(+,3)}\right) = C_2^2\left(\frac{1}{8\epsilon^3} - \frac{11\zeta_3}{4}\right) \tag{6.1c}$$

$$\left(4!B_0^{-4}\hat{\mathcal{M}}_{\text{NLL}}^{(+,4)}\right) = \frac{C_2^3}{16\epsilon^4} + C_A C_2^2\left(-\frac{3\zeta_4}{16} - \frac{\zeta_3}{8\epsilon}\right) \tag{6.1d}$$

$$\begin{aligned}\left(5!B_0^{-5}\hat{\mathcal{M}}_{\text{NLL}}^{(+,5)}\right) = {} & C_2^4\left(\frac{1}{32\epsilon^5} - \frac{53\zeta_5}{2}\right) + C_A C_2^3\left(\frac{253\zeta_5}{16} - \frac{\zeta_3}{16\epsilon^2} - \frac{3\zeta_4}{32\epsilon}\right) \\ & - \frac{5}{2}C_A^2 C_2^2\zeta_5\end{aligned} \tag{6.1e}$$

$$\begin{aligned}\left(6!B_0^{-6}\hat{\mathcal{M}}_{\text{NLL}}^{(+,6)}\right) = {} & C_2^5\left(\frac{1}{64\epsilon^6} - \frac{481\zeta_3^2}{16}\right) \\ & + C_A C_2^4\left(\frac{240975\zeta_3^2 - 945\zeta_6}{6048} - \frac{\zeta_3}{32\epsilon^3} - \frac{3\zeta_4}{64\epsilon^2} - \frac{3\zeta_5}{32\epsilon}\right) \\ & - \frac{141}{8}C_A^2 C_2^3\zeta_3^2 + \frac{39}{16}C_A^3 C_2^2\zeta_3^2\end{aligned} \tag{6.1f}$$

$$\begin{aligned}\left(7!B_0^{-7}\hat{\mathcal{M}}_{\text{NLL}}^{(+,7)}\right) = {} & C_2^6\left(\frac{1}{128\epsilon^7} - \frac{13443\zeta_7}{32}\right) \\ & + C_A C_2^5\left(\frac{180\zeta_3\zeta_4 + 2224155\zeta_7}{3840} - \frac{\zeta_3}{64\epsilon^4} - \frac{3\zeta_4}{128\epsilon^3} - \frac{3\zeta_5}{64\epsilon^2}\right. \\ & \left. + \frac{189\zeta_3^2 - 945\zeta_6}{12096\epsilon}\right) + C_A^2 C_2^4\left(\frac{360\zeta_3\zeta_4 - 1249395\zeta_7}{3840} + \frac{\zeta_3^2}{32\epsilon}\right) \\ & + \frac{21595}{256}C_A^3 C_2^3\zeta_7 - \frac{2135}{256}C_A^4 C_2^2\zeta_7\end{aligned} \tag{6.1g}$$

and we provide another four loop orders (i.e. up to eleven loops) in the ancillary file `amplitude_w11.txt`.

6.2 Outlook

There are several directions one may want to explore next. An obvious one is to pick up where we left off and devote more time to understanding the finite terms of the amplitude and, hopefully, resum them eventually. Going beyond the eleven-loop order which we provide with this work will likely be useful in this context and should be easy to do. (We did not invest much time to optimise our implementations.) A different approach to this problem is provided by the Fourier-Mellin representation of the two-dimensional wavefunction which has proven to be very useful in other (multi-)Regge scenarios [27, 50, 51, 64] and might uncover patterns we were unable to see with our methods. A better understanding of the wavefunction will most definitely provide clues what to look for in the amplitude (even though it will not be as straightforward as in the soft limit, as we argued in section 5.2). Furthermore investigating the physical

implications for the pomeron and 27 exchange (5.28) separately based on the results provided here might be fruitful and is something we barely had time for.

Parting with the signature-even amplitude, there could be ways to apply a modified version of our approach to the signature-odd exchange at NNLL [26], just like generalisation to $2 \to (n-2)$ processes in multi-Regge kinematics are surely worth exploring.

Appendix A

Ancillary files

With this thesis we provide the following plain text files.

`wavefunction_2dL_w13.txt` contains the two-dimensional wavefunction up to 13 loops expressed in terms of standard SVHPLs $\mathcal{L}_\sigma(z,\bar{z})$ using the standard letters $\{0,1\}$. The ℓ-loop contribution is called `WfL[l]`.

`wavefunction_2dF_w10.txt` contains the two-dimensional wavefunction up to ten loops expressed in terms of symmetrised SVHPLs $\mathcal{F}_\sigma(z,\bar{z})$ (4.61) using the letters $\{a,s\}$, cf. section 4.3.2. The ℓ-loop contribution is called `WfF[l]`.

`amplitude_w11.txt` contains the signature-even amplitude at NLL up to eleven loops. The ℓ-loop contribution is called `M[l]` and yields a list of the soft and hard terms. The sum of the two entries of the list equals the full ℓ-loop amplitude up to $\mathcal{O}(\epsilon^0)$.

The data inside the files use a shortened notation

`e` $\longrightarrow \epsilon$	`c1` $\longrightarrow 2C_A - \mathbf{T}_t^2$
`c3` $\longrightarrow C_A$	`c2` $\longrightarrow C_A - \mathbf{T}_t^2$
`Z[n]` $\longrightarrow \zeta_n$	`L[{a,b,c},z,zb]` $\longrightarrow \mathcal{L}_{a,b,c}(z,\bar{z})$
`g533` $\longrightarrow g_{5,3,3}$	`F[{a,b,c},z,zb]` $\longrightarrow \mathcal{F}_{a,b,c}(z,\bar{z})$

For easy viewing each file can be imported in `Mathematica` via the command

```
Get["path_to_file/filename.txt"];
```

Appendix B

Proof of the all-order singular amplitude

In this appendix we show that the singular terms in eq. (3.18) are equal to those in eq. (3.16). We start by noticing that the statement is equivalent to

$$\sum_{n=1}^{\ell}(-1)^{n+1}\binom{\ell}{n}\prod_{m=0}^{n-2}\left[1-\hat{B}_m(\epsilon)\frac{2C_A-\mathbf{T}_t^2}{C_A-\mathbf{T}_t^2}\right] - \left(1-\hat{B}_{-1}(\epsilon)\frac{(2C_A-\mathbf{T}_t^2)}{(C_A-\mathbf{T}_t^2)}\right)^{-1} = \mathcal{O}(\epsilon^\ell). \quad \text{(B.1)}$$

Multiplying both sides of this equality by $\left(1-\hat{B}_{-1}(\epsilon)\frac{(2C_A-\mathbf{T}_t^2)}{(C_A-\mathbf{T}_t^2)}\right)=1+\mathcal{O}(\epsilon^3)$ we get

$$\sum_{n=1}^{\ell}(-1)^{n+1}\binom{\ell}{n}\prod_{m=0}^{n-2}\left[1-\hat{B}_m(\epsilon)\frac{(2C_A-\mathbf{T}_t^2)}{(C_A-\mathbf{T}_t^2)}\right] \times\left(1-\hat{B}_{-1}(\epsilon)\frac{(2C_A-\mathbf{T}_t^2)}{(C_A-\mathbf{T}_t^2)}\right)-1=\mathcal{O}(\epsilon^\ell). \quad \text{(B.2)}$$

The additional factor multiplying the sum on the l.h.s. can be incorporated into the product. Similarly, the -1 on the l.h.s. can be included in the sum. We obtain

$$\sum_{n=0}^{\ell}(-1)^{n+1}\binom{\ell}{n}\prod_{m=-1}^{n-2}\left[1-\hat{B}_m(\epsilon)\frac{(2C_A-\mathbf{T}_t^2)}{(C_A-\mathbf{T}_t^2)}\right]=\mathcal{O}(\epsilon^\ell). \quad \text{(B.3)}$$

At this point, we realise that the structure of the sum and product is strikingly similar to that appearing in the wavefunction in eq. (3.14). In that case, finiteness of the ℓ-loop wavefunction implies

$$\sum_{n=0}^{\ell}(-1)^{n}n^q\binom{\ell}{n}\prod_{m=0}^{n-1}\left[1-\hat{B}_m(\epsilon)\frac{(2C_A-\mathbf{T}_t^2)}{(C_A-\mathbf{T}_t^2)}\right]=\mathcal{O}\left(\epsilon^{\ell-q}\right) \quad \text{(B.4)}$$

with $q \in \mathbb{N}_0$ which is obtained by expanding $(p^2/k^2)^{n\epsilon}$ around small ϵ inside the sum. Next, we bring the product in eq. (B.3) to the same form as in eq. (B.4), obtaining

$$\sum_{n=0}^{\ell}(-1)^{n+1}\binom{\ell}{n}\left(1-\hat{B}_{-1}(\epsilon)\frac{(2C_A-\mathbf{T}_t^2)}{(C_A-\mathbf{T}_t^2)}\right)\left(1-\hat{B}_{n-1}(\epsilon)\frac{(2C_A-\mathbf{T}_t^2)}{(C_A-\mathbf{T}_t^2)}\right)^{-1} \times\prod_{m=0}^{n-1}\left[1-\hat{B}_m(\epsilon)\frac{(2C_A-\mathbf{T}_t^2)}{(C_A-\mathbf{T}_t^2)}\right]=\mathcal{O}(\epsilon^\ell). \quad \text{(B.5)}$$

The extracted factor

$$\begin{aligned}&\left(1-\hat{B}_{-1}(\epsilon)\frac{(2C_A-\mathbf{T}_t^2)}{(C_A-\mathbf{T}_t^2)}\right)\left(1-\hat{B}_{n-1}(\epsilon)\frac{(2C_A-\mathbf{T}_t^2)}{(C_A-\mathbf{T}_t^2)}\right)^{-1}\\ &=1+\frac{(2C_A-\mathbf{T}_t^2)}{(C_A-\mathbf{T}_t^2)}\left[2\epsilon(n\epsilon)^2\zeta_3+3\epsilon^2(n\epsilon)^2\zeta_4+\left(4\epsilon^3(n\epsilon)^2+2\epsilon(n\epsilon)^4\right)\zeta_5\right]+\mathcal{O}(\epsilon^6) \quad \text{(B.6)}\end{aligned}$$

is a function which depends on n only through the combination $n\epsilon$, cf. eq. (3.9). This ensures that for each term in the ϵ expansion, the power of n is never greater than the power of ϵ.

This, then, together with eq. (B.4), proves eq. (B.3) and thus the conjectured amplitude (3.18).

Appendix C

HPLs and SVHPLs

C.1 Harmonic polylogarithms

Harmonic polylogarithms (HPLs) [65] extend the natural logarithm $\log z$ with $z \in \mathbb{C}$ to nested integrals. Similarly to the well-known polylogarithms $\mathrm{Li}_n(z)$ they are defined recursively namely

$$H_{0,\sigma}(z) = \int_0^z \mathrm{d}t \frac{H_\sigma(t)}{t} \qquad \text{and} \qquad H_{1,\sigma}(z) = \int_0^z \mathrm{d}t \frac{H_\sigma(t)}{1-t} \tag{C.1}$$

where σ is a "word" of any length made from the letters[1] $\{0, 1\}$. The number of indices of a HPL $H(z)$ is called the *weight* of the function. By means of eq. (C.1) it corresponds to the number of nested integrals. The recursion is closed by the weight-1 identities

$$H_0(z) = \log z \qquad \text{and} \qquad H_1(z) = -\log(1-z). \tag{C.2}$$

HPLs form a shuffle algebra and thus obey shuffle product identities

$$H_\rho(z) H_\sigma(z) = \sum_{\tau \in \rho \sqcup\!\sqcup \sigma} H_\tau(z) \tag{C.3}$$

where $\rho \sqcup\!\sqcup \sigma$ denotes the shuffle of the words ρ and σ.

The indices of a HPL may be shortened by means of a collapsed notation; one replaces strings of zeros followed by a one according to

$$\underbrace{0, 0, \ldots, 0}_{n \text{ zeros}}, 1 \longrightarrow n+1 \tag{C.4}$$

[1] The full alphabet of HPLs includes the letter -1. In the present work however we only encounter integrals corresponding to the letters 0 and 1.

for example $H_{0,1,0,0,1,1}(z) \to H_{2,3,1}(z)$. In the collapsed notation the number of indices is referred to as the *depth* of the function (while their sum now equals the weight).

Depending on the context it may be useful to view the HPLs as nested sums. One commonly used definition is

$$H_\sigma(z) = \sum_{j=1}^{\infty} z^j Z_j(\sigma) \tag{C.5}$$

with

$$Z_j(a,\sigma) = \frac{1}{j^a} \sum_{i=2}^{j} Z_{i-1}(\sigma) \qquad \text{and} \qquad Z_j(1) = 1/j \tag{C.6}$$

where we assume the collapsed notation. Note that the aforementioned depth is equal to the number of nested sums.

The Taylor series of HPLs, defined by eq. (C.1), whose rightmost index is non-zero, is given by eq. (C.5) with (C.6). Trailing zeros in the indices of a HPL point to logarithmic divergences at $z = 0$. The $\log z = H_0(z)$ terms can be exposed using the shuffle algebra; one considers

$$H_\sigma(z) H_0(z) = H_{\sigma,0}(z) + \ldots + H_{0,\sigma}(z) \tag{C.7}$$

and solves for $H_{\sigma,0}(z)$. This procedure can be applied recursivly until all trailing zeros are removed. Hence, HPLs can always be written as a series in z and $\log z$.

For arguments between 0 and 1 HPLs yield real values. They show branch cuts on the real axis where $z \in [1, \infty)$ and are thus multi-valued functions.

C.2 Single-valued harmonic polylogarithms

Single-valued harmonic polylogarithms (SVHPLs) [48] are the class of all branch cut-free, single-valued, combinations of HPLs. Their construction is somewhat involved and we will only provide a short summary here. Further details can be found in e.g. refs. [49, 66, 67].

SVHPLs are functions of a complex variable z and its complex conjugate $\bar{z}$. They correspond to the linear combinations of $H_\sigma(z) H_{\sigma'}(\bar{z})$ that solve

$$\frac{\mathrm{d}}{\mathrm{d}z} \mathcal{L}_{0,\sigma}(z,\bar{z}) = \frac{\mathcal{L}_\sigma(z,\bar{z})}{z} \qquad \text{and} \qquad \frac{\mathrm{d}}{\mathrm{d}z} \mathcal{L}_{1,\sigma}(z,\bar{z}) = \frac{\mathcal{L}_\sigma(z,\bar{z})}{1-z} \tag{C.8}$$

and obey the boundary conditions [66]

$$\mathcal{L}_\varnothing(z,\bar{z}) = 1, \qquad \mathcal{L}_{\vec{0}_n}(z,\bar{z}) = \log^n(z\bar{z})/n! \qquad \text{and} \qquad \lim_{z\to 0} \mathcal{L}_{\sigma \neq \vec{0}_n}(z,\bar{z}) = 0. \tag{C.9}$$

For the explicit construction one typically defines two alphabets $\{x_0, x_1\}$ and $\{y_0, y_1\}$ and the corresponding sets of all words X^* and Y^* formed from the respective alphabet. The letters of the former alphabet directly translate to $\{0, 1\}$ when they appear as the indices of a (SV)HPL. The letters y_0, y_1 are related to x_0, x_1 via

$$y_0 = x_0 \tag{C.10}$$

$$\tilde{Z}(y_0, y_1) y_1 \tilde{Z}(y_0, y_1)^{-1} = Z(x_0, x_1)^{-1} x_1 Z(x_0, x_1) \tag{C.11}$$

where Z is the so-called Drinfeld associator. It is defined as the generating series

$$Z(x_0, x_1) = \sum_{\sigma \in X^*} H_\sigma(1)\sigma \qquad \text{and} \qquad \tilde{Z}(y_0, y_1) = \sum_{\sigma \in Y^*} H_{\phi(\sigma)}(1)\tilde{\sigma} \tag{C.12}$$

where the "tilde" operation reverses words and ϕ maps $y_i \to x_i$. The values of the HPLs at $z = 1$ in the definition (C.12) are regularised by the shuffle algebra. Eq. (C.11) can be solved iteratively for y_1.

The SVHPLs can then be extracted from the product of another two generating series

$$\sum_{\sigma \in X^*} \mathcal{L}_\sigma(z, \bar{z}) = L_X(z) \tilde{L}_Y(\bar{z}) \tag{C.13}$$

where

$$L_X(z) = \sum_{\sigma \in X^*} H_\sigma(z)\sigma \qquad \text{and} \qquad \tilde{L}_Y(\bar{z}) = \sum_{\sigma \in Y^*} H_{\phi(\sigma)}(\bar{z})\tilde{\sigma} \tag{C.14}$$

with "tilde" and ϕ defined below eq.(C.12).

SVHPLs obey the same shuffle product as HPLs (C.3), namely

$$\mathcal{L}_\rho(z, \bar{z}) \mathcal{L}_\sigma(z, \bar{z}) = \sum_{\tau \in \rho \sqcup\!\sqcup \sigma} \mathcal{L}_\tau(z, \bar{z}). \tag{C.15}$$

C.2.1 Holomorphic part and single-valued map

SVHPLs are uniquely fixed by their holomorphic part (i.e. their functional dependence on z) and the requirement of single-valuedness. We define the holomorphic part of a function $\psi(z, \bar{z})$ as the limit

$$\psi^{(h)}(z) = \psi(z, 0)\big|_{\log \bar{z} \to 0}. \tag{C.16}$$

For a given linear combination of SVHPLs taking this limit simply amounts to replacing $\mathcal{L}_\sigma(z, \bar{z}) \to H_\sigma(z)$.

The dependence on $\bar{z}$ is reconstructed by the single-valued map

$$\mathbf{s}\left(\psi^{(h)}(z)\right) = \psi(z, \bar{z}) \tag{C.17}$$

which is discussed in detail in refs. [50, 56]. Again, we restrict ourselves here to stating the (obvious) replacement rule $H_\sigma(z) \to \mathcal{L}_\sigma(z, \bar{z})$ which generates the corresponding single-valued expression from a linear combination of HPLs of z. As the action of the Hamiltonian $\hat{H}_{\text{2d,i}}$ (4.15) removes constant terms from the wavefunction prior to integration we leave the discussion of those in the context of eqs. (C.16) and (C.17) to the above references.

C.2.2 Variable transformations

SVHPLs obey relations under certain variable transformations. For the most part they are, in some sense, the *same* relations that apply to HPLs due to the single-valued map discussed above in appendix C.2.1. While the latter are much better documented (for an overview we recommend ref. [68]) we struggled to find a comprehensive list for SVHPLs which motivated this appendix.

In section 4.3.2 we transform $z \to 1/z$ and $z \leftrightarrow \bar{z}$ to account for the symmetries of the two-dimensional wavefunction. In addition, we consider $z \to 1 - z$ in section 4.4.2 to facilitate the "last integration". Let us discuss the latter transformation in detail.

At the level of HPLs it is straightforward to find relations under $z \to 1 - z$. Effectively, the transformation moves the lower limit of the integral definition (C.1) from zero to one. Consider the weight-w HPLs with argument $1 - z$

$$\begin{aligned} H_{0,a_2,\ldots,a_w}(1-z) &= \int_0^{1-z} \frac{\mathrm{d}t}{t} H_{a_2,\ldots,a_w}(t) \\ &= \int_0^1 \frac{\mathrm{d}t}{t} H_{a_2,\ldots,a_w}(t) - \int_{1-z}^1 \frac{\mathrm{d}t}{t} H_{a_2,\ldots,a_w}(t) \\ &= H_{0,a_2,\ldots,a_w}(1) - \int_0^z \frac{\mathrm{d}t}{1-t} H_{a_2,\ldots,a_w}(1-t) \end{aligned} \tag{C.18}$$

and

$$\begin{aligned} H_{1,a_2,\ldots,a_w}(1-z) &= \int_0^{1-z} \frac{\mathrm{d}t}{1-t} H_{a_2,\ldots,a_w}(t) \\ &= \int_0^1 \frac{\mathrm{d}t}{1-t} H_{a_2,\ldots,a_w}(t) - \int_{1-z}^1 \frac{\mathrm{d}t}{1-t} H_{a_2,\ldots,a_w}(t) \\ &= H_{1,a_2,\ldots,a_w}(1) - \int_0^z \frac{\mathrm{d}t}{t} H_{a_2,\ldots,a_w}(1-t) \end{aligned} \tag{C.19}$$

with

$$H_0(1-z) = -H_1(z) \quad \text{and} \quad H_1(1-z) = -H_0(z). \tag{C.20}$$

Since the HPLs inside the integrals in eqs. (C.18) and (C.19) are of weight $w-1$ this defines a recursive prescription of how to write any HPL of $1-z$ in terms of HPLs of z.

By means of the holomorphic part of SVHPLs and the single-valued map, see appendix C.2.1, these relations can be applied to SVHPLs. However, it is also possible to solve the recursion and write the answer directly as a sum. We find

$$\mathcal{L}_{a_1,\ldots,a_w}(1-z,1-\bar{z}) = \sum_{j=0}^{w}(-1)^j \mathcal{L}_{\tilde{a}_1,\ldots,\tilde{a}_j}(z,\bar{z})\mathcal{L}_{a_{j+1},\ldots,a_w}(1,1) \tag{C.21}$$

with the "$\sim$" operation swapping the indices $0 \leftrightarrow 1$.

Similarly, on can derive identities for the transformation $z \to 1/z$, $\bar{z} \to 1/\bar{z}$. Again, the recursion can be solved and the resulting formula is simply yet slightly awkward to write out. To do so we define $n_0(\sigma)$ ($n_1(\sigma)$) to count the number zeros (ones) in the indices σ and $\hat{s}_{1\to 0+1}$ to split $\mathcal{L}_\sigma(z,\bar{z})$ into a sum of $2^{n_1(\sigma)}$ SVHPLs according to the index rule $1 \to 0+1$. For example,

$$\begin{aligned}\hat{s}_{1\to 0+1}\left[\mathcal{L}_{1,0,0,1,0}(z,\bar{z})\right] = \\ \mathcal{L}_{0,0,0,0,0}(z,\bar{z}) + \mathcal{L}_{0,0,0,1,0}(z,\bar{z}) + \mathcal{L}_{1,0,0,0,0}(z,\bar{z}) + \mathcal{L}_{1,0,0,1,0}(z,\bar{z})\end{aligned} \tag{C.22}$$

Then

$$\mathcal{L}_{a_1,\ldots,a_w}\left(\frac{1}{z},\frac{1}{\bar{z}}\right) = \sum_{j=0}^{w}(-1)^{n_0(a_1,\ldots,a_j)}\hat{s}_{1\to 0+1}\left[\mathcal{L}_{a_1,\ldots,a_j}(z,\bar{z})\right]\mathcal{L}_{a_{j+1},\ldots,a_w}(\infty,\infty). \tag{C.23}$$

The values of SVHPLs at $z,\bar{z} \to \infty$ are related to the values at $z,\bar{z}=1$ by yet another transformation: $z \to z/(z-1)$.

$$\mathcal{L}_{a_1,\ldots,a_w}\left(\frac{z}{z-1},\frac{\bar{z}}{\bar{z}-1}\right) = (-1)^{n_1(a_1,\ldots,a_w)}\hat{s}_{0\to 0+1}\left[\mathcal{L}_{a_1,\ldots,a_w}(z,\bar{z})\right] \tag{C.24}$$

with $\hat{s}_{0\to 0+1}$ defined like $\hat{s}_{1\to 0+1}$ (C.17) but based on the index rule $0 \to 0+1$. This last step is not strictly necessary but it reduces the amount of data needed to apply these kinds of transformations to a list of SVHPLs at $z,\bar{z}=1$.

Lastly, let us examine the transformation $z \leftrightarrow \bar{z}$ and how to related an SVHPL $\mathcal{L}_\sigma(\bar{z},z)$ to (a sum of) SVHPLs $\mathcal{L}_{\sigma'_i}(z,\bar{z})$. The easy yet computationally heavy way is to translate $\mathcal{L}_\sigma(z,\bar{z})$ to HPLs, swap $z \leftrightarrow \bar{z}$, extract the holomorphic part by means of eq. (C.16)

and finally apply $\mathbf{s}$ (C.17). For SVHPLs of weight less or equal to five this might be adequate but at higher weights it becomes inefficient due to the large size of expressions that the translation to HPLs causes. Like in the above examples this step can be avoided altogether.

The procedure relies on knowing the functional dependence of y_1 on the x_i, cf. eq. (C.11). Consider the weight-n SVHPL $\mathcal{L}_\sigma(z,\bar{z})$ with $\sigma = \sigma_1,\ldots,\sigma_n$ and swap $z \leftrightarrow \bar{z}$. Then

$$\mathcal{L}_\sigma(\bar{z},z) = \mathcal{L}_{\tilde{\sigma}}(z,\bar{z}) + \sum_{i=4}^{|\sigma|}\sum_{j=0}^{|\sigma|-i} y1(\sigma_j,\ldots,\sigma_{i+j})\mathcal{L}_{\underbrace{\sigma_1,\ldots,\sigma_{j-1}}_{(A)},\underbrace{\sigma_{i+j+1},\ldots,\sigma_n}_{(B)},1} \tag{C.25}$$

where the "tilde" map was defined below eq. (C.12) and $y1(\sigma)$ is the coefficient of the product of x_0 and x_1 corresponding to σ, e.g. if $\sigma = 1,1,0,1,0$ then $y1(\sigma)$ is the coefficient of $x_1x_1x_0x_1x_0$. The indices (A) in eq. (C.25) only appear if $j-1 \geq 1$ and likewise (B) if $i+j+1 \leq n$.

Acronyms

BFKL Balitsky–Fadeev–Kuraev–Lipatov

HPL harmonic polylogarithm

HPLs harmonic polylogarithms

Balitsky-JIMWLK Balitsky–Jalilian-Marian–Iancu–McLerran–Weigert–Leonidov–Kovner

LL leading logarithm(ic accuracy)

MZV multiple zeta value

MZVs multiple zeta values

NLL next-to-leading logarithm(ic accuracy)

NNLL next-to-next-to-leading logarithm(ic accuracy)

OEIS The On-Line Encyclopedia of Integer Sequences

QCD quantum chromodynamics

QFT quantum field theory

SVHPL single-valued harmonic polylogarithm

SVHPLs single-valued harmonic polylogarithms

Bibliography

[1] Simon Caron-Huot, Einan Gardi, Joscha Reichel, and Leonardo Vernazza. Infrared singularities of QCD scattering amplitudes in the Regge limit to all orders. *JHEP*, 03:098, 2018.

[2] E. A. Kuraev, L. N. Lipatov, and Victor S. Fadin. Multiregge Processes in the Yang-Mills Theory. *Sov. Phys. JETP*, 44:443–450, 1976. [Zh. Eksp. Teor. Fiz.71,840(1976)].

[3] E. A. Kuraev, L. N. Lipatov, and Victor S. Fadin. The Pomeranchuk Singularity in Nonabelian Gauge Theories. *Sov. Phys. JETP*, 45:199–204, 1977. [Zh. Eksp. Teor. Fiz.72,377(1977)].

[4] I. I. Balitsky and L. N. Lipatov. The Pomeranchuk Singularity in Quantum Chromodynamics. *Sov. J. Nucl. Phys.*, 28:822–829, 1978. [Yad. Fiz.28,1597(1978)].

[5] L. N. Lipatov. The Bare Pomeron in Quantum Chromodynamics. *Sov. Phys. JETP*, 63:904–912, 1986. [Zh. Eksp. Teor. Fiz.90,1536(1986)].

[6] Alfred H. Mueller. Soft gluons in the infinite momentum wave function and the BFKL pomeron. *Nucl. Phys.*, B415:373–385, 1994.

[7] Alfred H. Mueller and Bimal Patel. Single and double BFKL pomeron exchange and a dipole picture of high-energy hard processes. *Nucl. Phys.*, B425:471–488, 1994.

[8] Richard C. Brower, Joseph Polchinski, Matthew J. Strassler, and Chung-I Tan. The Pomeron and gauge/string duality. *JHEP*, 12:005, 2007.

[9] Ian Moult, Mikhail P. Solon, Iain W. Stewart, and Gherardo Vita. Fermionic Glauber Operators and Quark Reggeization. 2017.

[10] I. Balitsky. Operator expansion for high-energy scattering. *Nucl. Phys.*, B463:99–160, 1996.

[11] I. Balitsky. Factorization for high-energy scattering. *Phys. Rev. Lett.*, 81:2024–2027, 1998.

[12] Yuri V. Kovchegov. Small x F(2) structure function of a nucleus including multiple pomeron exchanges. *Phys. Rev.*, D60:034008, 1999.

[13] Jamal Jalilian-Marian, Alex Kovner, Larry D. McLerran, and Heribert Weigert. The Intrinsic glue distribution at very small x. *Phys. Rev.*, D55:5414–5428, 1997.

[14] Jamal Jalilian-Marian, Alex Kovner, Andrei Leonidov, and Heribert Weigert. The Wilson renormalization group for low x physics: Towards the high density regime. *Phys. Rev.*, D59:014014, 1998.

[15] Edmond Iancu, Andrei Leonidov, and Larry D. McLerran. The Renormalization group equation for the color glass condensate. *Phys. Lett.*, B510:133–144, 2001.

[16] Michael G. Sotiropoulos and George F. Sterman. Color exchange in near forward hard elastic scattering. *Nucl. Phys.*, B419:59–76, 1994.

[17] Gregory P. Korchemsky. On Near forward high-energy scattering in QCD. *Phys. Lett.*, B325:459–466, 1994.

[18] I. A. Korchemskaya and G. P. Korchemsky. Evolution equation for gluon Regge trajectory. *Phys. Lett.*, B387:346–354, 1996.

[19] I. A. Korchemskaya and G. P. Korchemsky. High-energy scattering in QCD and cross singularities of Wilson loops. *Nucl. Phys.*, B437:127–162, 1995.

[20] Vittorio Del Duca and E. W. Nigel Glover. The High-energy limit of QCD at two loops. *JHEP*, 10:035, 2001.

[21] Vittorio Del Duca, Giulio Falcioni, Lorenzo Magnea, and Leonardo Vernazza. High-energy QCD amplitudes at two loops and beyond. *Phys. Lett.*, B732:233–240, 2014.

[22] Vittorio Del Duca, Giulio Falcioni, Lorenzo Magnea, and Leonardo Vernazza. Analyzing high-energy factorization beyond next-to-leading logarithmic accuracy. *JHEP*, 02:029, 2015.

[23] Vittorio Del Duca, Claude Duhr, Einan Gardi, Lorenzo Magnea, and Chris D. White. An infrared approach to Reggeization. *Phys. Rev.*, D85:071104, 2012.

[24] Vittorio Del Duca, Claude Duhr, Einan Gardi, Lorenzo Magnea, and Chris D. White. The Infrared structure of gauge theory amplitudes in the high-energy limit. *JHEP*, 12:021, 2011.

[25] Simon Caron-Huot. When does the gluon reggeize? *JHEP*, 05:093, 2015.

[26] Simon Caron-Huot, Einan Gardi, and Leonardo Vernazza. Two-parton scattering in the high-energy limit. *JHEP*, 06:016, 2017.

[27] Vittorio Del Duca, Claude Duhr, Falko Dulat, and Brenda Penante. All two-loop MHV remainder functions in multi-Regge kinematics. *Submitted to: JHEP*, 2018.

[28] Claude Duhr and Zhengwen Liu. Multi-Regge kinematics and the scattering equations. *Submitted to: JHEP*, 2018.

[29] Robin Marzucca and Bram Verbeek. The Multi-Regge Limit of the Eight-Particle Amplitude Beyond Leading Logarithmic Accuracy. 2018.

[30] P. D. B. Collins. *An Introduction to Regge Theory and High-Energy Physics*. Cambridge Monographs on Mathematical Physics. Cambridge Univ. Press, Cambridge, UK, 2009.

[31] T. Regge. Introduction to complex orbital momenta. *Il Nuovo Cimento (1955-1965)*, 14(5):951–976, Dec 1959.

[32] Øyvind Almelid, Claude Duhr, and Einan Gardi. Three-loop corrections to the soft anomalous dimension in multileg scattering. *Phys. Rev. Lett.*, 117(17):172002, 2016.

[33] Einan Gardi, Øyvind Almelid, and Claude Duhr. Long-distance singularities in multi-leg scattering amplitudes. *PoS*, LL2016:058, 2016.

[34] S. Mert Aybat, Lance J. Dixon, and George F. Sterman. The Two-loop soft anomalous dimension matrix and resummation at next-to-next-to leading pole. *Phys. Rev.*, D74:074004, 2006.

[35] Einan Gardi and Lorenzo Magnea. Factorization constraints for soft anomalous dimensions in QCD scattering amplitudes. *JHEP*, 03:079, 2009.

[36] Thomas Becher and Matthias Neubert. Infrared singularities of scattering amplitudes in perturbative QCD. *Phys. Rev. Lett.*, 102:162001, 2009. [Erratum: Phys. Rev. Lett.111,no.19,199905(2013)].

[37] Thomas Becher and Matthias Neubert. On the Structure of Infrared Singularities of Gauge-Theory Amplitudes. *JHEP*, 06:081, 2009. [Erratum: JHEP11,024(2013)].

[38] Øyvind Almelid, Claude Duhr, Einan Gardi, Andrew McLeod, and Chris D. White. Bootstrapping the QCD soft anomalous dimension. *JHEP*, 09:073, 2017.

[39] J. Bartels, D. Colferai, S. Gieseke, and A. Kyrieleis. NLO corrections to the photon impact factor: Combining real and virtual corrections. *Phys. Rev.*, D66:094017, 2002.

[40] J. Bartels and A. Kyrieleis. NLO corrections to the gamma* impact factor: First numerical results for the real corrections to gamma*(L). *Phys. Rev.*, D70:114003, 2004.

[41] J. Bartels and L. Motyka. Baryon scattering at high energies: Wave function, impact factor, and gluon radiation. *Eur. Phys. J.*, C55:65–83, 2008.

[42] Jeffrey R. Forshaw and D. A. Ross. Quantum chromodynamics and the pomeron. *Cambridge Lect. Notes Phys.*, 9:1–248, 1997.

[43] Yu. L. Dokshitzer and G. Marchesini. Soft gluons at large angles in hadron collisions. *JHEP*, 01:007, 2006.

[44] Stefano Catani. The Singular behavior of QCD amplitudes at two loop order. *Phys. Lett.*, B427:161–171, 1998.

[45] Gudrun Heinrich. Sector Decomposition. *Int. J. Mod. Phys.*, A23:1457–1486, 2008.

[46] Jonathon Carter and Gudrun Heinrich. SecDec: A general program for sector decomposition. *Comput. Phys. Commun.*, 182:1566–1581, 2011.

[47] S. Borowka, G. Heinrich, S. Jahn, S. P. Jones, M. Kerner, and J. Schlenk. Numerical evaluation of two-loop integrals with pySecDec. *Acta Phys. Polon. Supp.*, 11:375, 2018.

[48] Francis C. S. Brown. Polylogarithmes multiples uniformes en une variable. *Compt. Rend. Math.*, 338(7):527–532, 2004.

[49] Lance J. Dixon, Claude Duhr, and Jeffrey Pennington. Single-valued harmonic polylogarithms and the multi-Regge limit. *JHEP*, 10:074, 2012.

[50] Vittorio Del Duca, Stefan Druc, James Drummond, Claude Duhr, Falko Dulat, Robin Marzucca, Georgios Papathanasiou, and Bram Verbeek. Multi-Regge kinematics and the moduli space of Riemann spheres with marked points. *JHEP*, 08:152, 2016.

[51] Vittorio Del Duca, Stefan Druc, James Drummond, Claude Duhr, Falko Dulat, Robin Marzucca, Georgios Papathanasiou, and Bram Verbeek. The seven-gluon amplitude in multi-Regge kinematics beyond leading logarithmic accuracy. *JHEP*, 06:116, 2018.

[52] Lance J. Dixon, James M. Drummond, Claude Duhr, and Jeffrey Pennington. The four-loop remainder function and multi-Regge behavior at NNLLA in planar N = 4 super-Yang-Mills theory. *JHEP*, 06:116, 2014.

[53] Lance J. Dixon, Matt von Hippel, and Andrew J. McLeod. The four-loop six-gluon NMHV ratio function. *JHEP*, 01:053, 2016.

[54] Simon Caron-Huot, Lance J. Dixon, Matt von Hippel, Andrew J. McLeod, and Georgios Papathanasiou. The Double Pentaladder Integral to All Orders. *JHEP*, 07:170, 2018.

[55] Oliver Schnetz. Graphical functions and single-valued multiple polylogarithms. *Commun. Num. Theor. Phys.*, 08:589–675, 2014.

[56] Francis Brown. Single-valued Motivic Periods and Multiple Zeta Values. *SIGMA*, 2:e25, 2014.

[57] Matthew D. Schwartz and Hua Xing Zhu. Nonglobal logarithms at three loops, four loops, five loops, and beyond. *Phys. Rev.*, D90(6):065004, 2014.

[58] Einan Gardi and Lorenzo Magnea. Infrared singularities in QCD amplitudes. *Nuovo Cim.*, C32N5-6:137–157, 2009. [Frascati Phys. Ser.50(2010)].

[59] Lance J. Dixon, Einan Gardi, and Lorenzo Magnea. On soft singularities at three loops and beyond. *JHEP*, 02:081, 2010.

[60] Valentin Ahrens, Matthias Neubert, and Leonardo Vernazza. Structure of Infrared Singularities of Gauge-Theory Amplitudes at Three and Four Loops. *JHEP*, 09:138, 2012.

[61] G. P. Korchemsky and A. V. Radyushkin. Loop Space Formalism and Renormalization Group for the Infrared Asymptotics of QCD. *Phys. Lett.*, B171:459–467, 1986.

[62] G. P. Korchemsky and A. V. Radyushkin. Infrared asymptotics of perturbative QCD: renormalisation properties of the Wilson loops in higher orders of perturbation theory. *Sov. J. Nucl. Phys.*, 44:877, 1986. [Yad. Fiz.44,1351(1986)].

[63] G. P. Korchemsky and A. V. Radyushkin. Renormalization of the Wilson Loops Beyond the Leading Order. *Nucl. Phys.*, B283:342–364, 1987.

[64] Vittorio Del Duca, Stefan Druc, James Drummond, Claude Duhr, Falko Dulat, Robin Marzucca, Georgios Papathanasiou, and Bram Verbeek. Amplitudes in the Multi-Regge Limit of $\mathcal{N}$=4 SYM. In *Diffraction and Low-x 2018 (Difflowx2018) Reggio Calabria, Italy, August 26-September 1, 2018*, 2018.

[65] E. Remiddi and J. A. M. Vermaseren. Harmonic polylogarithms. *Int. J. Mod. Phys.*, A15:725–754, 2000.

[66] Jeffrey Pennington. The six-point remainder function to all loop orders in the multi-Regge limit. *JHEP*, 01:059, 2013.

[67] Vittorio Del Duca, Lance J. Dixon, Claude Duhr, and Jeffrey Pennington. The BFKL equation, Mueller-Navelet jets and single-valued harmonic polylogarithms. *JHEP*, 02:086, 2014.

[68] D Maitre. HPL, a mathematica implementation of the harmonic polylogarithms. *Comput. Phys. Commun.*, 174:222–240, 2006.